Ministry of Higher Education and
Scientific Research
University of Babylon
College of Science
Department of physics

Effect of Annealing on Some Structure and Physical Properties of Ni:Al_2O_3 Thin Film by Using Thermal Chemical Spray

A Thesis

Submitted to the Council of College of Science, University of Babylon in Partial Fulfillment of the Requirements for the Degree of Master of Science in Physics

By

Mohamed Khaled Khalil Yassin

(B. Sc. in Physics 2007)

Supervised By

Prof. Dr.
Raheem G aayied Kadhim Hussein

Asst .Prof. Dr.
Saba A. Obaid ALShiaa

2023 A.D.

1444 A.H.

Supervisors Certification

We certify that this thesis is titled (Effect of Annealing on Some Structure and Physical Properties of Ni:Al_2O_3 Thin Film by Using Thermal Chemical Spray) was prepared by (Mohamed Khaled Khalil Yassin) under our supervision at the Department of physics - College of Science - University of Babylon, as partial fulfillment of the requirements for the degree of Master in Physics.

Signature:

Supervisor: Prof. Dr. Raheem Gaayied Kadhim Hussein

Title: Professor

Address: Department of physics
College of Science
University of Babylon

Date: / / 2023

Signature:

Supervisor: Dr. Saba Abdulzahra O. ALShiaa

Title: Asst .Prof.

Address: Department of physics
College of Science
University of Babylon

Date: / / 2023

Certification of the Head of the Department

In view of the available recommendation, I forward latter thesis for debate by the examination committee.

Signature
Name: Dr. Samira Adnan Mahdi
Title: Assistant Professor
Address: Head of Department of Physics, College of Science, University of Babylon
Date: / / 2023

Dedication

This Thesis is dedicated to

My parents .....The shortest way to win the satisfaction of Allah

My wife .....For her patience with me in all circumstances

My brothers.....The source of my strength

My children .....The most beautiful in life and hope for the future (Ayham , Sama and Slr).

And ..... All who helped .

Mohamed

Acknowledgments

In the name of Allah (the Almighty) ,the Great is the most Gracious and the most Merciful. Praise be to Allah (the Almighty), the lord of earth and heaven, for completing my dissertation .

I would like to thank my supervisors, Prof. Dr. Raheem Gaayied Kadhim Hussein, and Dr. Saba Abdulzahra O. ALShiaa for suggesting this topic to me and for their distinguished efforts and sound advice and directions that helped me. In alleviating all the difficulties, I encountered during my work.

Many thanks are the Deanery of the College of Science at University of Babylon and to Department of Physics for offering me the opportunity to complete my study. I wish success to all mentioned or not my thankfulness is to all who took part in this achievement.

Mohamed

وزارة التعليم العالي والبحث العلمي

جامعة بابل / كلية العلوم

قسم الفيزياء

تأثير التلدين على بعض الخصائص التركيبية والفيزيائية للأغشية الرقيقة $Ni:Al_2O_3$ بطريقة الرش الكيميائي الحراري

رسالة

مقدمة الى مجلس كلية العلوم - جامعة بابل وهي جزء من متطلبات نيل درجة الماجستير

في علوم الفيزياء

من قبل

(محمد خالد خليل ياسين)

بكالوريوس علوم في الفيزياء (٢٠٠٧)

بأشراف

أ.د. رحيم كعيد كاظم حسين **أ.م.د. صبا عبد الزهرة عبيد الشياع**

١٤٤٤ هـ ٢٠٢٣ م

الخلاصة

تعتبر المادة الاساسية هي كلوريد النيكل $NiCl_2$ والمادة المشوبة هي اوكسيد الالمنيوم Al_2O_3 وتم استخدام طريقة الرش الكيميائي الحراري حيث تم استخدام اوكسيد الالمنيوم بنسب تشويب مختلفة %(١,٢,٣) رُسبت الاغشية الرقيقة على ركائز زجاجية ثم لدُنتّ الاغشية بدرجة (٣٥٠ ^oC) .

تتميز الاغشية الرقيقة المصنعة $NiCl_2:Al_2O_3$ بسمك nm (٤٥ – ٦٢ ± ٦) لخصائص حيود الاشعة السينية (XRD) وميكروسكوب القوة الذرية (AFM) والتحليل الطيفي للأشعة فوق البنفسجية (UV) والماسح الضوئي للمجهر الالكتروني (SEM) وخصائص (I-V) .

اظهرت انماط (XRD) ان جميع الاغشية الرقيقة من $NiCl_2:Al_2O_3$ كانت ذات طبيعة متعددة التبلور تنتمي الى الطور المعيني القائم وباتجاه سائد (١١١) ، وحُسب الحجم الحبيبي (d) ، ثابت الشبيكة (a) ، عرض منتصف القمة (FWHM) واطهرت ان زيادة نسبة التشويب يؤدي الى زيادة متوسط الحجم الحبيبي nm (٣-٥) .

ودُرست التضاريس والتشكل السطحي للأغشية الرقيقة المحضرة باستخدام مجهر القوة الذرية (AFM) ، حيث وجد أن الخشونة تزداد مع زيادة التشويب وتقل عند التلدين.

أما بالنسبة لصور نتائج المجهر الإلكتروني الماسح (SEM) ، فإن الزيادة في حجم الجسيمات النانوية عن طريق زيادة التشويب ويحدث العكس أثناء عملية التلدين.

حُسبتْ المعلمات الضوئية الاساسية مثل الامتصاصية والنفاذية ومعامل الامتصاص (α) ومعامل الخمود (K) ومعامل الانكسار (n) والاجزاء الحقيقة (ε_{rel}) والخيالية (ε_{img}) لثابت العزل الكهربائي وفجوة الطاقة المحظورة (E_g) من اطياف الامتصاص .

وجد ان طيف الامتصاصية يزداد مع زيادة نسب التشويب ويقل عند التلدين ويحث العكس لطيف النفاذية . ثم وجد ان الانتقال البصري لهذه الاغشية من النوع المباشر المسموح حيث تقل فجوة الطاقة من (٣.٨ eV) الى (٣.٦ eV) مع زيادة الحجم الحبيبي .

وشملت الخواص الكهربائية خصائص (I-V) حيث تم حساب التوصيلية الكهربائية (σ) .

Summary

The basic material is considered $NiCl_2$ and the doped material was Al_2O_3using the thermal chemical spray , where aluminum oxide used with different doping ratios (1,2,3) % . The thin films were deposited on glass substrates and annelid at a temperature of 350 º C.

The synthesized $NiCl_2$:Al_2O_3 thin films of thickness (45 – 62 ± 6) nm have been characterized by x-ray diffraction (XRD) , atomic force microscopy (AFM) , UV-VIS spectroscopy , scanners electron microscopy (SEM) and I-V characteristics.

The XRD patterns show that all thin films of $NiCl_2$:Al_2O_3 were polycrystalline nature belonging to orthorhombic phase , with performed orientation in the direction(111). The grain size (D),lattice constant (a),width of the middle of the peak (FWHM) have been calculated and showed that the doping ratio leads to increase the average particles size (3-5)nm .

The topography and surface morphology of the prepared films were studied using atomic force microscopy (AFM), where it is found that the roughness increased with increasing doping and decreased with annealing.

As for the images of the results of the scanning electron microscope (SEM), the increase in the size of the nanoparticles by increasing the doping and the opposite occurs during the annealing process.

The fundamental optical parameters like absorption , transmittance , absorption coefficient (α),extinction coefficient (K),refractive index (n) , and real and imaginary parts of dielectric constant , and band gap have been calculated from transmission spectra . It was found that the

absorbance increases with the increase in doping and decreases upon annealing, and the opposite happens for the transmittance spectra .

The possible optical transition in these films is found to be direct and allowed where band gap decreased from (3.8 eV) to (3.6 eV) with increase the grain size . By using the reflectance and transmittance spectra , the refractive index (n) , real dielectric constant (ε_{real}) and imaginary dielectric constant (ε_{imag})have been calculated and discussed graphically .

The electrical properties include I-V characteristic have been studied and found that resistivity and conductivity (σ).

Contents

List of Symbols

Symbol	Physical meaning	Unit
A	Absorption	-
R	Reflectance	-
T	Transmittance	-
α	Absorption Coefficient	cm^{-1}
n	Refractive Index	-
K	Extinction Coefficient	-
ε_r	Real Part of Dielectric Constant	-
ε_i	Imaginary Part of Dielectric Constant	-
G.S	Grain Size	M
θ	Bragg Diffraction Angle	Deg
δ	Dislocation Density	cm^{-2}
N_0	Crystals Layers Number	cm^{-3}
a	Lattice Constant	Nm
hkl	Miller indices	-

Symbol	Physical meaning	Unit
λ	Wavelength	M
Eg^{opt}	optical energy gap	eV
I_0,I	The intensity of the transmitted and incident ray	$eV/m^2.s$
t	Thin film thickness	Nm
$h\upsilon(E)$	photon energy	eV
E_F	Fermi level energy	eV
E_v	Valence Band energy	eV
E_c	Conduction Band energy	eV
ρ	Resistivity	Ω cm
σ	Electrical Conductivity	$(\Omega\ cm)^{-1}$

List of Abbreviations

Symbol	Physical meaning
XRD	X-Ray Diffraction
UV	Ultra Violet Spectrum
AFM	Atomic Force Microscope
SEM	Scanning Electron Microscope
CSP	Chemical Spray Pyrolysis
R.M.S.	Root Mean Square
β (FWHM)	Full Width at Half Maximum
I-V	Current-Voltage

List of Figures

List of Tables

﴿ قَالُواْ سُبْحَانَكَ لاَ عِلْمَ لَنَا إِلاَّ مَا عَلَّمْتَنَا

إِنَّكَ أَنتَ الْعَلِيمُ الْحَكِيمُ ﴾

صدق الله العظيم

سورة البقرة / الآية ٣٢

1.1. Introduction

The study of matter in the form of a thin film is one of the important topics of solid-state physics, and thin-film technology has made a great contribution to the study of semiconductors, and many of its physical and chemical properties have been identified in order to determine its use in various practical applications [1,2].

The term thin film is used to describe one or more layers of atoms of matter, the thickness of which does not exceed one micron (1 μ) [3].

The study of thin films had a great impact on attracting the interest of physicists, as Bunsen and Grove prepared thin metal films in 1852 by the chemical reaction method, and in 1857 Faraday managed to obtaining a thin film using thermal evaporation technology(Thermal Evaporation) , In 1876, Adams prepared thin films of selenium adjacent to platinum, and in 1887 the possibility of evaporating metals was reached using the vacuum evaporation technique, which was followed by the world (Kenett) in 1888 in preparing thin films for metals, and the study of thin films was advanced through measurements Both Jamin , Fizeau and Quink and the theoretical side by Drude. As for the physical properties, they began to be studied at the beginning of the twentieth century, and research in this field made a rapid leap [4-6].

The development in the field of preparation of thin films has led to the diversification of research on the study of the physical properties of these films, and the preparation of thin films with specifications of a high degree of purity , accuracy and control of the thickness of the film and its homogeneity requires complex and precise systems and devices that require exorbitant costs. All of this led to research methods in which preparation costs are low and with less complex equipment, note that the

films prepared in this way may be of less quality and efficiency when balancing them with the films prepared using advanced methods. However, they are films with good specifications for study and can be used in important practical applications in various fields [7]. Therefore, the thermal chemical precipitation method was chosen in this research.

1.2. Thin Films Growth Process

There are three main stages that form a typical thin-film deposition process which are:

(i) Production of the appropriate atomic, molecular, or ionic species ،

(ii) Transport of these particles to the substrate through a technic ،

(iii) Condensation of the vapor on the substrate, either directly or via a chemical and/or electrochemical reaction, to form a solid deposit [8,9].

Based on the various experimental and theoretical studies, a general picture of the step-by-step growth process is as follows [10]:

1. The vaporized species, when impacting the substrate, lose their velocity to the substrate (provided that the incident energy not to be high) and are adsorbed on the substrate surface physically .

2. Especially when heated, the adsorbed material is not in thermal equilibrium with the substrate initially and moves over the substrate surface. In this process, by interacting among themselves, form clusters .

3. The clusters or the nuclei are unstable thermodynamically and may have tendency to desorb in time, depending on the deposition parameters. If the deposition parameters are so that a formed cluster collides with other adsorbed clusters it will start increasing in size, forming islands. After getting a certain critical size, the cluster becomes stable

thermodynamically; the nucleation barrier is said to be overcome. This step is called the nucleation stage which includes the formation of stable, chemisorbed, critical-sized nuclei.

4. The number and size of critical cluster will increase until it reaches a saturation nucleation density. Parameters such as the energy of the impinging species, the rate of impingement, the activation energies of adsorption, desorption, thermal diffusion, the temperature, topography, and chemical nature of the substrate will strongly change nucleation density and the average nucleus size.

5. The next stage in the process of film formation is the coalescence stage in which the small islands begin to coalescing with each other in an attempt to reduce the substrate surface area. This tendency to form bigger islands is called agglomeration and is increased by increasing the surface mobility of the adsorbed species, for an example, by enhancing the substrate temperature .

6. Larger islands growth takes place together by leaving channels and holes of uncovered substrate. The structure of the films at this step changes from rough discontinuous island to porous network type. Formation of a completely continuous film occurred when filling of the channels and holes [10] .

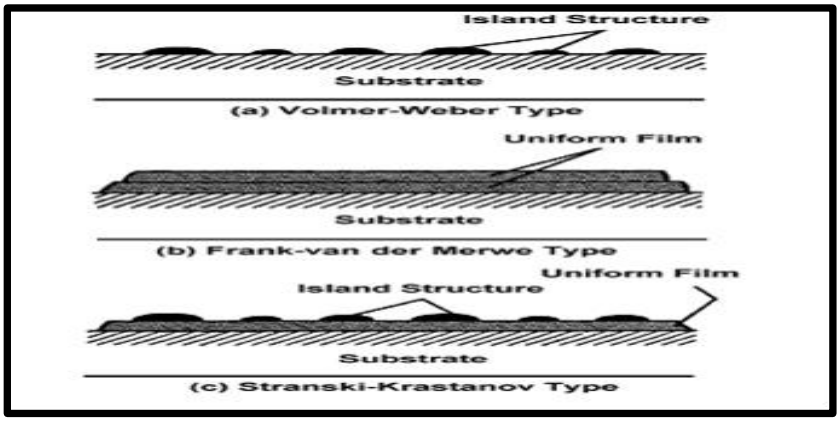

Fig (1.1): Three modes of thin film growth processes [11].

What is available in almost all practical cases is Island type; the most common growth process; except for special conditions which are necessary for the crystallographic orientations and the topographical details; different islands are randomly distributed. [9]. Films will show a ring-type diffraction pattern and will be polycrystalline if the grains are randomly located. Even if the location and orientation of different islands is the same during the technique; as obtained under special deposition conditions on suitable single crystal substrates; a single-crystal film won't be accessible. These films show diffraction patterns similar to those of single crystals and are called epitaxial single-crystal films [12].

1.3. Physical Mechanisms of Thin Film Growth

In this section, we will examine the effect of the growth parameters on the structure and microstructure of thin films. We will discuss the main physical mechanisms involved in the nucleation and crystallization of the films on the substrate. Studies have done through x- ray diffraction, optical diffraction and, mainly through electron diffraction; have allowed creating three mechanisms of the nucleation and growth of thin films which is dependent on the thermodynamic parameters of the deposit and the substrate surface interaction between the atoms and the substrate material. The three basic modes are: (i) Volmer–Weber model, (ii) Frank–Van der Merwe model and (iii) Stranski– Krastanov model. [13,14].

1.4. Thin Film Applications

Thin films are used in many technical and scientific fields and some of them are listed below [15,16]. Thin films have great importance and importance for a large variety of industrial applications. Some of the significant applications are wear and corrosion resistant depositing which

are capable of largish the lifetime of a large number of critical products [17]. In addition optical and electrically active as well as magnetic films can be usefully used in sensors actuators solar cells thin film electroacoustic devices porous nanocomposite films etc[18,19].

Thin film technology is available for tailoring depositing materials for specific applications e.g, properties varying from hard diamond to soft polymer films. The thin film technology for technological applications are capable of attaining super hard and tough coatings, and also self-lubricating coatings are available. Smart windows based on electronic controlled transparency have already been investigated [20,21],

Thin films have been used in many optical industries, such as making mirrors, as well as in reflective and non-reflective coatings. They have also been used in the manufacture of optical filters, photographic processes, and photocopying devices[21].

Thin films have been used in recent years in many electronic devices due to their small size and light weight, as they are used in digital computers, rectifiers, and transistors, as well as in integrated circuits[20].

1.5. Annealing of Thin Film

Annealing is widely used in industry as a primary process and as a heat treatment to give the product the required properties, as annealing is widely used in the production of non-ferrous metals and alloys [22].

Annealing means heating the sample to a certain temperature below its melting point and stabilizing the temperature for a specific time in order to achieve thermal homogeneity for all the sample slowly inside the furnace. Annealing generally aims to remove stresses and remove the inhomogeneity that arises from casting. The second goal of annealing is

to recrystallize the metal granules. Or any sample where new granules are formed with almost equal axes, because these granules differ from the previous ones in terms of shape, angle, and atomic composition, as well as what they contain of low concentrations of dislocations. And the driving force for recrystallization is the energy of distortions of the crystalline arrangement of the granules, which are stored in dislocations, and which are liberated when the concentrations of dislocations decrease, during the annealing process, where the granules swell after the end of recrystallization and grow one at the expense of the other due to the movement of some atoms or a group of atoms across the separating boundaries from the diminishing granule to the next. the developing granule [23].

The heat treatment may take place in a vacuum or in the presence of gas or air and it is done using an oven and it is called traditional thermal annealing or using laser technology and it is called rapid thermal annealing and its effect varies according to the type of material and heating conditions of temperature and type of gas, that the thermal treatment rearranges the crystal for itself and reduces crystal defects in some Sometimes it is used to obtain the crystallized state.

Sometimes the resistance decreases as a result of the formation of objective levels within the energy gap [24]. A study appeared on the effect of annealing on the physical properties, where the researchers (Hsiuang & Wang) [25] found that the effect of heat treatment for random semiconductors is to reduce the voids and regularity of the atoms (at low temperature) and reduce the dangling bonds and structural relaxation (at high temperatures) as well. Increasing the annealing time and the number of annealing times lead to the stability of the membrane properties.

1.6. Nickel (Ni)

Nickel is a chemical element with symbol Ni and atomic number 28. It is a silvery-white lustrous metal with a slight golden tinge . Nickel is a hard and ductile transition metal. Pure nickel is chemically reactive but large pieces are slow to react with air under standard conditions because a passivation layer of nickel oxide forms on the surface that prevents further corrosion. Even so, pure native nickel is found in Earth's crust only in tiny amounts, usually in ultramafic rocks [26] and in the interiors of larger nickel–iron meteorites that were not exposed to oxygen when outside Earth's atmosphere.

Nickel has the following properties:

Table (1.1): the physical properties of nickel [26].

Ni	Properties
Color	Grayish white
Size of Particle	75-100 microns
Melting Point	1453 °C
Boiling Temperature	2732 °C
Density	8.9 g/ cm^3
Electrical Conductivity at T=20°C	0.146×10^6 $(\Omega.cm)^{-1}$
Crystal Structure	Cube with a concentric face (a=0,352mm)

Nickel chloride is one of the nickel salts used in this research is the chemical compound ($NiCl_2$). The anhydrous salt is yellow, but the more familiar hydrate $NiCl_2 \cdot 6H_2O$ is green. Nickel chloride, in various forms, is the most important source of nickel for chemical synthesis. The nickel chlorides are deliquescent, absorbing moisture from the air to form a solution[2٧].

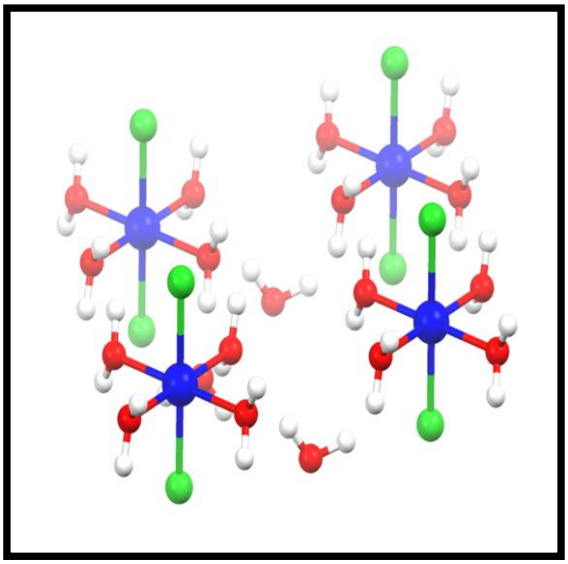

Fig: (1.2) : structure of hexahydrate[27].

Table(1.2): Some Physical Properties of Nickel Chloride [28] .

$NiCl_2$	Properties
Color	Green
Density	1.92 g/ cm^3
Melting point	140 °C
Solubility	123.8g/100ml water
Molecular Weight	129.20 g/mol

1.7. Aluminum Oxide (Al_2O_3)

Aluminum is the third element in the earth's crust, after oxygen and silicon . Aluminum turns into an intermediate or catalyst to spontaneously combine with oxygen, forming that thin film of oxide aluminum, which protects aluminum or allows it to be colored after anode oxidation, or forming aluminum metals such as (Bauxite), which gives, through the famous Bayer method , aluminum oxide (Al_2O_3) ، which ends either in aluminum metal and its alloys or in aluminum oxide ceramics, which appears in the form of a crystal single in a (ruby) gemstone, the first

polycrystalline ceramic material in which unique properties combine to attract diverse engineering applications[29-31].

Table (1.3): Some of Physical Properties of Al_2O_3 [30].

Al_2O_3	Properties
Hardness (Mohs)	9
Young coefficient (GPa)	300-400
Specific heat (J/kg.K)	900
Melting temperature (°C)	2050
Molecular Weight	101.96 g/mol

1.7.1. Aluminum Oxide Applications

The importance of alumina stems from its use as a raw material for the extraction of aluminum metal, as a raw material for the manufacture of a wide range of advanced and traditional ceramic products, and as an active agent in various chemical industries. used more than 90% of the alumina produced globally is in aluminum production. However, this number does not detract from the uses and applications of this material itself in the industry, as the global consumption of alumina is estimated at more than 4 million tons in material applications, and its many applications are related to its abundance, its relatively low production cost, and its outstanding characteristics mentioned above. These applications include the following[32-35]:

A- Insulating Material (Electrical Insulator) :

1. Very high frequency applications (UHV), such as television, transmission tubes, or transmitters in collectors.
2. Microwave generators for heating .

B- Electronics :

1. Passive elements such as internal or interstitial links , resistors and capacitors .
2. Manufacture of hybrid circuit substrates and substrates or computer chips .

C- Military Applications :

1. Armor manufacturing and plating .
2. Bulletproof vests .

D - Medical and Biological Applications :

1. Orthopedic surgery artificial joint replacements.
2. Dental implants and dental restoration .
3. Manufacture of tubes or medical tools and equipment .

E – Enameling :

1. Coating of sheet metal in home appliances structures .
2. Painting ceramic tiles for floors and walls .
3. Oxidation and wear resistant coating on metal sheets .

F - Refractory Uses :

1. Manufacture of refractory bricks for lining furnaces .
2. high-temperature cements .
3. Metal casting moulds .

1.8. Literature Survey

1- **Khudheir A. Mishjil**, (2003) [36], has prepared a thin films of Al2O3 by chemical spray pyrolysis method and studied the optical properties and dc conductivity, the results showed that the film have a direct electronic transition allowed and forbidden of energy gap and have two activation energy for dc conductivity (0.00255 eV and 0.527 eV).

2- **Abeer K. J. Al-Azawee** (2006) [37] , The effect of annealing (450) was studied on the optical and structural properties of Al_2O_3 films prepared by thermal chemical spray method. The X-ray diffraction results showed that the films are polycrystalline and that the annealing increases the prohibited energy gap values.

3- **SA. Mahmoud *et al.* (2011)** [38], where the effect of varying substrate temperatures on the optical structural properties of NiO films was studied, and nickel acetate was deposited from a 0.05 M solution in ethanol. sedimentation time was 15 seconds and spray time was 3 minutes. The spray nozzle height is fixed at 35 cm. Moreover to obtain a homogeneous film, the spraying rate was kept at 15 cm^3/min. For temperature measurements, a thermocouple was used. At a low substratum temperature of 225 °C, the XRD model presented amorphous films. .

4- **Caglar and Yakuphanoglu**, (2009) [39] pure and doped cadmium oxide films with aluminum in proportions (1.3%) on glass bases. The examination by X-ray diffraction revealed that all the prepared films were pure and doped with aluminum it has a polycrystalline crystalline structure, with a preference for growth in the direction (111) for all as for the optical properties, they were studied by both percentage transmittance and reflectance spectroscopy. Percentage

as a function of wavelength within the range (300-700 nm), and the results of visual examinations showed that the optical energy gap value of pure cadmium oxide films increases with increasing percentages

5- **Y. Zhao *et al.* (2014)**[40], showed the effect of partial oxygen pressure on the properties of NiO films was investigated, the XRD patterns show that when the partial oxygen pressure drops from 80% to 0%, the strength of the (200) peak decreases.

6- **M. Jlassi *et al.* (2014)** [41], NiO film was prepared at different annealing temperatures using the sol gel method. The XRD study shows that there were polycrystalline structures in all annealed films. Meanwhile a single large unstructured XRD line is shown in as-deposited films. It was possible to find a prevailing peak corresponding to (200). As the annealing temperature decreased from 600 to 300 ^{o}C, the intensity of this peak decreased. On the other hand, as the annealing temperature rises, it is clear that all the films display high clarity in the visible and near infrared sections. This results in films with strong transmission for that purpose.

7- **M. Vigneshkumar *et al.* (2016)**[42], Focus on the antireflection coating for NiO thin films in solar cells. NiO films were deposited on glass substrate using a 0.5 M aqueous solution from nickel chloride of a temperature at 350 °C, A reflectance of 7% was obtained of 550 nm. This low value gives an indication that it can be used as an antireflection coating material in solar cells. The refractive index was recorded at 550 nm to be 1.871. Calculated optical direct band gap energy from the prepared NiO thin film was found to be 3.25 eV.

8- **AA. Yadav, and U. Chavan. (2016)**[43], studied effect of substrate temperature on various physical and electrochemical

properties of NiO thin films. This was done by using nickel chloride precursor spray deposition of NiO thin films. The thin films were deposited at 425 °C, 450 °C, 475 °C and 500 °C temperatures. Cubic polycrystalline nickel oxide confirmed the structural analysis. The surface morphology showed a porous surface with randomly formed heaps that were inhomogeneous. It was found that optical band gap energy was in the range of 3.04-3.28 eV. The electrical resistivity confirms NiO semiconducting behavior with energies of activation at room temperature of 0.30 to 0.38 eV.

9- **R. O. Ijeh *et al.* (2019)** [44], prepared nickel oxide (NiO) thin films with p-type Cu doped (5 a%) using a sol–gel solution process and investigated their structural, optical, and electrical characteristics by X-ray diffraction (XRD), optical transmittance and current–voltage (I–V) characteristics. The crystallinity of the NiO films improved with the addition of Cu dopants, and the grain size increased from 38 nm (non-doped) to 50 nm (Cu-doped). The transmission of the Cu-doped NiO film decreased slightly in the visible wavelength region, and the absorption edge of the film red-shifted with the addition of the Cu dopant. Therefore, the width of the optical band gap of the Cu-doped NiO film decreased as compared to that of the nondoped NiO film.

10- **Zaid M. J. Zwaid (2021)** [45], Studied Preparation and Characterization of (NiO:Cu/Si) Solar Cell by Aerosol Assisted Chemical Vapor Deposition. This was done by using the spray deposition of a nickel chloride precursor of NiO thin films. Thin films were deposited and doped with copper. Cubic nickel oxide polycrystalline confirmed the structural analysis. The surface morphology showed a porous surface with randomly formed

heterogeneous piles. It was found that the optical bandgap energy was in the range of 3.5–2.8 eV. The electrical resistivity confirms the semiconducting behavior of NiO.

1.9. Aims of the Work

The aims of this work can be summarized in the following points :

1- Study of structural , optical and electrical properties of $NiCl_2$:Al_2O_3 thin film on glass substrate by chemical thermal spray technique .

2- Study the effect of temperature (350 ºC) on the thin film in terms of structural , optical and electrical propertie.

3- Crystallization processes improved the properties by adding aluminum oxide with nickel chloride and cohesion and its applications in the medical field (dental filling).

2.1. Introduction

This chapter includes a general description of the side of the theoretical to the subject of current study the concept of nanotechnology and its importance , fundamental difference between the material in general bulk material and nanoscale material . It also includes a theoretical description of structure , morphological ,optical and electrical properties and their scientific explanation , mathematical relation and laws .

2.2. Nanomaterials

Nanomaterials are defined as materials with size in the range of (1 to 100) nm at least in one of the three dimensions. Because of this very small size scale, they possess a massive surface area per unit volume, ahigh proportion of atoms in the surface and near surface layers, and the ability to exhibit quantum effects. The resulting unique properties of nanomaterials cannot be anticipated from a simple extrapolation of the properties of bulk materials [46] . The nanomaterials have the following two features; activation of particle surface and increasing the surface area [47].

Figure (2.1) shows the two approaches. Attrition or milling is a typical top-down method in making nanomaterials, whereas chemical thermal spray technology method is a good example of bottom-up [48,49].

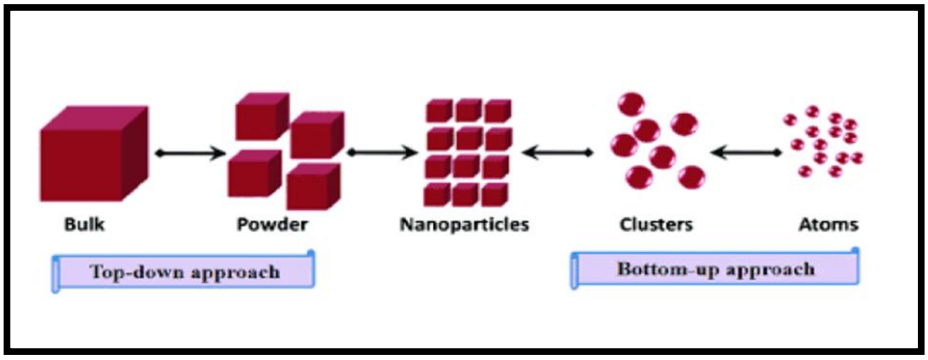

Fig (2.1) : Schematic representation of the 'bottom up' and 'top down' synthesis represents processes of nanomaterials [5٠]

2.2.1. Classification of Nanostructures

There are different classifications of nanostructures in nanotechnology. Nanostructures usually categorized by their geometrical properties. Nanostructures usually consist of nanocages, nanobelts, nanocrystallites, nanoneedles, nanoflowers, nanofabrics, nanofibers, nanoflakes, nanocomposites, nanofoams, nanomeshes, nanopin films, nanopillars, nanoparticles, nanorings, nanorods, nanoclusters, nanopowders, nanoshells, nanowires, nanotubes, quantum hetero structures, quantum dots and sculptured thin films [51]. Classifying nanostructures according to their dimensions is the most favorite mode of their classification.

The shape (dimensionality) of their microstructural constituents (boundary regions and crystallites, Depending on the chemical composition of the crystallites, the three categories of (Nano Structure Material) NSM may be grouped into four families; Figure (2.2) [52]. Nanostructures can be described as zero- (0D), one- (1D), two- (2D), and three-dimensional (3D) nanomaterials as shown in Figure (2.3) [53].

0D- all dimensions (x,y,z) at nanomatric scale. Example : Nanoparticles

1D- tow dimensions (x,y) at nanomatric scale one other dimension (L) is not. Example : Nanorods, Nanotubes

2D- one dimension (t) at nanomatric scale tow other dimensions (Lx,Ly) are not. Example : Thin nanofilms

3D- all of three dimensions (Lx, Ly, Lz) are not at nanomatric scale. Example : Nanocrystalline and nanocomposite material [52-54].

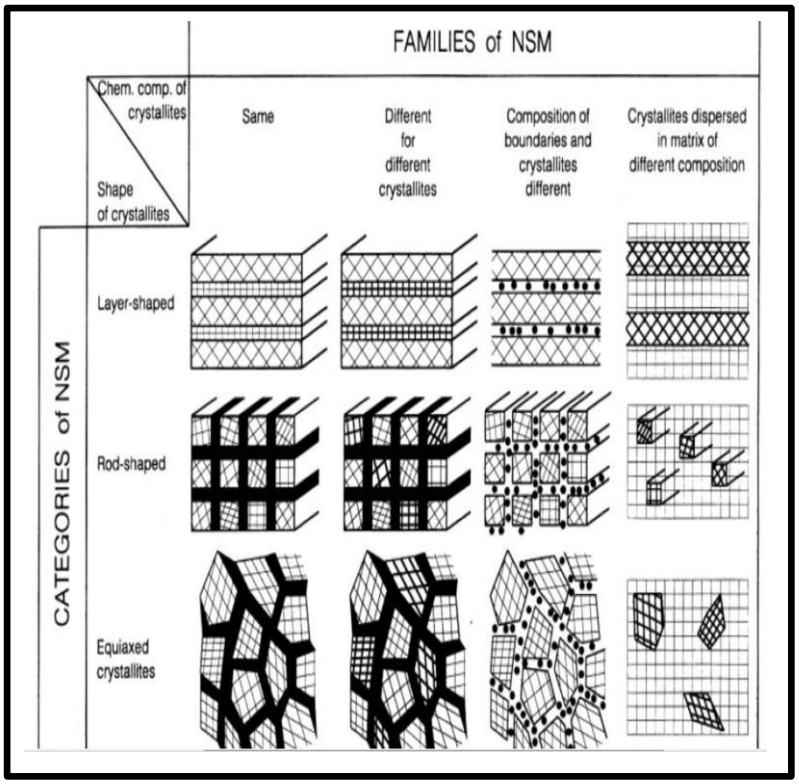

Fig: (2.2) Classification schemas for nanostructured material according to their chemical composition and the dimensionality (shape) of the crystallites (structural elements) forming the NsM. [46].

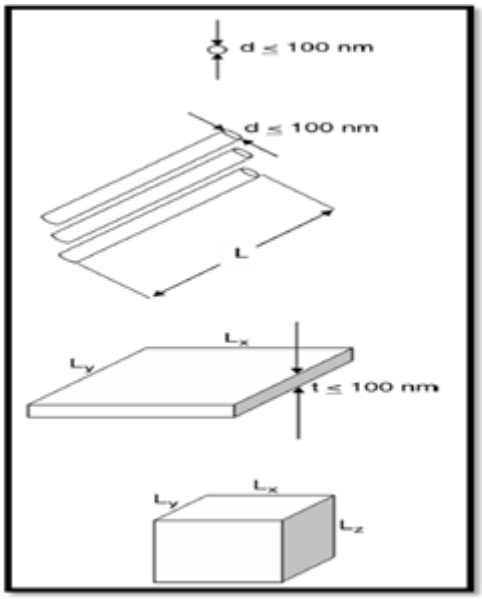

Fig: (2.3) Classification of nanostructures according to 0-D, 1-D, 2-D, and 3-D [51].

Dimensions of 0D nanostructures are in the nanometric size range (such as nanoparticles or well-separated nanopowders). 1D nanostructures have a dimension that is outside the nanometric size range.

These 1D nanostructures have a rod shape, and form of nanotubes, nanorods, nanowires and nanoneedles. The 2D nanostructures have two dimensions outside of the nanometric size range. Hence, these 2D nanostructures indicate plane-like structures, and consist of thin films, nanolayers and nanocoatings. The 3D nanostructures have three dimensions big side of the nanometric size range. These bulk 3D nanostructures form of many various kinds themselves, and usually include nanocrystalline units that show the influenced properties of nanoscale due to the size effect.

A 3D nanostructure can include different distributions of nanoparticles or nanocrystallites, groups of nanowiresand nanotubes, and also different nanolayers. 0D, 1D, 2D and 3D nanostructures can be amorphous or nanocrystalline. The 2D and 3D nanostructures may also be categorized in more details. The simplest shape of a 2D nanostructure is a plane with a depth below 100 nm and other dimensions are bigger than nanometric dimensions. In spite of its external dimensions, this plan can show interior nanostructural dimensions, for example, nanocrystals (or nano grains) with nanoscale dimension. This 2D nano-crystalline layer can show some new size-related properties different from those of a microcrystalline layer. If the external thickness leaved in the nanometric size range, the inside grains (crystallites) can be outside of the nanoscale and yet still classified as a nanostructured matter. So the insider structural dimensions (for crystallites or grains) and outsider surface dimensions (exclusively its depth) can be in the nanometricsize range, and this difference will divide the 2D nanostructures as interior nanostructured and non-internal nanostructured layers [55].

The dimensions of 3-D nanostructures will not be located in any nanometric size range but they still show such size-influenced properties. For example, 3D nanocomposites can be gained with two or more phases

with various properties and their total synergistic properties cannot be obtained by each phase alone. The matrix of the nanocomposite has dimensions bigger than nanometric scale and the amplifying material is generally at the nanometric size range. These 3D nanostructures can be categorized by the type of amplifying phases, for example, nanoparticles, nanoflakes, nanotubes or nanorods.

The 3D nanostructure may be microcrystalline or nanocrystalline in its inside structure, such as mentioned for 2D nanostructures. Table (2.1) which shows the general figures and different classes of nanostructures with their dimensionality [55].The position of nanostructures in engineering materials can also be seen in Figure (2.4) [52]. The overlapping regions in this figure are related to binary and tertiary nanomaterials. The areas of zones covered by the triangle of nanostructures cannot be compared with each other but the overall coverage of the different circles and the triangle show the position of nanostructures among engineering materials [52-56].

Table (2.1): General features and different classes of nanostructures [55].

Dimensionality	Separated	Surface Bulk
	Nano materials	
0 – D	Well – dispersed Nano crystalline Materials Nano powders thin layer	Nano crystalline
1 – D	Nano tube reinforced Nano composites	
2 – D	Nano rods and nanotubes Thin Nano films Nano layers	Nano connections

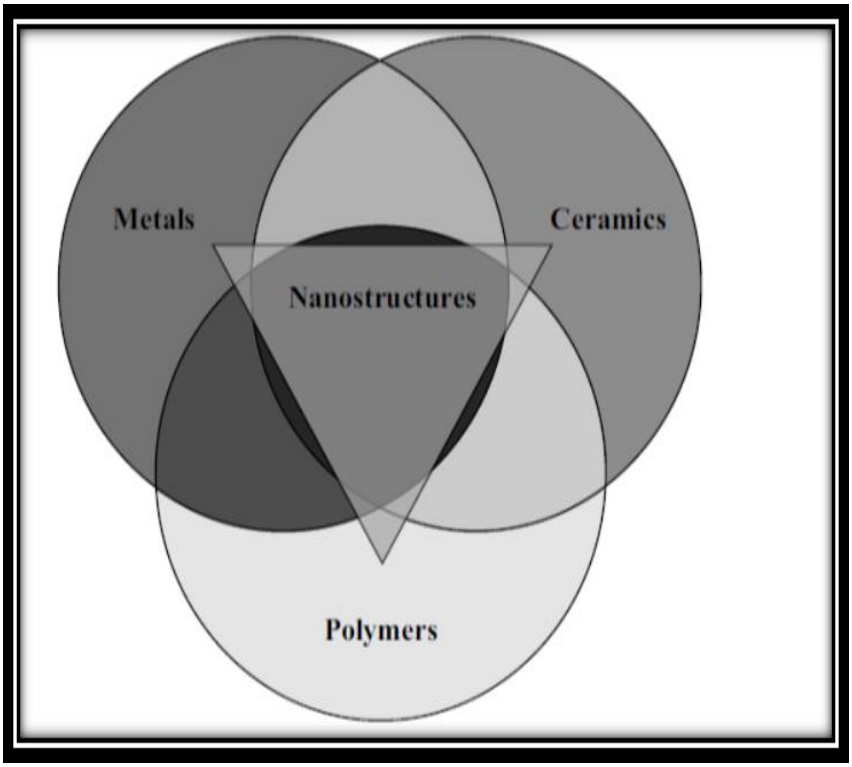

Fig: (2.4) Position of nanostructures in engineering materials (areas of covered surfaces are not Related to actual contributions) [52].

2.3. Thin Film Deposition Principle

For the purpose of depositing a thin film on the surface of a solid substrate, particles of the material forming the slide must pass through a carrier so that this medium is in direct contact with the substrate once the particles reach a surface . The substrate is a part of it that adheres to the surface by (van der waals) forces or reacts chemically with it [59] . These particles can be atoms, molecules or ions, and they may be the means of transporting materials to the substrate, either through materials (liquid, gaseous or in a vacuum) [57].

2.4. Methods for Preparing Thin Films

Membranes are prepared by physical and chemical methods, among which we briefly mention:

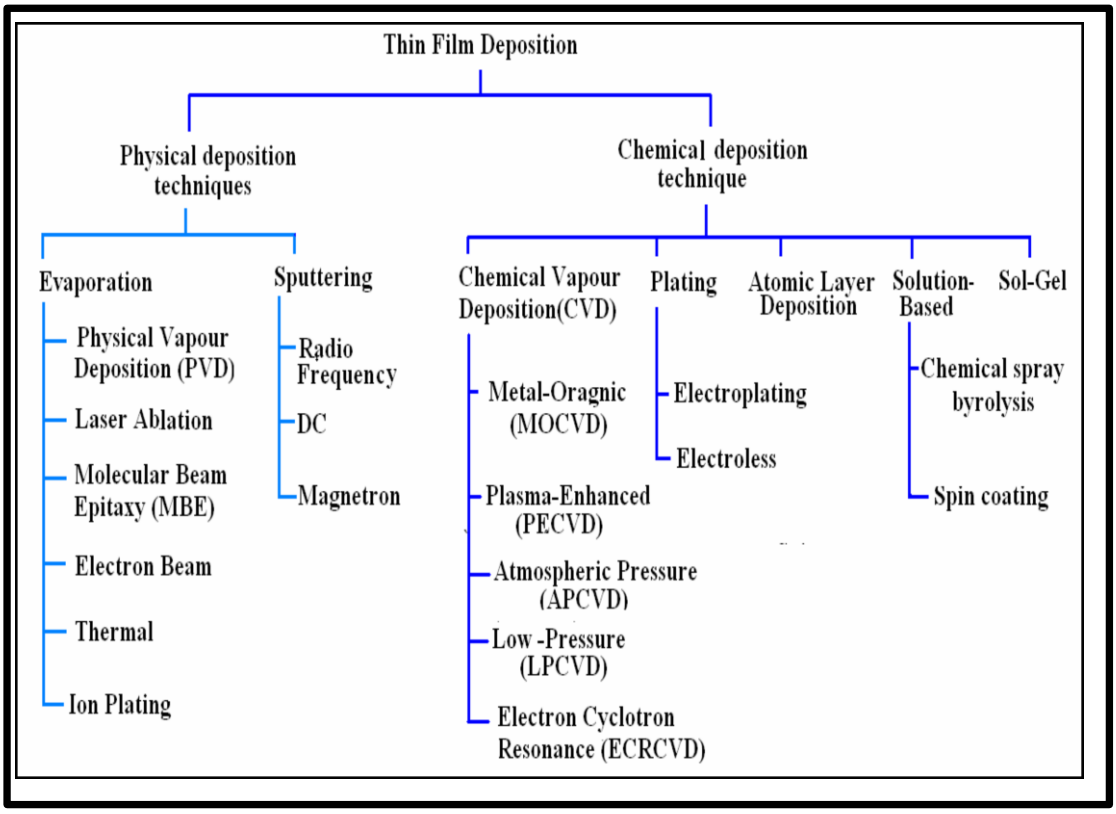

Fig (2.5) : The classifications of thin film deposition methods [58].

2.4.1. Chemical Methods

There are several chemical methods for the deposition of thin films will address here two methods chemical vapor deposition (CVD) and thermal chemical spraying .

2.4.1.1. Chemical Vapor Deposition (CVD)

This method is used to obtain pure thin films of metals, semiconductors and insulators from during the vaporization of a substance from a volatile compound (Volatile Compound) [59] . The vapor of the substance is reacted with gases or liquids or with other vapors on the base on which the film is to be deposited, and this reaction results in non-products volatile deposits gradually (atom by atom) on the base, forming a thin film [60] .

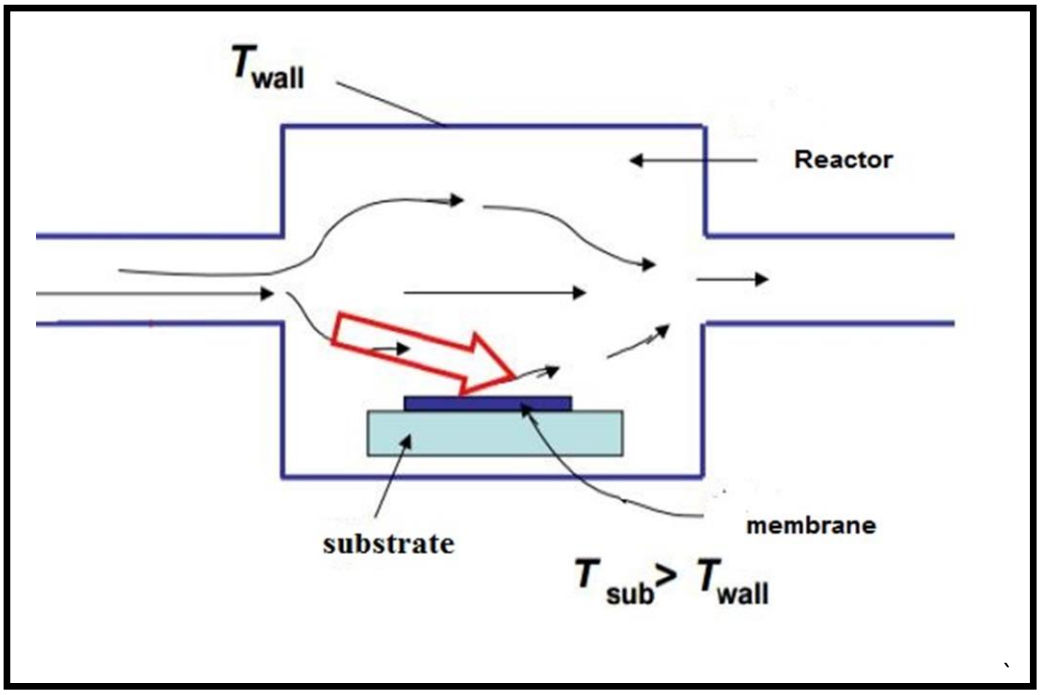

Fig (2.6) :Diagram showing thin-film vapor deposition[61].

2.4.1.2. Thermal Chemical Spraying (CSP)

This is the method used in our research, this technique is one of the chemical methods, and it was developed during the sixties of the last century due to the urgent need for a less expensive technology to prepare large area devices in the photovoltaic industries. Thin films of inorganic sulfides and cyanides have been prepared by hydrolysis on a hot base. The first to use this method were the two researchers (Auger & Hotle) in the year 1959, where they intended to do by preparing a black copper film on an aluminum base using a selective surface [62]

Only chemical solutions are used, i.e. the powder of the substance cannot be precipitated directly or using alloys. This technique depends on spraying the material to be deposited in the form of a film on hot bases under a temperature (temperature certain) depending on the type of material used, a thermochemical reaction takes place between the atoms of the hot base material، as a result of this reaction, a thin film is formed .

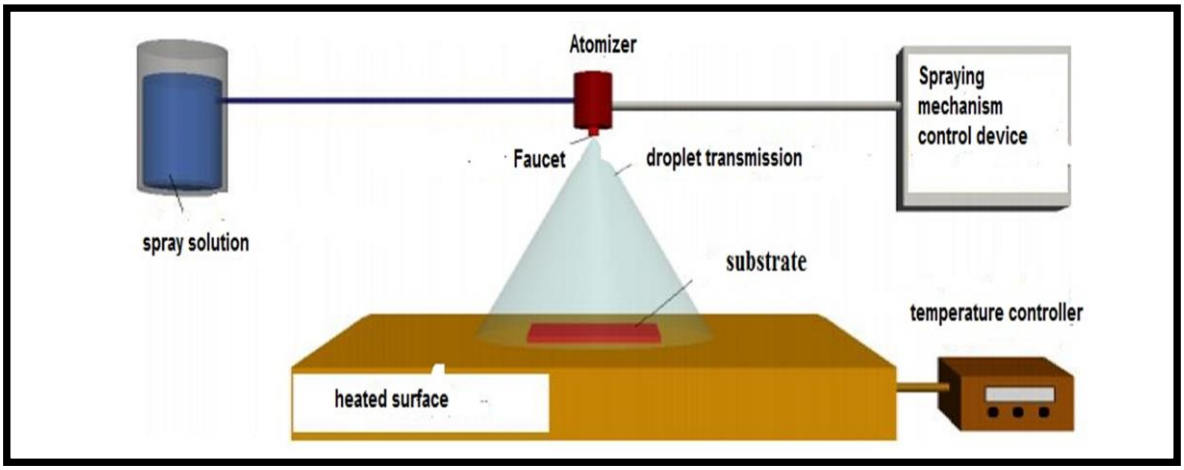

Fig (2.7) : Diagram showing the deposition process by spray pyrolysis [63]

2.5. Physical Properties of Thin Films

The physical properties of thin films vary with the diversity of the purpose for which the film was prepared and the diversity of research conducted . It is concerned with this field, so will focus studying the structural and optical properties of thin films.

2.5.1. Structural Properties

The structural properties of films are studied by several techniques, and X-ray diffraction (XRD) is one of the most reliable methods that were adopted in this research, so will explain it in some details [64].

2.5.1.1. X-Ray Diffraction(XRD)

X-ray is electromagnetic waves that result from the collision of high-energy accelerated electrons with the target material with a large atomic weight. They are radiation of relatively high energy. Its wavelength range ranges between (0. 1 - 10) nm, and this wavelength range means that it fulfills the condition that must be met for the transmittance of radiation from the material ($\lambda \leq 2d_{hkl}$) . Therefore it can be used in crystal diffraction technology [65].

The use of X-Ray diffraction is one of the effective and common techniques for studying the crystal structure of thin films that provides us with a lot of information about the unit cell. X-ray spectrometer is used to draw the diffraction spectrum of the subject materials - which records the intensity as a function of the angle change shown in Figure (2.8).

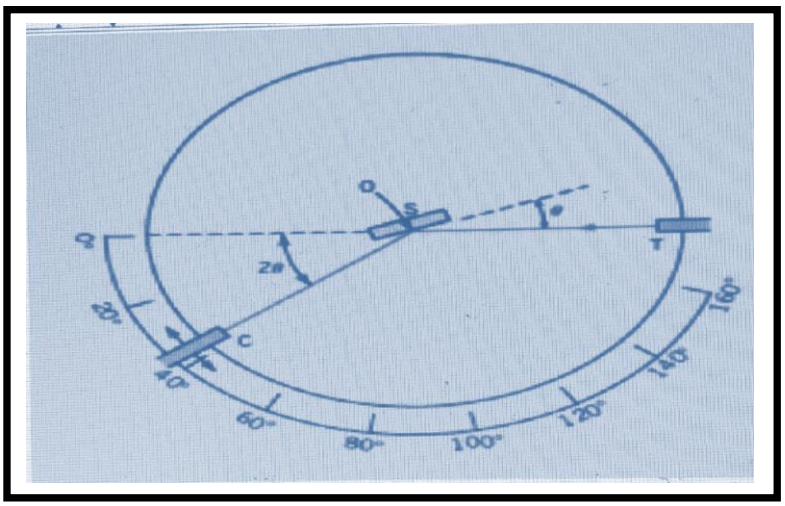

Fig (2.8) : Schematic diagram XRD [66].

In the above figure it shows , Detector (C) , sample (S) , X-ray source (T) , Rotation axis of sample and detector (O) .

The single-wavelength X-ray fall from the source (T) on the sample to be examined (S) at an angle of (θ), which represents the angle of incidence of the X-rays measured in degrees, and it is reflected at an angle of twice the angle of incidence time after time to record the readings starting from the value of the angle is zero down to the angle (160) degree, according to the need for this range.

This technology provides us with information about the locations of the characteristic peaks that represent the dominant crystal growth direction within the crystal lattice and the width of the middle of the greatest intensity level through which it is possible to obtain information about the grain

boundaries and thus know the growth in the grain size of the test sample [67].

2.5.1.2. The Distance Between the Surfaces (d_{hkl})

The device that was explained represents the mechanism through which the scientist (W. Bragg) was able to put his well-known law represented by the following equation (2-1) , and it is the same law that enables us to calculate the value of the interfacial surfaces shown in the figure of the equation [68] .

$$n\lambda = 2d_{hkl} \sin\theta \qquad (2\text{-}1)$$

Where (n) is an integer that indicates the order of the reflection, (θ) represents the angle of incidence of the X-ray at the wavelength (λ), (hkl) Miller's coefficients (Miller index).

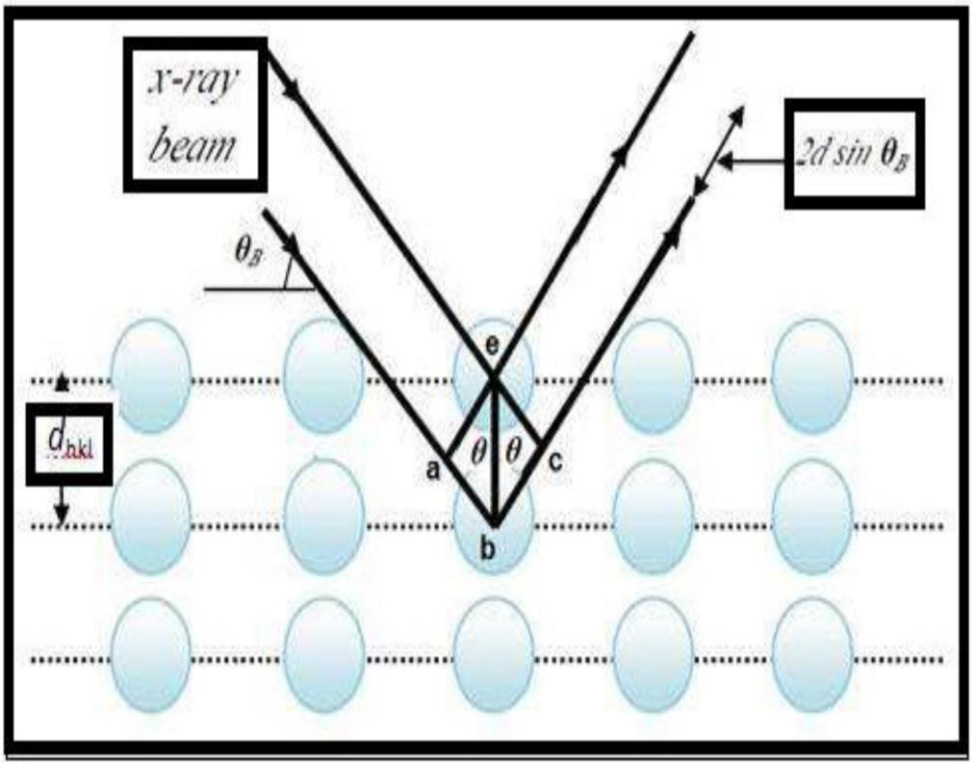

Fig (2.9) : represents the diffraction pattern , distance between the surfaces (d_{hkl})and lattice constant [69] .

2.5.1.3. Grain Size (G.S)

The information provided by the obtained diffraction pattern, we can find from it the rate at which the crystals grew inside the crystal lattice, we find the average grain size by adopting (Scherer's equation), then we can find the exposure amount of the characteristic peaks (β) depending on the width of the middle of the peak (FWHM) measured in radial units(rad), the granular size is measured in units (nm) according to the equation (2-2) [69 , 70].

$$\mathbf{G.S = (0.94\ \lambda) / \beta_{FWHM} .\cos\theta} \qquad \mathbf{(2\text{-}2)}$$

So (β_{FWHM}) is the width of the curve at the midpoint of the vertex (FWHM) and (θ) is the Bragg angle.

2.5.1.4. Dislocation Density (δ)

This term is given to the number of lines in which the dislocation appears within the crystal structure of the substance within the unit area, measured by the unit (m^2), which is an indicator of the quality of the crystal structure and can be found from the relation (2-3)[71] .

$$\mathbf{\delta = 1 / (G.S)^2} \qquad \mathbf{(2\text{-}3)}$$

2.5.1.5. Crystals Films Number (N_o)

It is the number of grains within a unit volume measured in units (m^3) and can be directed from the relation (2-4): [72].

$$\mathbf{N_o = t / (G.S)^3} \qquad \mathbf{(2\text{-}4)}$$

Where (t) represents the thickness of the membrane measured in units (cm^3).

2.5.1.2 Scanning Electron Microscopy (SEM)

The scanning electron microscope (SEM) uses a focused beam of high-energy electrons to generate a variety of signals at the surface of solid specimens. The signals that derive from electron reveal information about the sample including external morphology (texture), chemical composition, and crystalline structure and orientation of materials making up the sample. In most applications, data are collected over a selected area of the surface of the sample, and a 2-dimensional image is generated that displays spatial variations in these properties. Areas ranging from approximately (1) cm to (5) microns in width can be imaged in a scanning mode using conventional SEM techniques (magnification ranging from (20) X to approximately (30,000) X, spatial resolution of (50 to 100) nm). The SEM is also capable of performing analyses of selected point locations on the sample; this approach is especially useful in qualitatively or semi-quantitatively determining chemical compositions (using EDS), crystalline structure, and crystal orientations (using EBSD).

Accelerated electrons in an SEM carry significant amounts of kinetic energy, and this energy is dissipated as a variety of signals produced by electron-sample interactions when the incident electrons are decelerated in the solid sample. These signals include secondary electrons (that produce SEM images), backscattered electrons (BSE), diffracted backscattered electrons (EBSD that are used to determine crystal structures and orientations of minerals), photons (characteristic X-rays that are used for elemental analysis and continuum X-rays), visible light (cathodoluminescence--CL), and heat.

Secondary electrons and backscattered electrons figure (2.10) are commonly used for imaging samples: secondary electrons are most valuable

for showing morphology and topography on samples and backscattered electrons are most valuable for illustrating contrasts in composition in multiphase samples (i.e. for rapid phase discrimination SEM analysis is considered to be "non-destructive"; that is, X-rays generated by electron interactions do not lead to volume loss of the sample, so it is possible to analyze the same materials repeatedly [٧3].

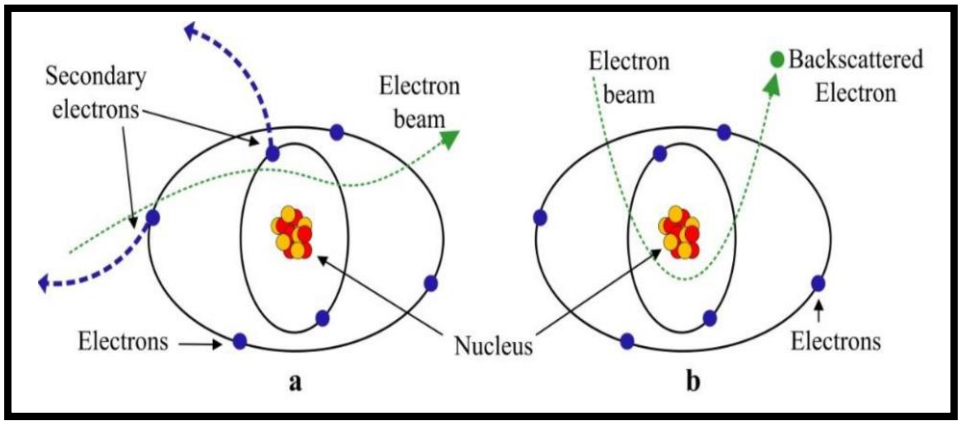

Fig (2.10): Secondary and backscattered electrons [74].

2.5.1.3. Atomic Force Microscopy (AFM)

The atomic force microscopy AFM is a mechanical imaging instrument that measures the three dimensional topography as well as physical properties of a surface with a sharpened probe. The sharpened probe is positioned close enough to the surface such that it can interact with the force fields associated with the surface. Then the probe is scanned across the surface such that the forces between the probe remain constant [75]. An image of the surface is then reconstructed by monitoring the precise motion of the probe as it is scanned over the surface. Typically, the probe is scanned in a raster-like pattern. AFM analyses in order to find the average grain size and surface topography at atomic scale of the samples [76].

2.5.2. Optical Properties

To study the optical properties of thin films is of great importance in finding the optical constants through which it is possible to identify the amount of the optical energy gap according to the specific preparation conditions (pressure, temperature, thickness of the film, etc.), as well as can know the other constants of absorbance and transmittance and their coefficients and the inertia coefficient and the real and imaginary dielectric coefficients [77].

In our research, used this optical spectrometer (UV-VIS Spectrophotometer / 2700 ,UK) which records the absorbance as a function of the wavelength within the range (290- 1100 nm).

2.5.2.1. Optical Absorption (A)

It is one of the important and highly effective studies in the field of semiconductor and membrane physics. The fall of electromagnetic ray with an energy (hυ) greater than the value of the energy gap and intensity (I_o) on the material whose thickness (t) will absorb part of it to run out of the intensity of (I_t), this we can find the relationship by which we calculate the absorption coefficient (α) according to the equation [72,78].

$$\mathbf{I_t = I_0}\, e^{(-\alpha t)} \qquad \textbf{(2-5)}$$

Since (α) is the optical absorption coefficient measured in the unit (cm^{-1}), which is the percentage of the decrease in the incident radiant energy and it changes according to the change in the wavelength of the incident rays and the nature of the material on which it falls, this process excites an electron in the valence band, moving it to the conduction band, releasing energy (hυ – E_g) as in Figure (2.11 a). But if the value of this energy is equal to the value of the prepared energy gap (E_g), then this energy will be absorbed by the material that fell on it, generating a pair (electron-hall) as in the

figure (2.11 b) and these two transitions represent the class of self-transfer (Intrinsic) from the valence beam to the conduction beam (Band to Band)

But in the case of the energy of these rays is less than the value of the prepared energy gap, the local levels within the prepared gap that can be found by crystalline physical defects will be the local levels to which the electron can move in this case and this is represented by the self-transfer (Extrinsic) which is shown in the figure (2.11 c) [79] .

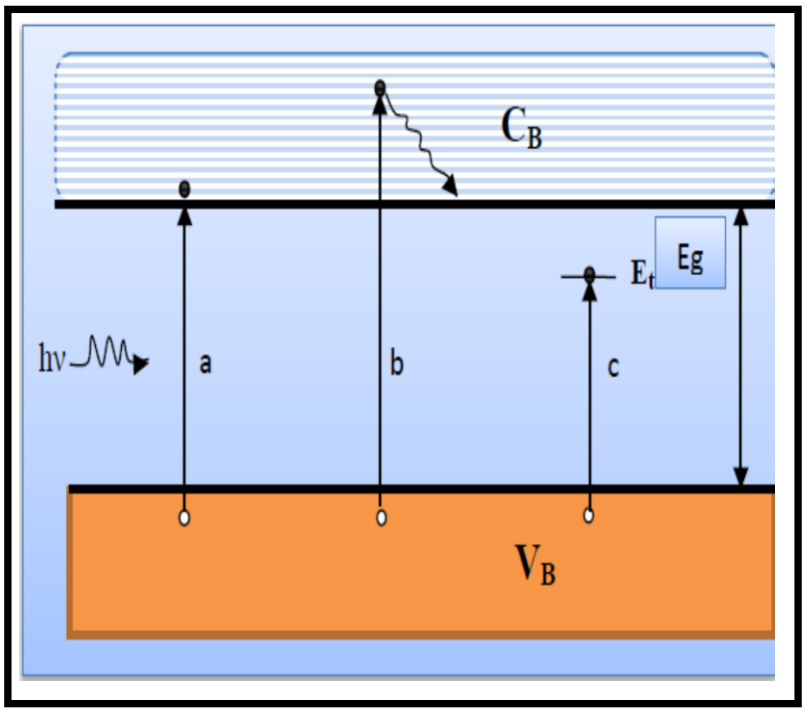

Fig (2.11) : Transfers Intrinsic and Extrinsic in semiconductors [79] .

2.5.2.2. Transmittance (T)

The transmittance represents the amount of radiant energy falling on the thin film after the radiation falls on it, and it can be found from the equation(2-6): [79] .

$$T = 10^{-A} \qquad (2\text{-}6)$$

2.5.2.3. Reflectance (R)

Reflectance represents the amount of radiant energy falling on the thin film to the medium from which it was provided, and its amount can be found from the equation (2-7): [80] .

R = 1 – T – A **(2-7)**

2.5.2.4. Absorption Edge

The amount of radiant energy that the photons fall on the material varies. In the case that this amount reaches a value equal to the width of the forbidden energy gap of the semiconductor material, the amount that the material will absorb will increase significantly, and this characteristic is shared by almost all semiconducting materials[81].

This magnitude, which starts with a rapid increase in absorption, is called the optical absorption edge, and the wavelength at which the absorption edge is formed is called cutoff wavelength .

Figure (2.12) shows that the amount of absorption at the wavelength less and more than the cut-off wavelength is little. As the absorption edge is distinguished when drawing the spectrum of the absorption coefficient as a function of the energy of the incident rays or the wavelength of these rays in the form of a distinctive linear cut-off edge that appears relatively wide in the case of polycrystalline semiconductors and sharp in monocrystalline semiconductors[٨1].

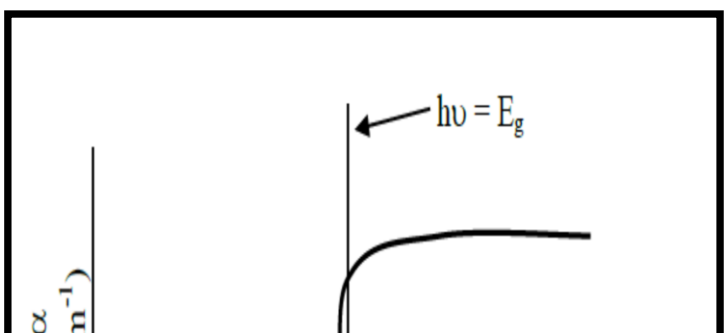

Fig (2.12) : The amount of the absorption coefficient before, after and then the absorption edge[82].

2.5.2.5. Optical Constants Values

Optical constants are one of the important functions, which by knowing their values can determine the applications of semiconducting materials or the optimal use of the thin film. These constants are:

2.5.2.5.A. Optical Absorption Coefficient (α)

It is defined as the percentage that decreases from the radiation energy falling on the material relative to the distance it traveled in the direction of propagation of this wave inside the semiconducting material. The calculation of this ratio depends on the energy of the incident rays (hv) and on the optical properties of the semiconducting material such as the amount of energy gap width of the semiconducting material and the type of electronic transition that occurs between the valence band and the conduction band [73].

To calculate the absorption coefficient, we start by calculating the photon energy of the incident rays from the equation (2-8) [77].

$$E = h\upsilon \qquad (2\text{-}8)$$

And the amount of this energy permeated (T) through the semiconductor material will reflect some of it (R), so the permeable part is given according to the equation (2-9) [77]

$$T = (1 - R)^2 e^{-\alpha t} \qquad (2\text{-}9)$$

In order to calculate how much material absorbs (A) of these rays, the equation is based [77]

$$T = e^{-2.303\,A} \qquad (2\text{-}10)$$

Now we substitute the value of (T) from equation (2-9) into equation (2-10) and we get the equation :

$$e^{-2.303\,A} = (1\text{-}R)^2 e^{-\alpha t} \qquad (2\text{-}11)$$

In the event that the amount of what is absorbed by the substance and the amount of what is permeated from it is approximately one, that is, the amount of what is reflected by the substance is close to zero, then the equation (2-11) will become in the form:

$$e^{-2.303\,A} = e^{-\alpha t} \qquad (2\text{-}12)$$

From it we can find the value of the absorption negligible (**α**) from the equation:

$$\alpha = 2.303\,(A / t) \qquad (2\text{-}13)$$

2.5.2.5.B. Optical Energy Gap

The energy gap of semiconducting materials is the amount of energy needed to move an electron from the valence band to the bottom of the conduction band or the local plane closest to the transition. The width of this gap is affected by the percentage of impurities added to the semiconductor material[83].

The energy gap value of the permissible and forbidden direct transmission and the permissible and forbidden indirect transmission is calculated from the experimental Tauss equation as follows [77] :

$$\alpha h\upsilon = B (h\upsilon - E_g^{opt})^r \qquad (2\text{-}14)$$

Where (B) represents the transfer constant , if the transfer is of a direct or indirect type, then its value is one. As for the value of the constant (r), it takes the values (1/2) in the case of permissible direct transmission, and takes the value (3/2) in the case of prohibited direct transmission, and takes the values (2) and (3) in the case of permissible and prohibited indirect transmission, respectively , as shown in the figure (2.13).

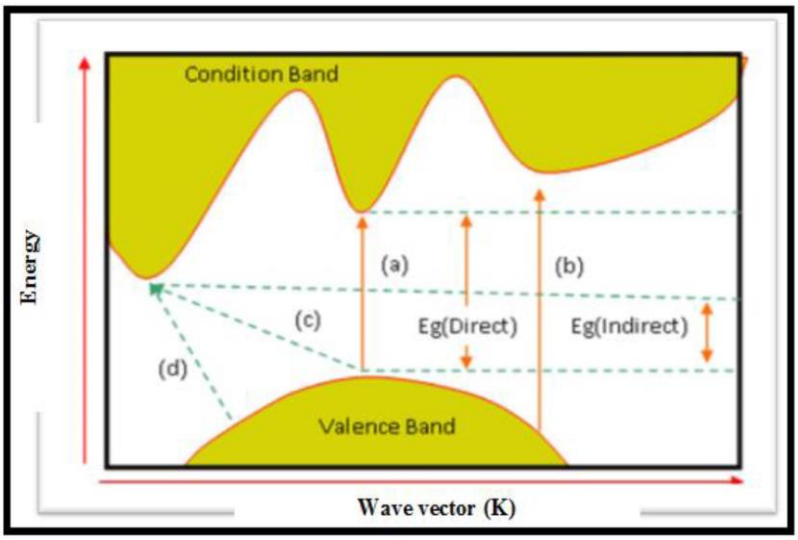

Fig (2.13) : Electronic transfers [84].

A graphic relation is drawn between the energy of the incident photons (hυ) for the x-axis and the amount $(\alpha h\upsilon)^{1/r}$ for the y-axis, and the amount

of the energy gap is determined by dropping a tangent line of the resulting curve in the direction of the x-axis and interrupts it at the point $(\alpha h\upsilon)^{1/r} = 0$ and this point represents the value of the energy gap[84].

2.5.2.5.C. Refractive Index (n)

A term given to designating the ratio between the speed of light in a vacuum to its speed in any other material medium, and it can be found depending on the value of the inertia constant (K) and the value of the reflectivity of the film (R). Its value will be according to the equation (2-15): [85]

$$\mathbf{n = \left[\left(\frac{1+R}{1-R}\right)^2 - (K^2+1)\right]^{1/2} + \frac{1+R}{1-R}} \qquad \mathbf{(2\text{-}15)}$$

2.5.2.5.D. Extinction Coefficient (K)

That is, the amount of electron energy put out from the incident rays or the attenuation in the energy of the incident rays, and it depends on the value of wavelength of the incident wave and on the value of the absorption coefficient (α) for each material and is calculated from the relation (2-16) : [85]

$$\mathbf{K = \alpha\lambda / 4\pi} \qquad \mathbf{(2\text{-}16)}$$

2.5.2.5.E. Dielectric Constant (ε)

The fall of electromagnetic rays on the material leads to the interaction of these rays with the charges of the falling material, which polarizes and absorbs a certain amount of the incident energy, which is usually called the dielectric constant of the material (ε), which is given by the relation (2-17) : [85].

$$\varepsilon = \varepsilon_r - \varepsilon_i \qquad (2\text{-}17)$$

Where (ε_r) the real part of the dielectric constant and (ε_i) the imaginary part of the dielectric constant

The real part of the dielectric constant (ε_r), which expresses the polarization of the medium regardless of the value of the energy lost as a result of light falling on it, is related to the value of the refractive index (n) and the damping coefficient (K) according to the equation (2-18):[85].

$$\varepsilon_r = n^2 - K^2 \qquad (2\text{-}18)$$

The imaginary part of the dielectric constant represents a measure of the absorption of the energy of the incident radiation from the atoms of the material and it is also related to the refractive index and the damping factor from us in the equation (2-19):[85].

$$\varepsilon_i = 2nK \qquad (2\text{-}19)$$

2.5.3. Electrical Properties

The semiconductor materials are insulator material at (0K) temperature, but they can be conductor materials when the temperature increases to the limit values that converted to increase in conducted electron density. Therefore, the material can be classified according to the values of its electrical conductivity into three types : conductor ($\sigma = 10^3$-10^8) S/m, Semiconductor ($\sigma = 10^3 - 10^{-8}$) S/m, and Insulator ($\sigma = 10^{-8}$-10^{-18}) S/m [86].

The electrical properties measurement of semiconductor thin films allows the determination of the impurity levels present in the materials these parameters are critical to their utilization in various electronic and optoelectronic applications. The electrical properties depend upon the

nature of semiconductor, if they are pure , doped and crystalline or amorphous [87] . According to Ohm's law the current (I) (in amperes) in a sample is proportional directly to the potential difference (V) (in Volts) across two points on this sample [88].

$$R=V/I \qquad (2\text{-}20)$$

Where (R) is the sample resistance measured in Ohms.

Electrical resistivity (also known as resistivity, specific electrical resistance, or volume resistivity) is an intrinsic property that quantifies how strongly a given material opposes the flow of electric current. A low resistivity indicates a material that readily allows the movement of electric charge. Resistivity is commonly represented by the Greek letter ρel. (rho). The (SI) unit system of the electrical resistivity is the Ohm multiplies by meter (Ω·m) although other units like (Ω·cm) are also in use [86].

Consider that the current passes through a peace of material with length (l) (m) and a cross section area (A) (m^2). The electrical resistivity (ρ) can be defined as [88].

$$\rho=R\,A/l \qquad (2\text{-}21)$$

Electrical conductivity or specific conductance is the reciprocal of electrical resistivity and measures a material's ability to conduct an electric current. Electrical conductivity or specific conductance is the reciprocal of electrical resistivity and measures a material's ability to conduct an electric current.It is commonly represented by the Greek letter (σ) (sigma), but (κ) (kappa) (especially in electrical engineering) or (γ) (gamma) are also occasionally used. Its (SI) unit is Siemens per meter (S/m)[86].

Where conductivity (σ), is the inverse of the resistivity (ρ) [88].

2.5.3.1. Current-Voltage (I-V) Characteristics

The current-voltage (I-V) characteristics in heterojunction are influenced by various mechanisms depending on the band discontinuities at the interface and the density of interface states. For e.g. if the barrier to holes is much higher than that for electrons, then the current will consist almost entirely of electrons; or if the density of interface states is very high then the dominant current will be generation-recombination current from the interface. The dominant current can also be due to tunneling if the barrier width is very thin, or to thermionic emission if the interface acts as a metal-semiconductor contact [87, 89].

2.5.3.1.1 Electrical Conductivity

It is a criterion for the extent to which the medium is able to move the electric charge through it, and it is symbolized by the symbol (σ), and it is measured in unit s of $(\Omega.cm)^{-1}$, it is the inverse of the resistivity(ρ) and it can be calculated through the following equation [90] :

Slope = I / V

R= 1 / slope

ρ = R × 0.000035

$$\sigma = 1/\rho \qquad (2\text{-}22)$$

where : R : Resistance

ρ : resistivity

σ : Conductivity

3.1. Introduction

This chapter includes a description of the deposition system by thermal chemical spray method, the process of preparing membranes, and the practical steps that were conducted in this research, starting with the process of preparing samples and conducting the sedimentation process, and then conducting structural, optical and electrical measurements, as shown in the following diagram(3.1).

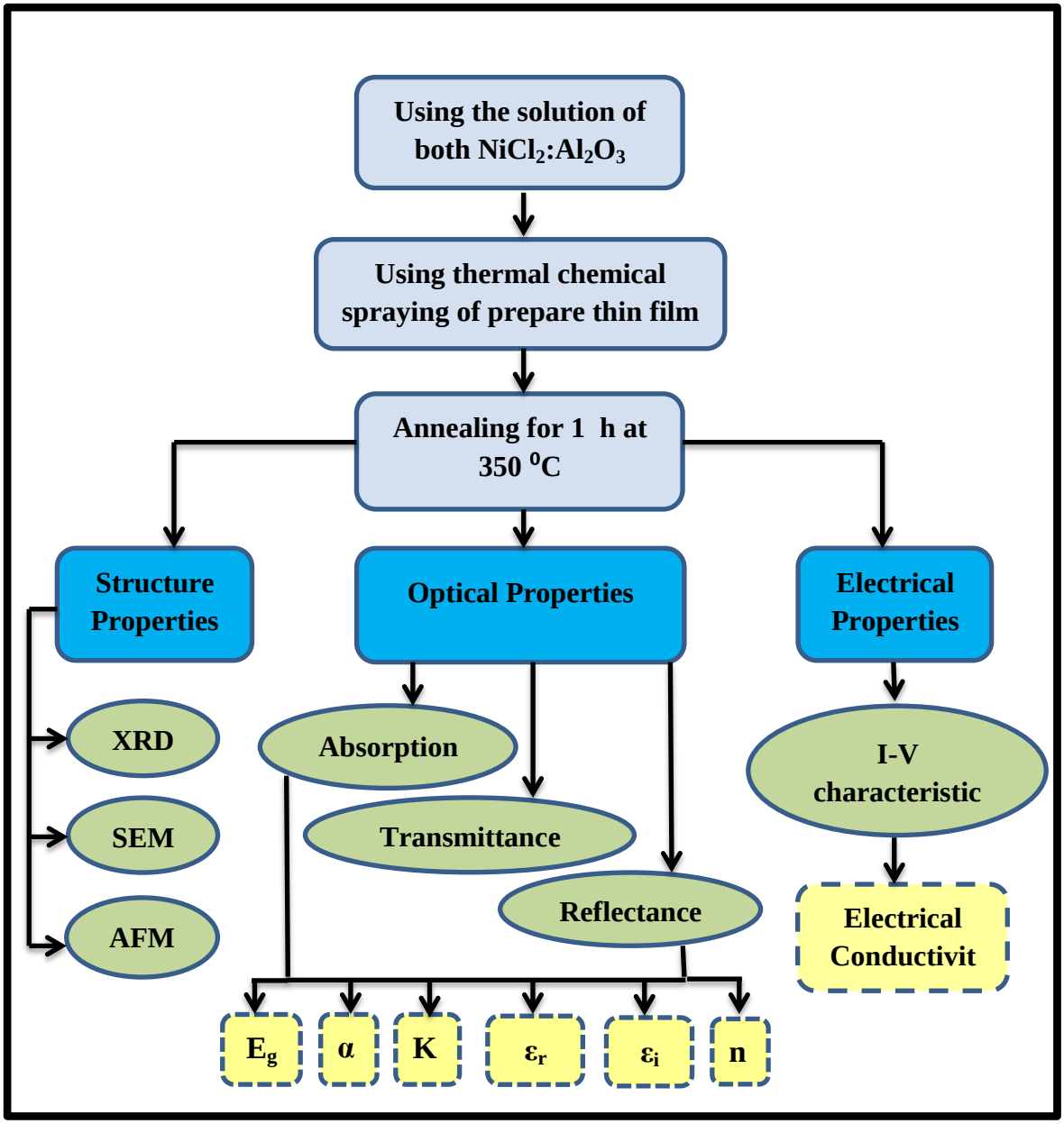

Fig(3.1) : Schematic diagram of the experimental .

3.2. Preparing the Solution

Prepared of the films ($NiCl_2$) hexahydrate nickel chloride was used, which is a substance in the form of green salts with an equivalent weight 58.693 g / mol and a purity of 99% supplied by College of Chemistry Sciences, also, doping aluminum oxide with an equivalent weight 101.96 g / mol was used, which is a white powder with purity 99% supplied by the Euphrates Spring Company also was to deposited the thin films of thickness (45-62 ± 6) nm. To find the weight of the material used in the reaction, we use the following equation:

$$\mathbf{M = W_t / M_{wt} \times 1000 / v} \qquad \mathbf{(3\text{-}1)}$$

Where M : The molar concentration is 0.1

W_t : Material weight

M_{wt} : Molecular weight

V : Volume of distilled water (100ml)

Where used 2.9 g of nickel chloride was dissolved in 100 ml of distilled water using a hotplate stirrer for 14 min at a temperature of 50 ^{0}C Celsius, and the dissolution was good .

Fig (3.2) : Nickel Chloride before

It is also melted 5 g of aluminum oxide (Al_2O_3) in (100 g) of distilled water using a hotplate stirrer for 30 min minutes at a temperature of 50 degree Celsius but the dissolution was not complete as there was plankton present in the solution, and for the purpose of dissolving completely and quickly, drops of dilute hydrochloric acid (HCl) were added for the purpose of dissolving the bonds of chlorides present in the solution the final solution is filtered with filter paper.

Fig (3.3) : Aluminum Oxide of powder.

Table (3.1) : Show the concentrations taken from Al_2O_3 added to $NiCl_2$ to obtain the proportions needed for the preparation.

Sample	$NiCl_2$ (ml)	Al_2O_3 (ml)	Deposition time (min)	Temp.	Annealing
$NiCl_2$	5	0	9	150 ºC	All samples are annealed for 1 hour at 350 ºC
$NiCl_2$:Al_2O_3	5	1	9	150 ºC	
$NiCl_2$:Al_2O_3	5	2	9	150 ºC	
$NiCl_2$:Al_2O_3	5	3	9	150 ºC	

3.3. Glass Substrate Preparation

To study the structural and optical properties of the prepared films, glass slides with dimensions (7.6 × 2.6 × 0.1) cm^3 were used, fixed on the upper base of the system.

The glass slides were cleaned in two stages. In the first stage, ethanol alcohol was used to dissolve the fat that may be present on the surface of the glass. In the second stage, the glass slides were immersed in distilled water for ten minutes then it was dried.

3.4. Thermal Chemical Spraying System

The thermochemical precipitation system consists of the following parts :

1- Sprayer Nozzle

2- Iron bearer

3- Electrical heater

4- Thermocouple

5- Digital counter

6- Air pump

7- Preparation room

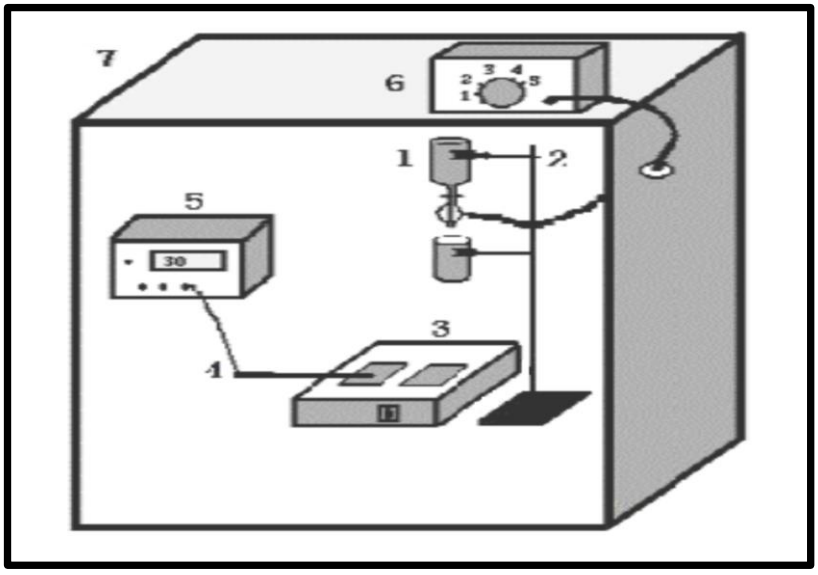

Fig(3.4) : The thermal chemical deposition system used in the work[91].

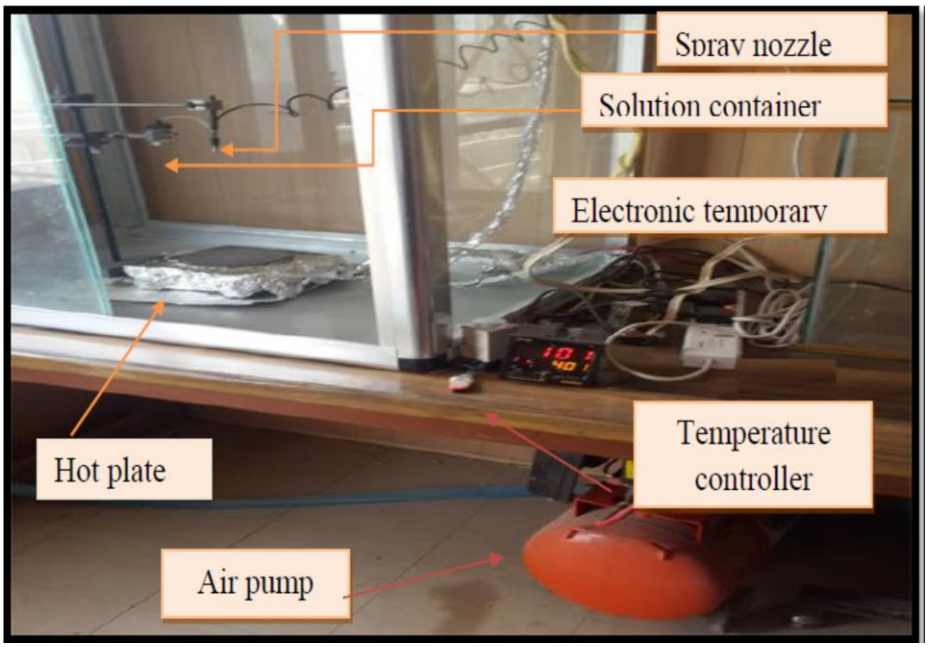

`Figure (3.5): Chemical Spray Pyrolysis System.

3.4.1. Sprayer Nozzle

This device was made locally from ordinary glass. It contains a cylindrical tank with a capacity of 100 ml, open from the top, with a radius of 1.5 cm and a height of 8 cm. Its diameter is (1 mm), the capillary tube is surrounded by a bulging glass chamber closed from the top because it is connected to the outer edge of the capillary tube and open from the bottom and the opening of the glass chamber surrounds the opening of the capillary tube so that the two holes are concentric and at one level, the glass chamber contains a side opening that allows the passage of compressed air inside it, which causes a pressure disturbance inside the glass chamber, leading to the conversion of the drop coming from the capillary tube into a spray in the form of a cone towards the glass base on which the film is to be deposited, as shown in Figure (3.6). The holder is used it is necessary to control the height of the spraying device from the surface of the electric heater, as well as the position of the spraying device (the angle of falling of the spray on the glass base), as it must be controlled the end of the capillary tube from which the solution

comes out should be perpendicular to the base on throuh the film is to be deposited.

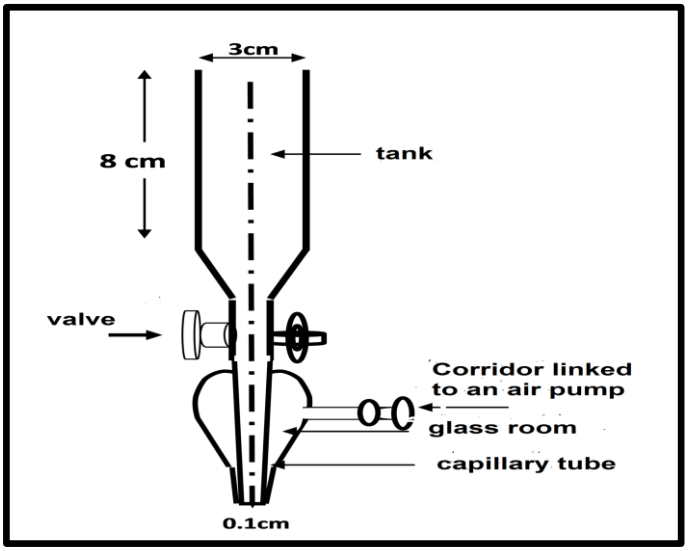

Fig (3.6) : Schematic diagram of the Sprayer Nozzle [92].

3.4.2. Electrical Heater

An electric heater (homemade) is used to control the temperature of the glass base on which the film is to be deposited .

3.4.3. Thermocouple

Use a thermocouple to measure the temperature of the heater and the glass bases used. The thermocouple consists of a sensitive thermocouple placed on the surface of the glass base. The thermocouple is connected to a digital counter that records the temperature in degrees Celsius.

3.4.4. Air Pump

In order to control the air entering the sprayer, a pump was used, as this pump pushes compressed air into the glass chamber through the side opening in the glass chamber, through the connection of the pump with the sprayer through a rubber tube, which pushes the solution The drop from the capillary tube onto the surface of the glass base in the form of a fine mist.

3.5. Factors Affecting Thin Film Preparation

There are several factors to consider while preparing the films, namely :

1- Base Temperature

Some of the previous studies that used the thermochemical deposition method agree on the value of the temperature between (673-773K) to obtain the required film, and it was found that the best film we get is at a temperature of (773K), which is close to many previous studies.

2- Deposition Rate

The sedimentation rate affects the homogeneity of the membrane, as it was found that the best sedimentation rate from which we obtain homogeneous films is ($10cm^3$/min), and this rate is controlled by the valve in the sedimentation device.

3- Deposition of Point Distance

It means the vertical distance between the glass base and the end of the capillary tube, and it was found that the best homogeneous membrane we get at a height of (30 ± 1 cm) approximately, in which the spray of the solution is not collected in one spot and is not volatile away from the glass base.

4- Deposition Time

The deposition time used is (10s) only to avoid sudden cooling of the bases, which leads to cracks in the glass base, and after the deposition process is followed by a pause of (3 min) to ensure the return of the temperature of the base to its original value and to complete the crystal

growth process, and this process is repeated several times until obtaining to the required thickness.

5- Air Pressure

The compressed air must be inside the glass chamber in a way that makes the solution in the form of a fine mist so as not to cause the glass base to cool and break, as the air pressure inside the glass chamber was fixed in the spraying device when preparing all membranes within 105N/m^2 to obtain a homogeneous film for the material prepared.

3.6. Structural Measurements

After completing the deposition process, we select a number of membranes that are homogeneous and free from gaps and apparent defects to conduct structural tests to know the crystal structure of the films prepared using X-ray diffraction technique.

3.6.1. X-Ray Diffraction Measurements (XRD)

X-ray diffraction (XRD) analysis shown in Figure (3.7) is used to determine the crystal structure of thin films. The source of radiation is Cu (k) with wavelength (=1.54060), current (30) mA, and voltage (40) kV in the (X-ray) diffractometer type (PW1730 Philips) made in (USA). At University of Tehran, Iran.

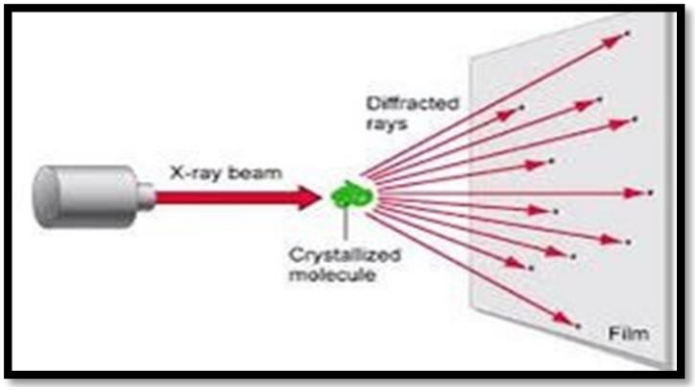

Fig (3.7): Diagram for X-ray diffraction (XRD) [93].

Measure

Axis : Theta – 2 Theta

Scan Mode : Continuous Scan

Range : 30-80 (deg)

Step : 0.0500 (deg)

Speed : 5.0000 (deg/min)

3.7. Surface Morphology Measurements

For the purpose of examining the surfaces of the thin films, they were photographed using:

3.7.1. Scanning Electron Microscopy (SEM)

Field emission scanning electron microscope with energy-dispersive X-ray spectroscopy (SEM) shown in Figure (3.٨) was used in this research. The SEM type (Mira3) is Made in the Czech Republic. The energy dispersive X-ray at University of Tehran, Iran.

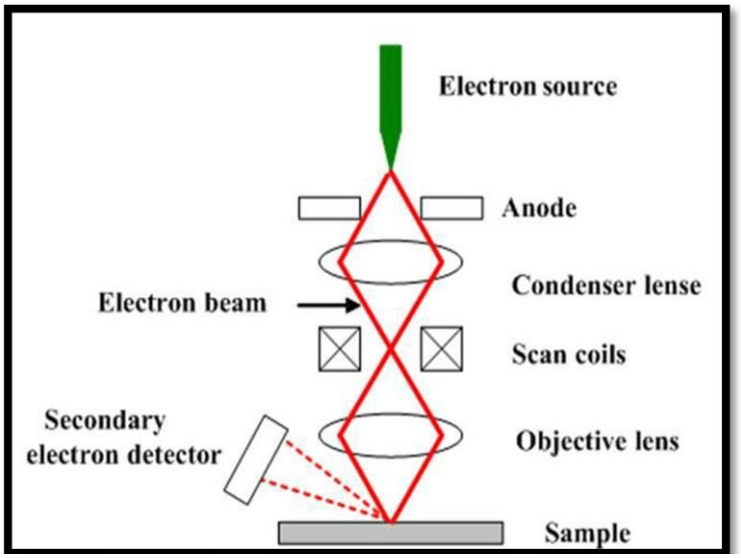

Fig (3.8):Diagram for Scanning electron microscopy (SEM)[94].

3.7.2. Atomic Force Microscopy (AFM)

The atomic force microscope provides us with three-dimensional images with a capacity of one million times magnification, through which the homogeneity of the membrane and its nanostructure are identified. This device consists of a needle with micro dimensions that passes over the surface to be scanned. This carrier and on the surface to be scanned, a laser beam falls on the carrier, which rises and falls with the rise and fall of the needle, and thus the surface topography varies from high and low. The laser beam is captured on the carrier by a special receiver, then the topography of the scanned surface is determined and drawn according to the movement of the reflex of the laser beam. This device also gives us information about the surface roughness and the granular size of the film. Examined at the University of Tehran, Iran.

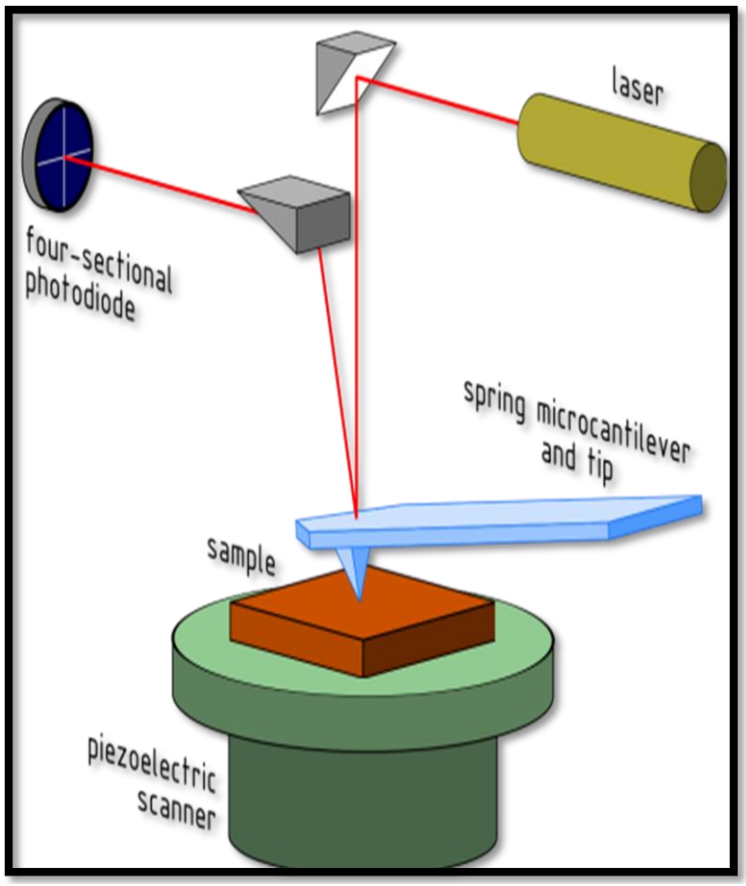

Fig (3.9): Diagram for atomic force microscope (AFM) [94].

3.8. Optical Measurement

A spectrometer of the type (UV-VIS-NIR-Double Beam Spectrometer) from (Perkin Elmere) company was used with two beams of light placed in the path of one of them the glass plate on which the film is deposited and the measurements are to be made for it, while the reference is placed in the path of the second beam which is a non-deposited glass plate Accordingly, measurements were made for pure, doped and annealed ($NiCl_2$) films within a range of wavelengths (1100-200 nm). Examined Advanced Polymer Lab / Department of Physics / College of Science / University of Babylon .

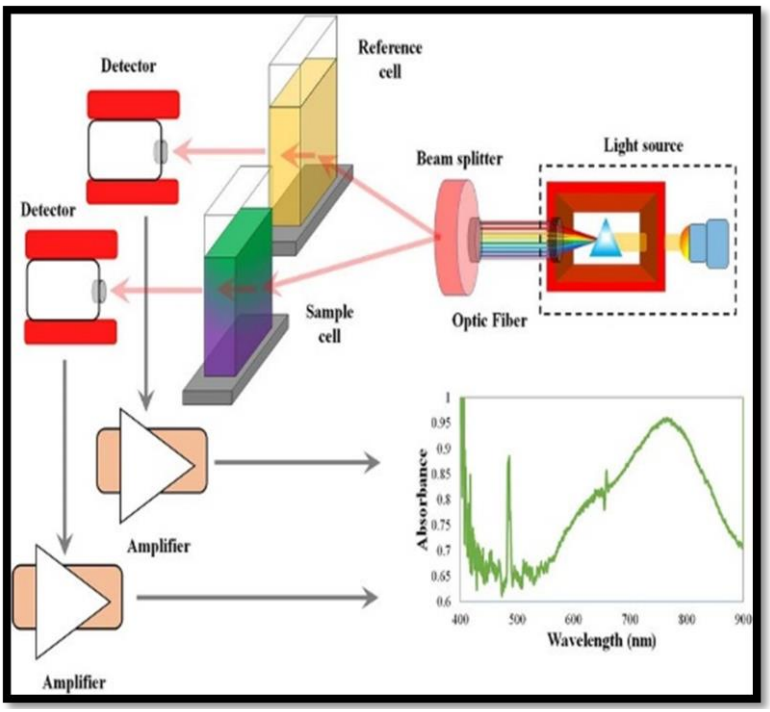

Fig (3.10): Diagram for UV Spectrophotometer [95] .

3.8.1 Absorption Coefficient Calculation

The absorption coefficient is one of the important physical coefficients through which the basic absorption edge and the energy gap can be identified. The absorption coefficient is calculated from the relation (2-11).

3.8.2. Calculate the Energy Gap

The value of the direct energy gap allowed for (NiCl2) films has been calculated using the relation (8-2) by drawing a curve between (αhν)2 and the photon energy (hυ), where the value of the energy gap can be found by extending the straight part of the relation curve to cut the x-axis at Photon energy values, where the point of intersection represents the value of the energy gap.

3.8.3. Calculation of Optical Constants

The optical properties of materials are usually described by optical constants that include the passivity coefficient, the refractive index, and the dielectric constant in both its real and imaginary parts, which were calculated by applying equations (2-13), (2-14), (2-15) and (2-16) respectively, where it is possible to identify the type of optical applications appropriate to the material under study.

2.9. Electrical Measurements

2.9.1. I-V Measurements

The system shown in Figure (3.11) was used to deposit gold electrodes on both sides of the substrate ($NiCl_2$ / $NiCl_2$: Al_2O_3) with a carrier density (5 × 1015 cm^{-3}) and in a direction using the spraying technique of the type (CRESSINGTON-108) for the purpose of studying the current-voltage characteristics of the circuit diagram The electric current shown in Figure (3.12) consisting of a device (DEGETAL MULTIMTER) of the type (DEGETAL MULTIMTER) AUTO - RANGE DMM for the purpose of measuring current and voltage, and through current, voltage and graphs, inclination, resistance, resistivity and conductivity are extracted. These

measurements were made at room temperature 300 K and the surface area of the samples was (4 x 4) mm^2.

Fig (3.11) : Electrode deposition system by sputtering technic

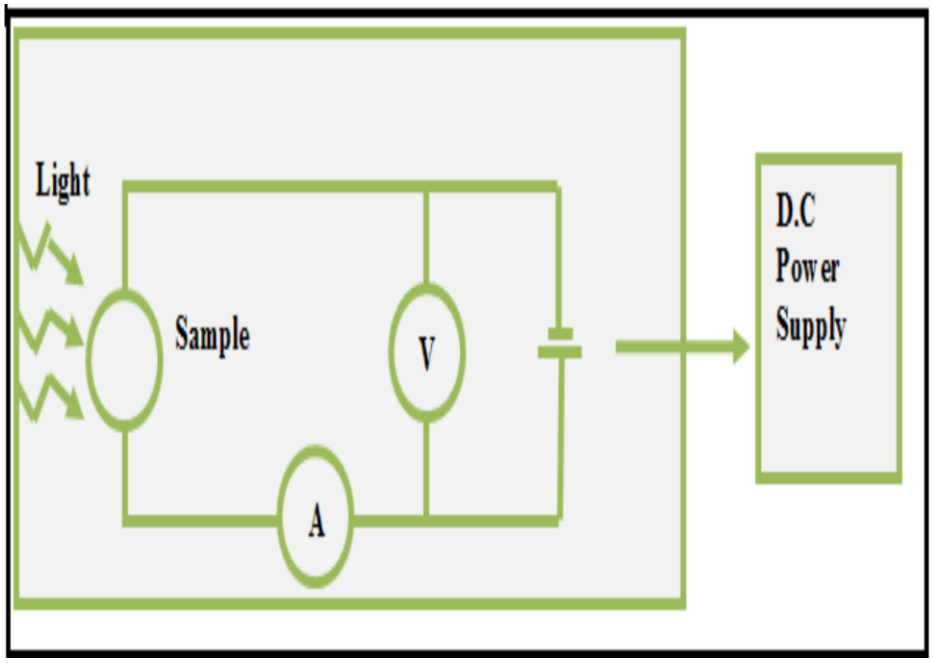

Fig (3.12) : Circuit diagram for measuring current-voltage characteristics.

4.1. Introduction

This chapter reviews the results obtained from studying the structural and optical properties of ($NiCl_2$) films pure and doped with aluminum oxide (Al_2O_3) in percentages (1,2,3)% and annealed at 350 °C prepared by thermal chemical spraying and discuss and compare them in light of the researches and studies available in this field, with a presentation of our conclusions and proposals that we reached after completion. from research .

4.2. Structural Properties

The synthesized $NiCl_2$:Al_2O_3 thin films are characterized by X-Ray Diffraction (XRD) , Atomic Force Microscopy (AFM) and Scanning Electron Microscopy (SEM) .

4.2.1. X-ray Diffraction Investigations

The importance of this measurement lies in knowing the crystal structure of the materials and showing the phases of the deposited materials and the nature of the arrangement the atoms in them and their orientation . Figure (4.1) represents the X-ray diffraction diagram of the pure $NiCl_2$ film, and it is noticed that there are diffraction peaks corresponding to levels (111), (241), and (222), and when comparing these results with (ASTM) cards (American Standard of Testing Materials) numbered (03-065-0601) and as Shown in Table (4-1), the results were somewhat consistent. The highest peak occurs at $2\theta=32.944°$ which is referred to (111) as a proffered plane. The positions of the peaks and the presence of more than one diffraction peak lead to the conclusion that the films are polycrystalline with an orthorhombic crystalline structure.

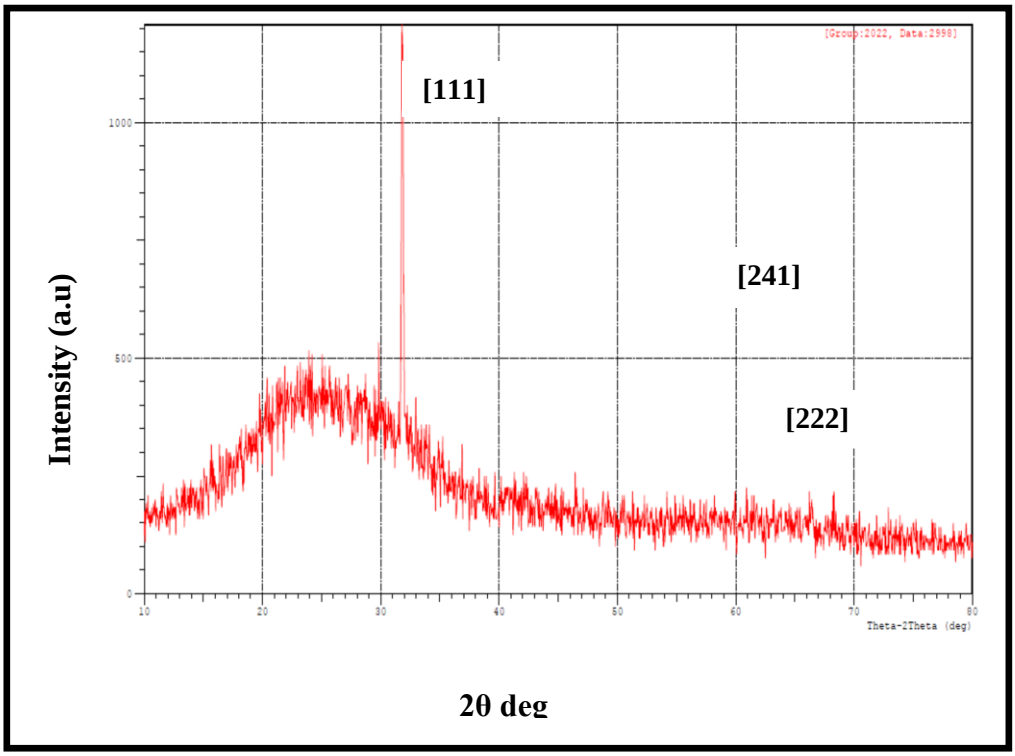

Figure (4.1) : X-ray diffraction of $NiCl_2$ thin film (pure) .

Table (4.1):X-ray Diffraction Screening Parameters for $NiCl_2$ films(pure).

No	2θ	hkl	d(Å)	G.S (nm)	FWHM	I %	a	Sys.
1	32.944	111	2.716	33.7	0.254	99	a=3.778 b=10.365 c=4.221	orthorhombic
2	64.908	241	1.435	35.1	0.254	5.8		
3	69.123	222	1.357	61.4	0.165	2.1		
				Av.=43.4	Av.=0.231			

noticed through Figures (4.2),(4.3) and (4.4) which represents the results of X-ray diffraction of ($NiCl_2$) films doped with (Al_2O_3), with different inoculation percentages (1,2,3)% with the appearance of atomic growth in the dominant and characteristic crystallographic directions (111) ,(241) , (222) , with a slight displacement in the locations of the peaks (2θ) which indicates that the grafted films were of polycrystalline structure and of type (orthorhombic) .

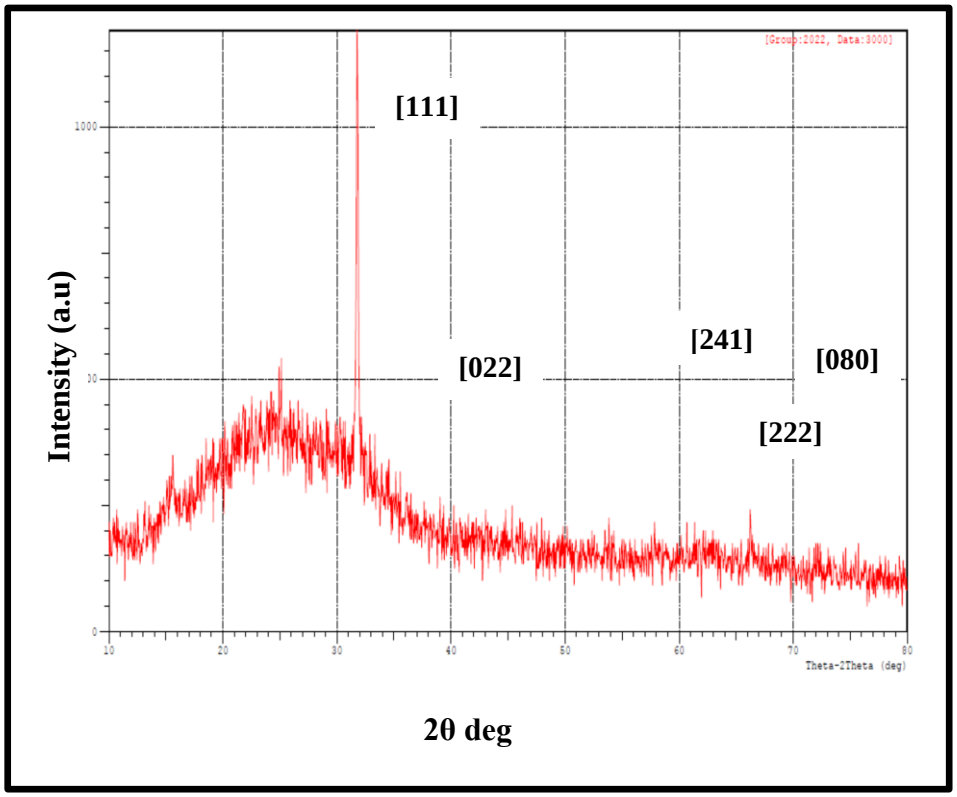

Fig (4.2) :X-ray diffraction of $NiCl_2$:Al_2O_3 thin film at 1% .

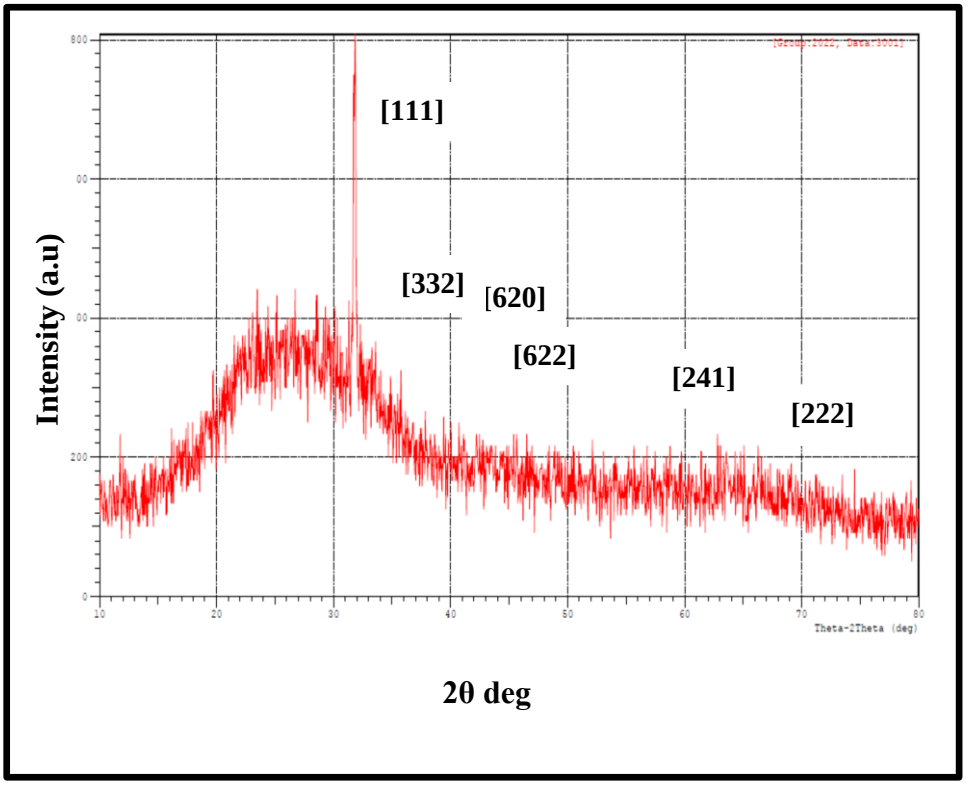

Figure (4.3): X-ray diffraction of $NiCl_2$:Al_2O_3 thin film at 2%.

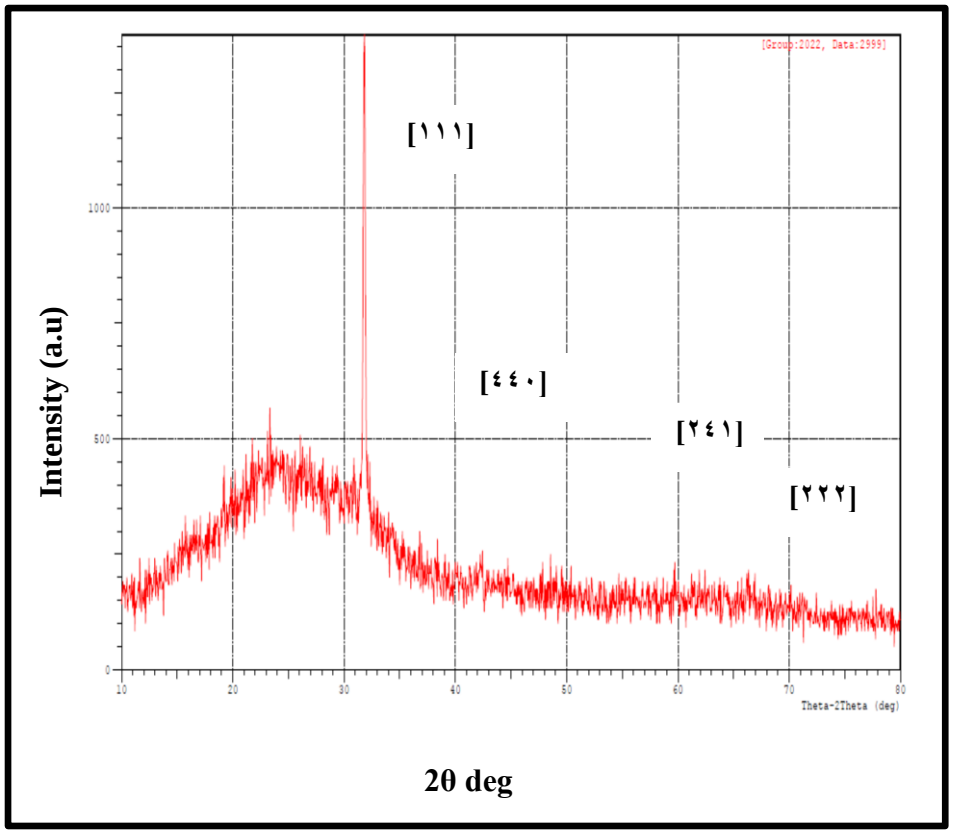

Figure (4.4): X-ray diffraction of $NiCl_2$:Al_2O_3 thin film at 3%.

It is noted that a noticeable change occurred in the intensity of the diffraction peaks for some levels after doping, so the intensity of the peaks decreased at the orientation (241), (222), and the intensity of the peaks increased at the orientation (111). The crystal structure, that is, there are some levels that are preferred for the growth of crystals, and this indicates that the crystallization process is improved by adding aluminum oxide (Al_2O_3) to the films ($NiCl_2$), and the best level for crystal growth is (111) , whose intensity is (I=99).This agree with refer [96].

Table (4.2): X-ray Diffraction Screening Parameters for $NiCl_2$:Al_2O_3 thin film at 1%.

No	2θ	hkl	d(Å)	G.S (nm)	FWHM	I %	a	Sys.
1	44.924	022	2.016	18.5	0.472	0.2	a=3.77 b=10.46 c=4.37	Orthorhombic
2	72.192	080	1.307	14.8	0.672	0.4		
3	32.944	111	2.716	43.8	0.197	99	a=3.778 b=10.365 c=4.221	Orthorhombic
4	64.908	241	1.435	35.1	0.276	5.8		
5	69.123	222	1.357	113.5	0.093	2.1		
				Av.=45.14	Av.=0.342			

Table (4.3): X-ray Diffraction Screening Parameters for $NiCl_2$:Al_2O_3 thin film at 2%.

No.	2θ	hkl	d(Å)	G.S (nm)	FWHM	I %	a	Sys.
1	46.107	620	1.967	59.5	0.135	0.1	a=b=c= 12.441	Cubic
2	48.498	622	1.875	9.3	0.945	0.3		
3	33.765	332	2.652	14.8	0.578	22		
4	32.944	111	2.726	43.8	0.197	98		
5	64.908	241	1.432	35.1	0.276	5.8		
6	69.123	222	1.354	113.5	0.093	2.2		
				Av.=46	Av.=0.370			

Table (4.4): X-ray Diffraction Screening Parameters for $NiCl_2$:Al_2O_3 thin film at 3%.

No.	2θ	hkl	d(Å)	G.S (nm)	FWHM	I %	a	Sys.
1	40.964	440	48.7	48.7	0.128	6.5	a=b=c= 12.433	Cubic
2	32.944	111	2.716	43.8	0.197	98	a=3.778 b=10.365 c=4.221	Orthorhombic
3	64.908	241	1.436	35.1	0.276	5.8		
4	69.123	222	1.315	113.5	0.093	2.2		
				Av.=60.275	Av.=0.187			

When annealing, noticed that an increase in the width of the middle, and this leads to a decrease in the particle size with an increase in temperature, which, as shown in the figures.

temperature leads to a decrease in the secondary levels, in addition to an increase in the crystallization of the membrane, and also the membrane becomes more regular and crystalline defects decrease and increase also the sharpness of the peaks, and this is due to the increase in crystallinity and regularity that occurs in the thin film, and that the increase in the height of the peaks when the base temperature is increased is attributed to the fact that the heat works to reduce crystal defects by giving the atoms of the material potential energy to rearrange themselves in the crystal lattice. This agree with refers [٩6,97].

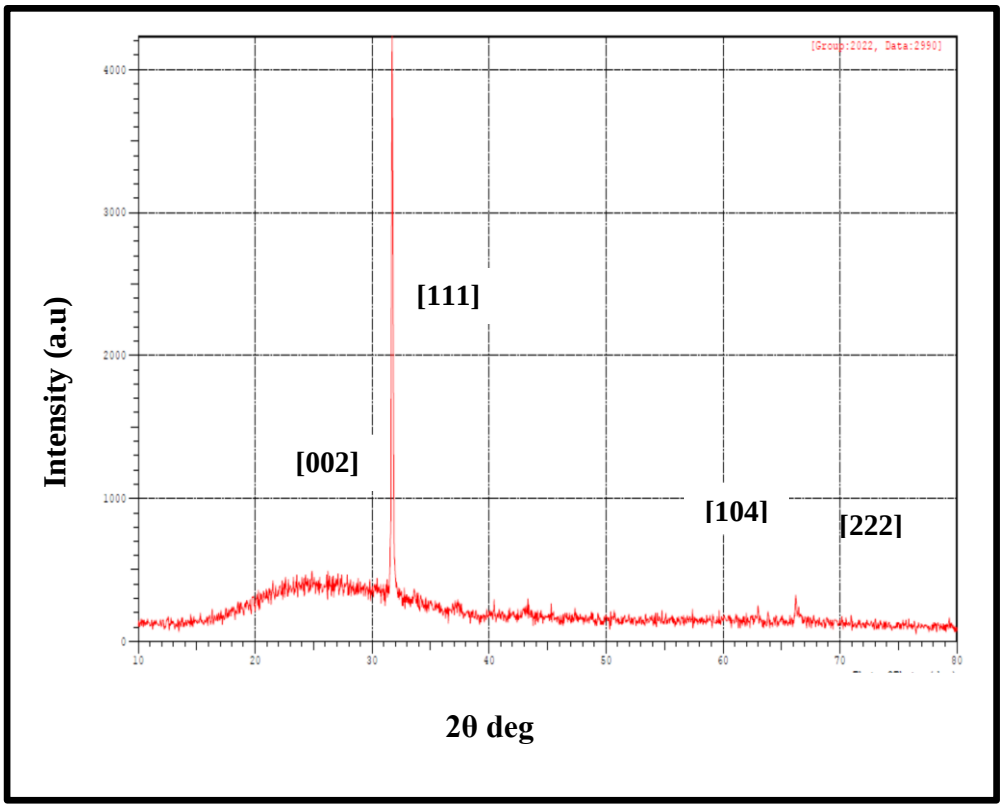

Fig (4.5) : X-ray diffraction of $NiCl_2$ thin film (pure) at 350^0 C.

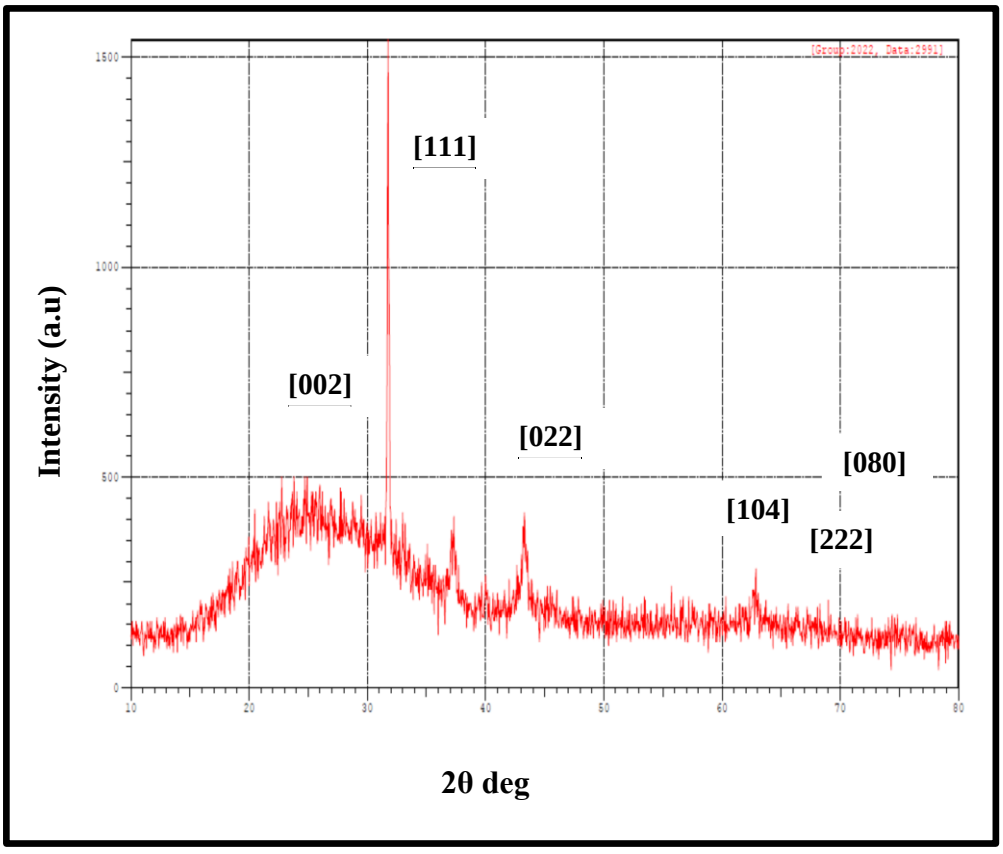

Fig (4.6) : X- ray diffraction of $NiCl_2$:Al_2O_3 thin film (1%) at 350 °C.

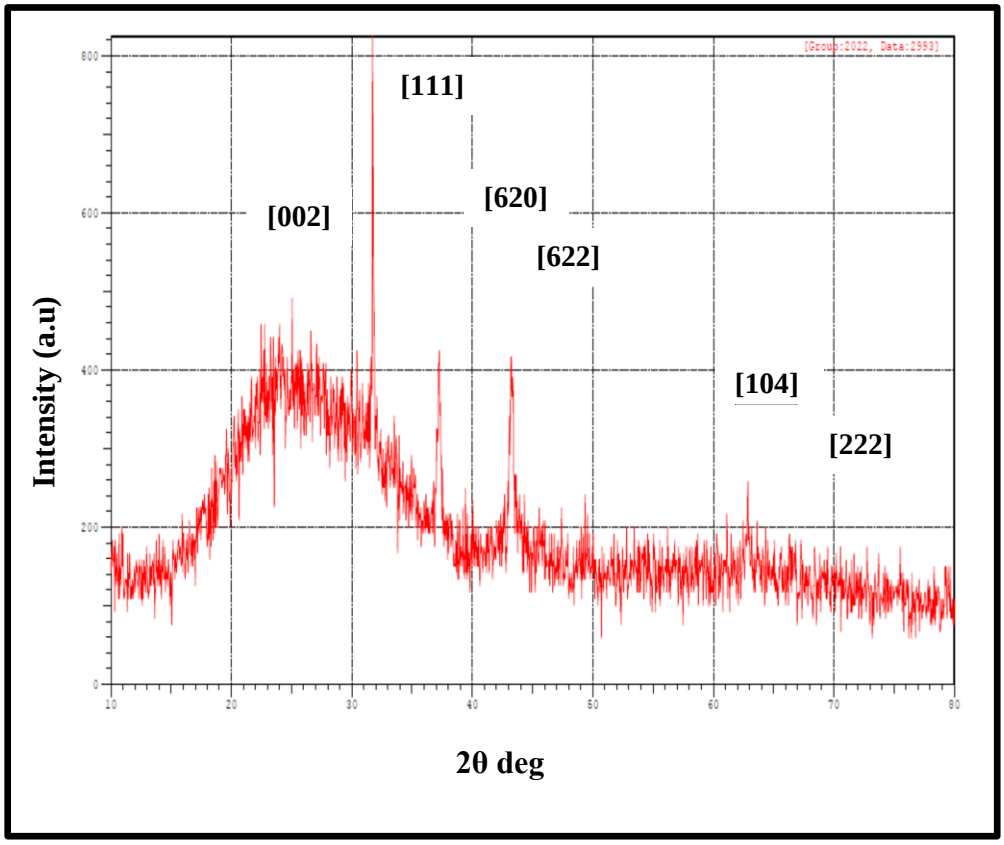

Fig (4.7) : X- ray diffraction of $NiCl_2$:Al_2O_3 thin film (2%) at 350 °C.

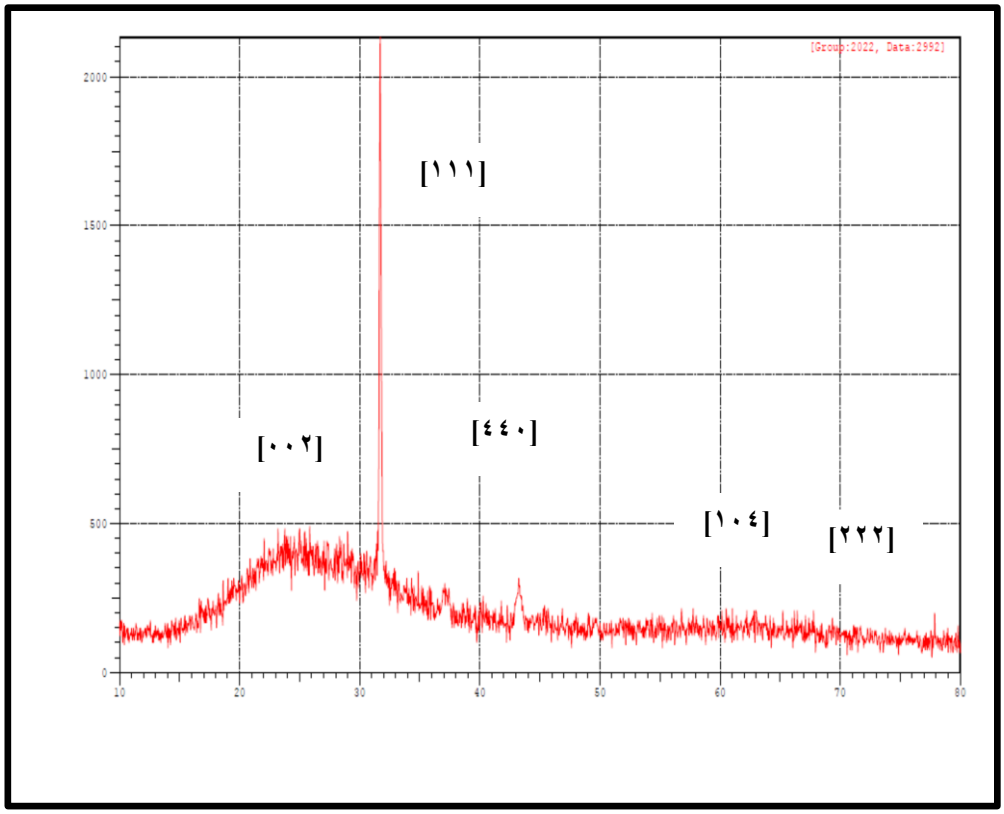

Fig (4.8) : X- ray diffraction of $NiCl_2$:Al_2O_3 thin film (3%) at 350 °C.

Table (4.5): X-ray Diffraction Screening Parameters for $NiCl_2$ (pure). thin film at 350 ºC.

No	2θ	hkl	d(Å)	G.S(nm)	FWHM	I %	A	Sys.
1	33.653	111	2.661	36.4	0.236	98	a=3.875 b=4.552 c=6.162	Orthorhombic
2	65.099	104	1.431	50.4	0.195	6		
3	70.743	222	1.33	46.6	0.217	7		
4	28.957	002	3.081	37.1	0.229	20		
				Ave=42.652	Ave=0.237			

Table (4.6): X-ray Diffraction Screening Parameters for $NiCl_2$:Al_2O_3 (1%) thin film at 350 ºC.

No	2θ	Hkl	d(Å)	G.S(nm)	FWHM	I %	A	Sys
1	46.418	022	1.954	55.8	0.472	0.613	a=3.77 b=10.365 c=4.221	Orthorhombic
2	72.96	080	1.295	42.6	0.678	0.24		
3	33.653	111	2.661	36.4	0.236	98	a=3.875 b=4.552 c=6.162	
4	65.099	104	1.431	50.4	0.195	6		
5	70.742	222	1.33	46.6	0.217	7		
6	28.957	002	3.081	37.1	0.229	20		
				Av.=44.816	Av.=0.350			

Table (4.7): X-ray Diffraction Screening Parameters for $NiCl_2$:Al_2O_3 (2%) thin film at 350 ºC.

No	2θ	hkl	d(Å)	G.S(nm)	FWHM	I%	A	Sys
1	46.06	620	1.968	28.1	0.153	0.1	a=b=c=12.42	Cubic orthorhombic
2	48.449	622	1.877	51.2	0.945	22	a=3.875 b=4.552 c=6.162	
3	33.653	111	2.654	55	0.578	22		
4	65.099	104	1.431	50.4	0.195	9		
5	70.742	222	1.33	46.6	0.217	6		
6	28.957	002	3.081	37.1	0.229	5		
				Av.=43.54	Av.=0.386			

Table (4.8): X-ray Diffraction Screening Parameters for $NiCl_2$:Al_2O_3 (3%) thin film at 350 ºC.

No	2θ	Hkl	d(Å)	G.S(nm	FWHM	I%	A	Sys
1	41.061	440	2.196	49.6	0.182	9.3	a=b=c=12.425	Cubic Orthorhombic
2	33.653	111	2.661	36.4	0.236	97	a=3.875 b=4.552 c=6.162	
3	65.099	104	1.431	50.4	0.195	8		
4	70.742	222	1.33	46.6	0.217	5		
5	28.957	002	3.081	37.1	0.229	19		
				Av.=44.02	Av.=0.211			

4.2.2. AFM Investigation

The imaging of the prepared films using the atomic force microscope (AFM), which has the ability to photograph and analyze the deposited surfaces, was to give measurements of the values of the surface roughness (Root Mean Square -RMS), showing the topography of the surfaces of the pure films (Root Mean Square -RMS) for the mean square of the roughness and the impurity and the extent of the spread of the doped aluminum oxide material throughout the unit area and the extent of its homogeneity, inferring this from the average size of the grains and their distribution shown in the attached figures from (4.9) to (4.12) form a film of pure nickel chloride doped with aluminum oxide, and the images show the effect of doping in the formation of the surface, where an increase in the size of the grains appears, and this is shown by the results of the roughness rate values (RMS) showing that the ratio of doping with (Al_2O_3) increases the rate of surface roughness, which indicates an increase in grain size and a decrease in grain boundaries, this agree with refer[98].

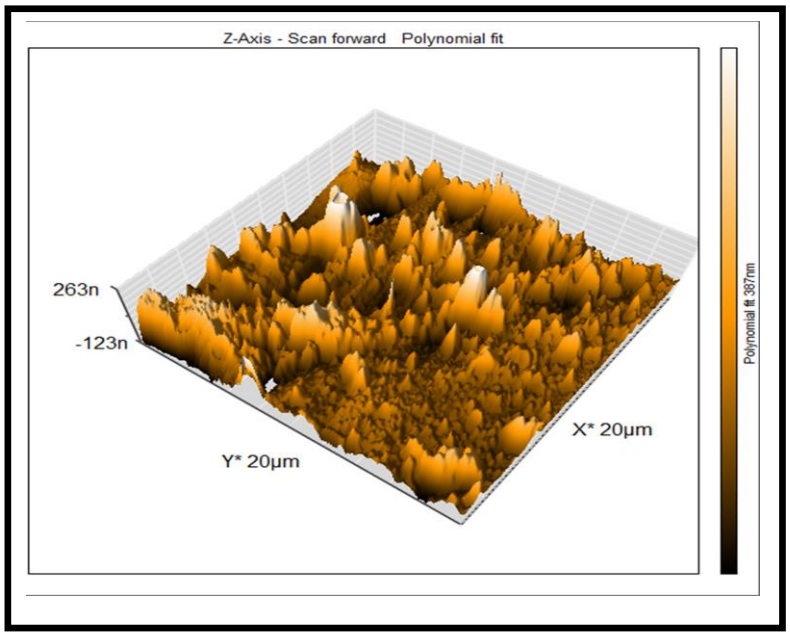

Fig (4.9): AFM image of $NiCl_2$ thin film (pure).

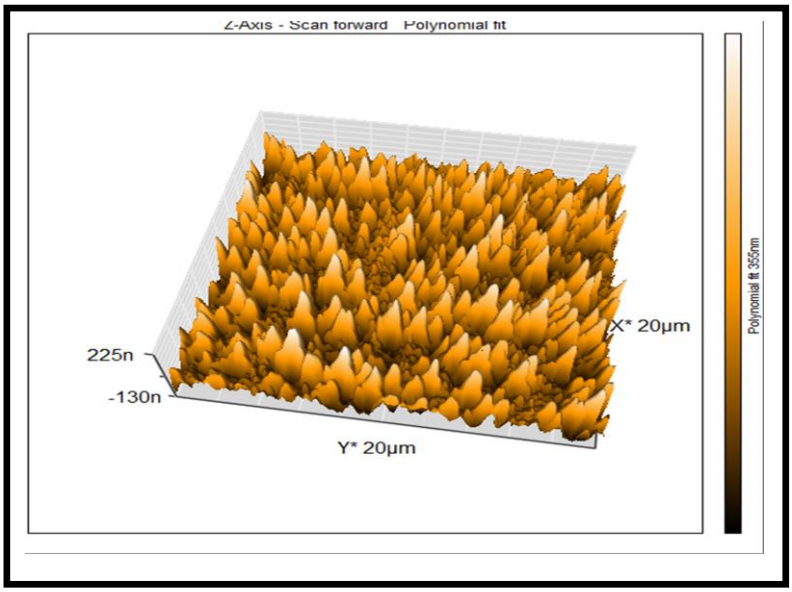

Fig (4.10): AFM image of $NiCl_2$ doped with 1% Al_2O_3 thin film.

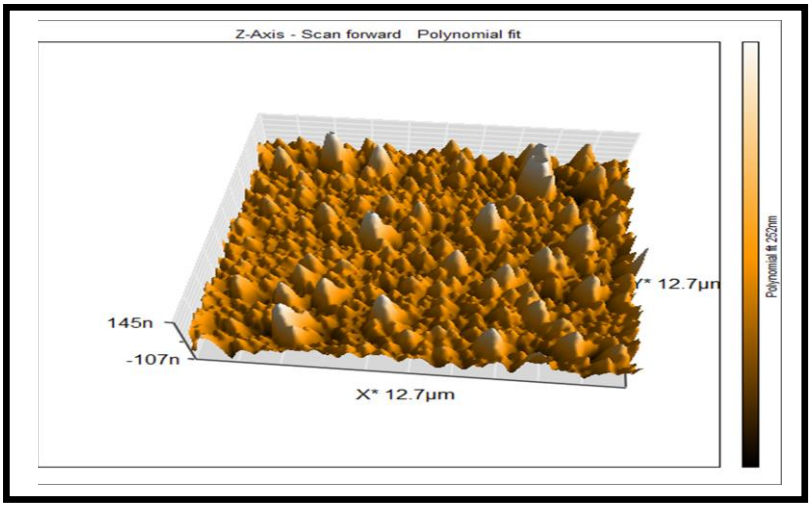

Fig (4.11): AFM image of $NiCl_2$ doped with 2% Al_2O_3 thin film .

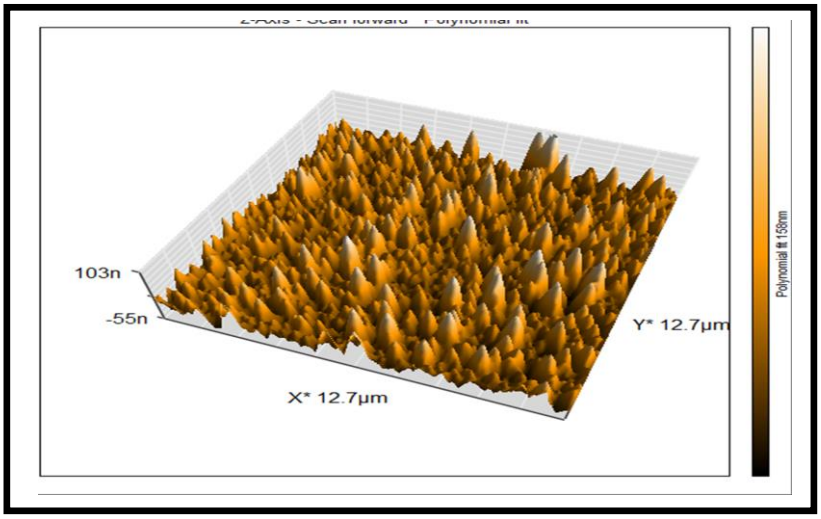

Fig (4.12): AFM image of $NiCl_2$ doped with 3% Al_2O_3 thin film.

When annealing increasing the temperature , noticed that the roughness decreases because the particle size decreases, and this is due to the decrease in the homogeneity of the membrane, as the increase in temperature reduces the aggregation of atoms with each other.

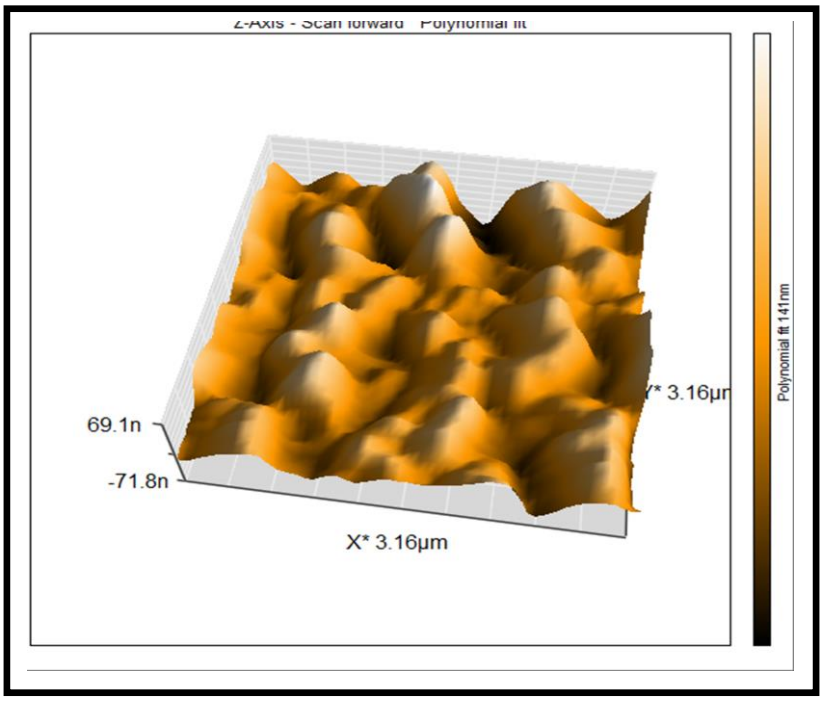

Fig (4.13): AFM image of $NiCl_2$ thin film (pure) at 350 °C.

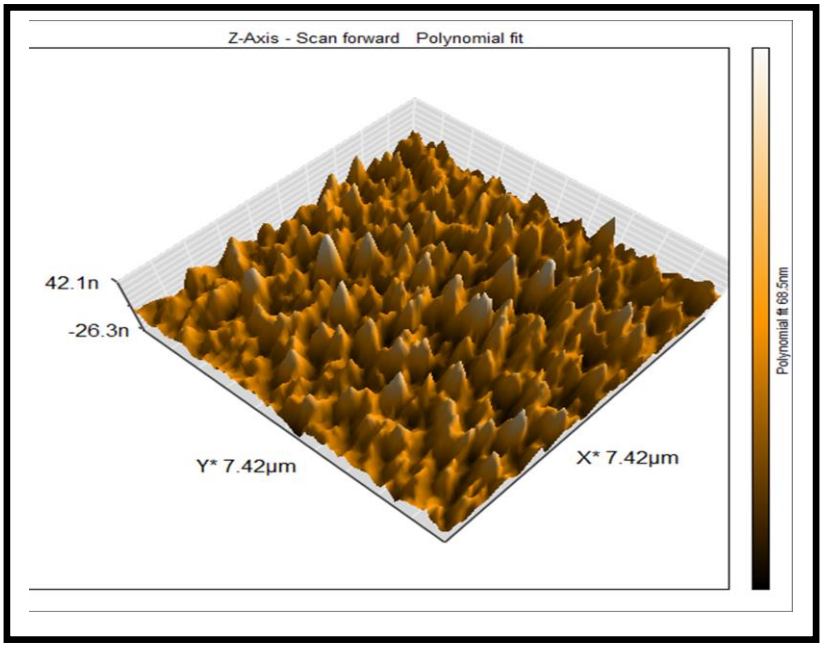

Fig (4.14): AFM image of $NiCl_2$ doped with 1% Al_2O_3 thin film at 350 °C.

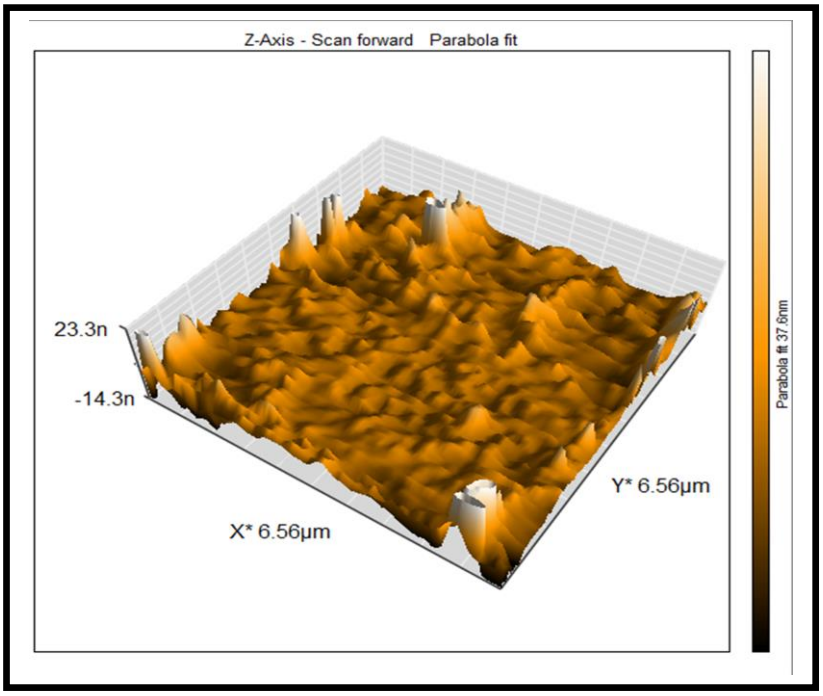

Fig (4.15): AFM image of $NiCl_2$ doped with 2% Al_2O_3 thin film at 350 °C.

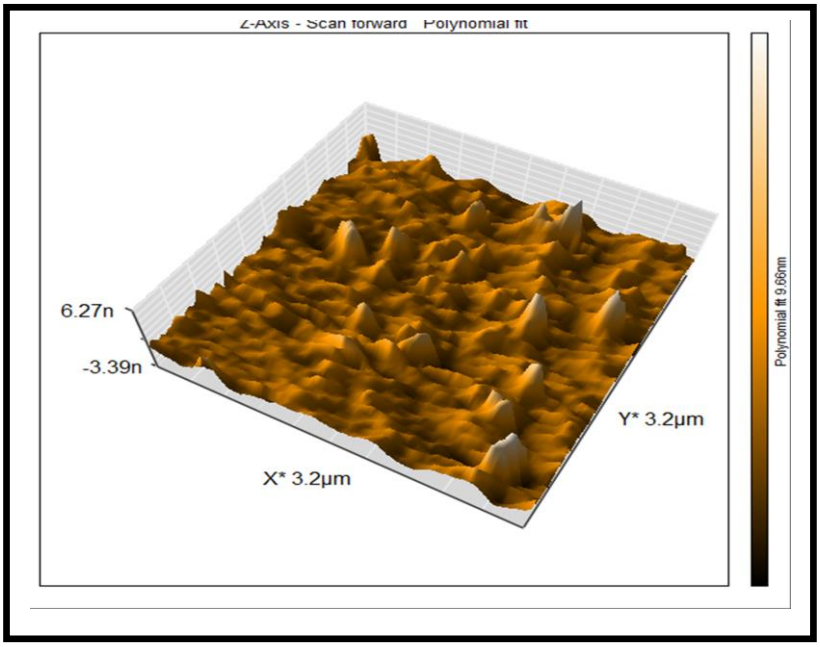

Fig (4.16): AFM image of $NiCl_2$doped with 3% Al_2O_3 thin film at 350 °C.

Table (4.9): Effect of doping on roughness.

Doping	RMS (nm)	Roughness (nm)
Pure	18.03	13.37
1%	38.17	27.91
2%	52.68	37.06
3%	70.54	46.99

Table (4.10): Effect of annealing on roughness.

Annealing 350 °C	RMS (nm)	Roughness (nm)
Pure	15.55	4.25
1%	37.17	11.68
2%	44.58	29.04
3%	56.99	41.99

4.2.3. SEM Investigation

Scanning electron microscopy is used to investigate the surface shape of the samples and the dispersion of aluminum oxide (Al_2O_3) in the thin film ($NiCl_2$). Figures (4.17), (4.18), (4.19) and (4.20) show the increase in pollination rates has a clear effect. When the inoculation rates increase, we notice an increase in the density and granule size of the film. It should also be noted that the composition of the thin films is polycrystalline, where the grain boundaries can be clearly distinguished, such as aluminum oxide when grafted. Are also present in the thin films with atoms of the substance ($NiCl_2$), and this increases the collisions between the atoms, which leads to the loss of the energy of the molecules in an adequate amount. To form molecular clusters where they align with each other. Increased surface roughness which is consistent with the (AFM) results and is consistent with the refer [99].

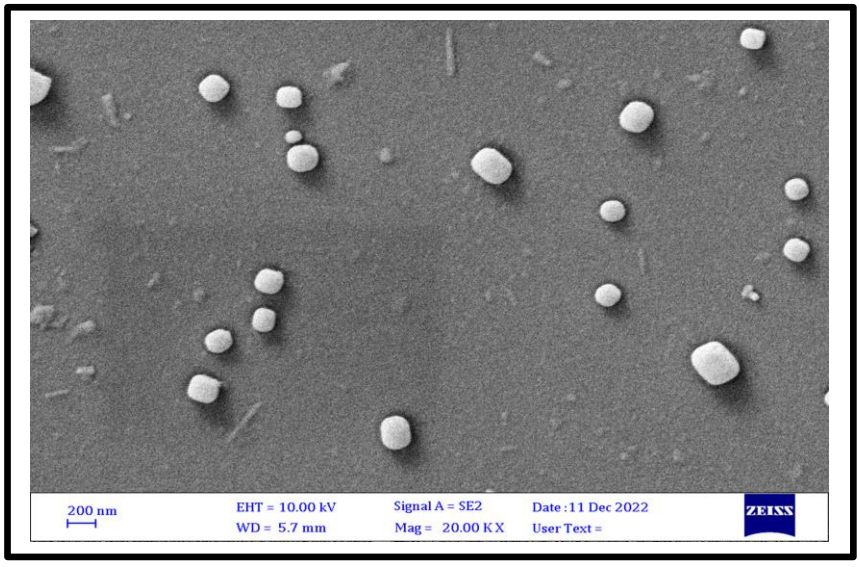

Fig(4.17) : SEM image of $NiCl_2$ thin film (pure).

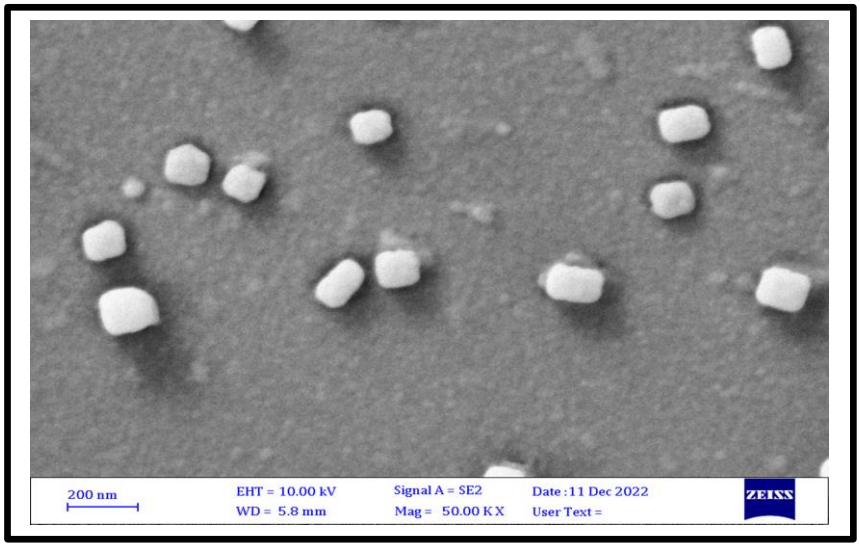

Fig(4.18) : SEM image of $NiCl_2$ doped with 1% Al_2O_3 thin film .

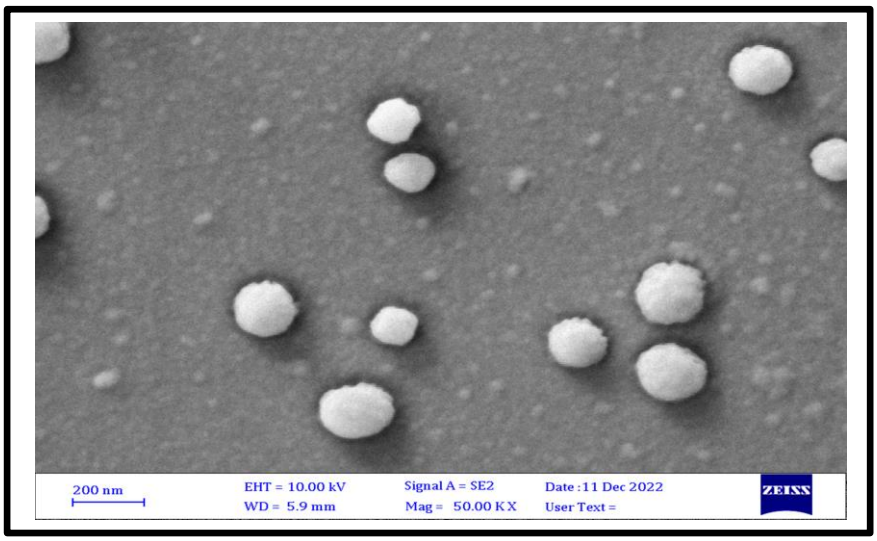

Fig(4.19) : SEM image of $NiCl_2$ doped with 2% Al_2O_3 thin film.

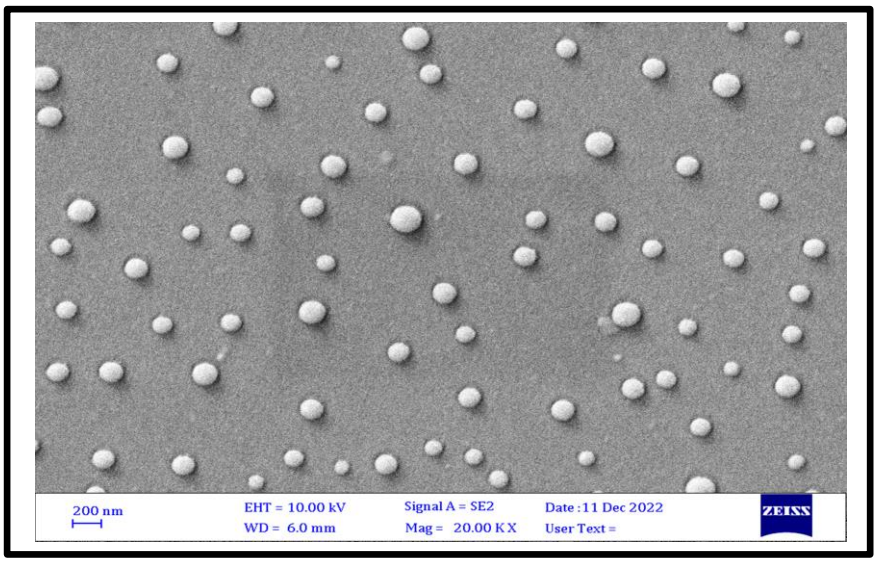

Fig(4.20) : SEM image of $NiCl_2$ doped with 3% Al_2O_3 thin film .

Figures (4.21) , (4.22) , (4.23) and (4.24) show pictures of pure ($NiCl_2$) film doped with aluminum oxide (Al_2O_3) deposited at different degrees with an annealing degree of 350 ^{0}C , where we note that the average particle size decreases with increasing temperature and (FWHM) increases, and this is consistent with the results of (XRD) and also with the results of (AFM), where the roughness decreases .

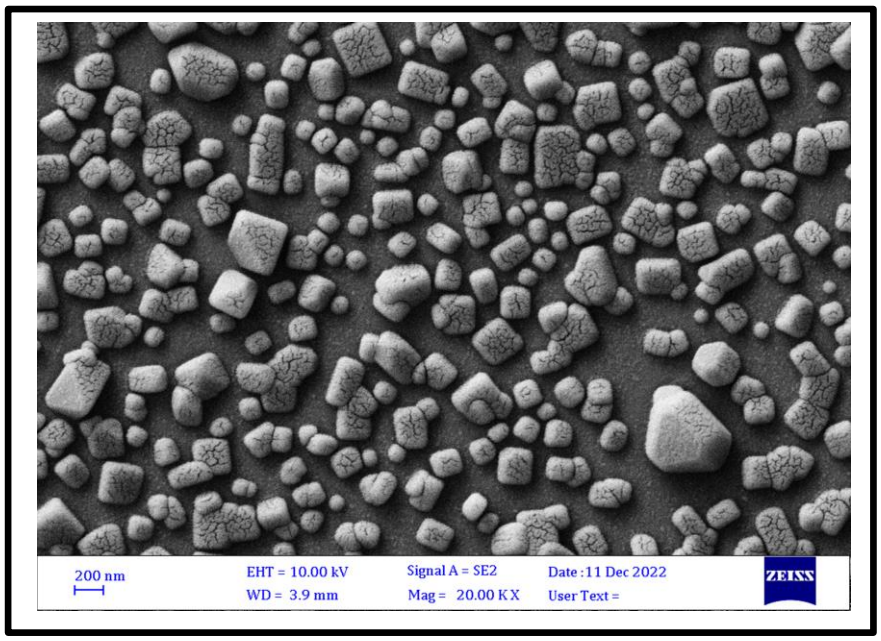

Fig (4.21) : SEM image of $NiCl_2$ thin film (pure) at 350 °C .

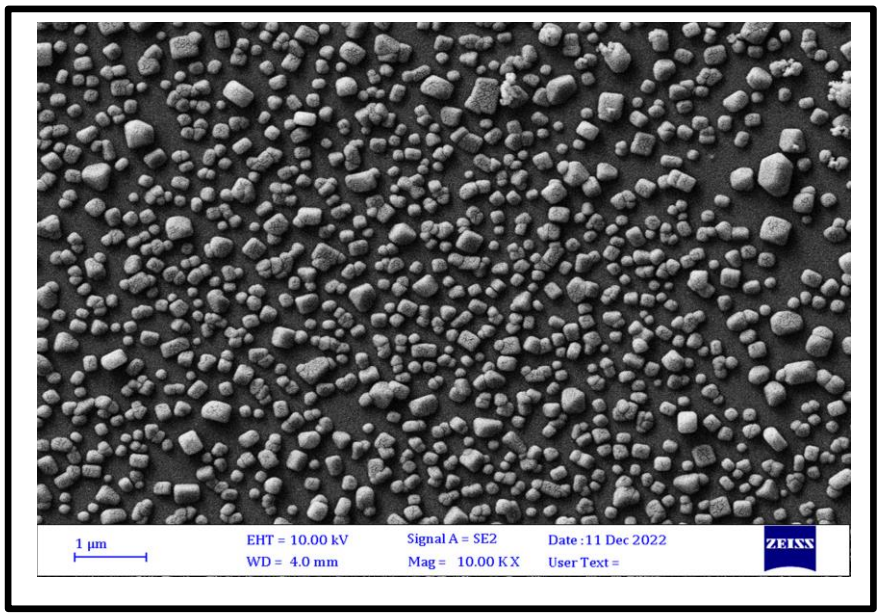

Fig(4.22) : SEM image of $NiCl_2$ doped with 1% Al_2O_3 thin film at 350^{0}C .

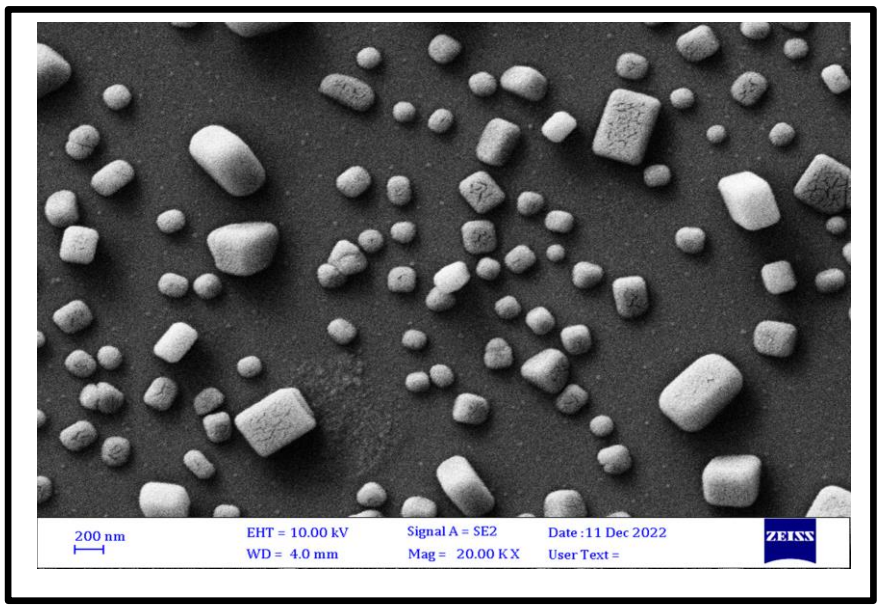

Fig(4.23) : SEM image of $NiCl_2$ doped with 2% Al_2O_3 thin film at 350^{0}C .

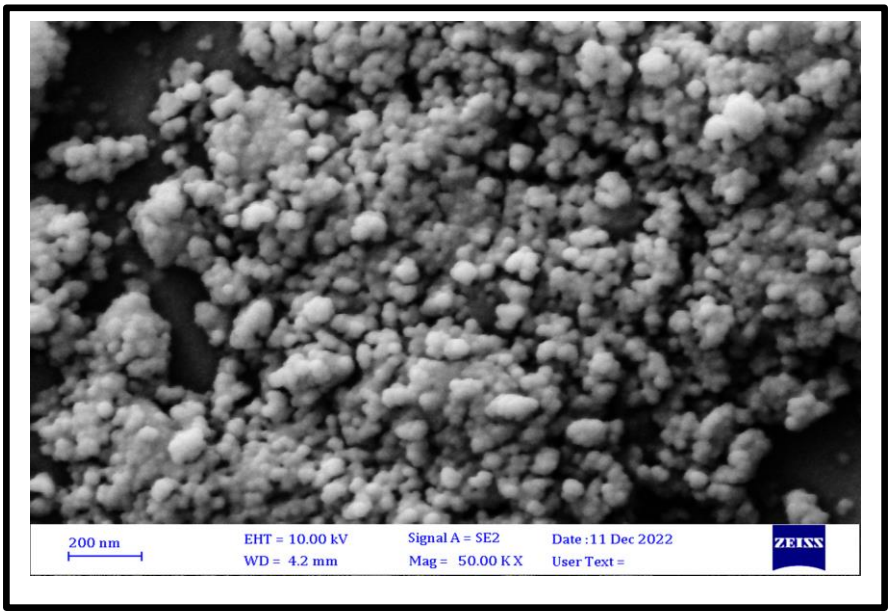

Fig(4.24) : SEM image of $NiCl_2$ doped with 3% Al_2O_3 thin film at 350^{0}C .

4.3. Results of Optical Properties Measurements

The study of the optical properties provides important information about the optical materials and their placement within the appropriate practical application. The optical behavior is closely related to the composition of the energy levels and the crystal structure of the material prepared for pure ($NiCl_2$) films doping with aluminum oxide (Al_2O_3) with different inoculation ratios. The optical properties were studied and

discussed. For membranes prepared by thermal chemical spraying and with different preparation conditions and thicknesses ranging, this part includes the results of transmittance and absorbance measurements and their relation to wavelength , absorption coefficient and its relationship to the energy of the incident photon on the membrane, and the optical energy gap was calculated, as well as the optical constants (absorption coefficient, refractive index, and the true dielectric constant , and imaginary) and its relation to photon energy.

4.3.1. Absorption Spectrum

Many optical constants can be found by studying the absorbance spectrum for wide ranges of wavelengths. Figure (4.25) represents the change of the absorbance spectrum as a function of wavelength , pure ($NiCl_2$) film and doped with aluminum oxide (Al_2O_3) with doping ratios (1, 2, 3)% .

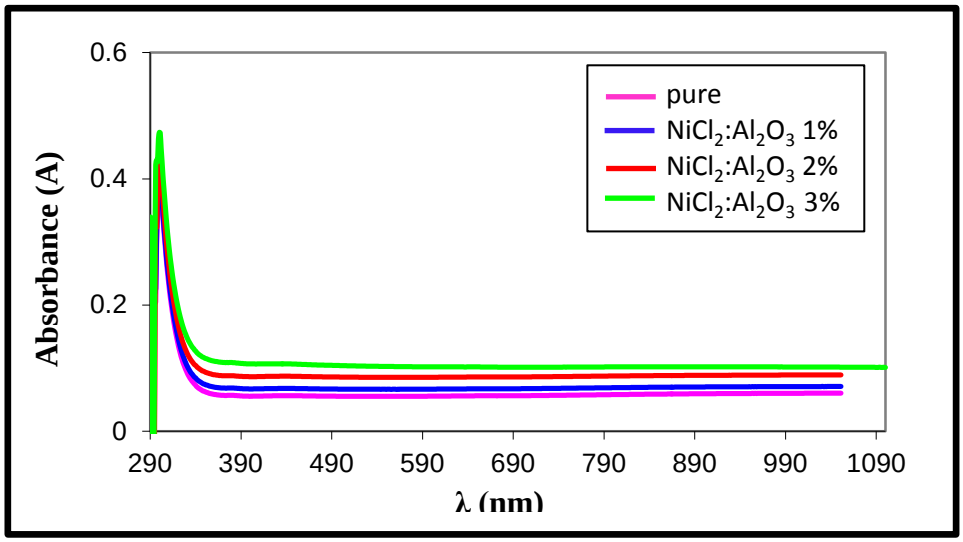

Fig (4.25): The effect of doping on absorption spectrum .

As noticed that the absorbance spectrum of the prepared pure ($NiCl_2$) thin films it is located within the visible region and its absorption was very low and noticed that the absorbance increases with the increase in the

doping ratios because the particle size increases, also due to the decrease in the optical energy gap to form levels of aluminum oxide (Al_2O_3) impurities within the energy gap, this result agree with refer [103].

Noticed that the films absorption less with the increase annealing 350 °C due to the increase in the permeability and porosity of the films, as shown in the figure (4.26) below, this result is consistent with the refer [101, 102].

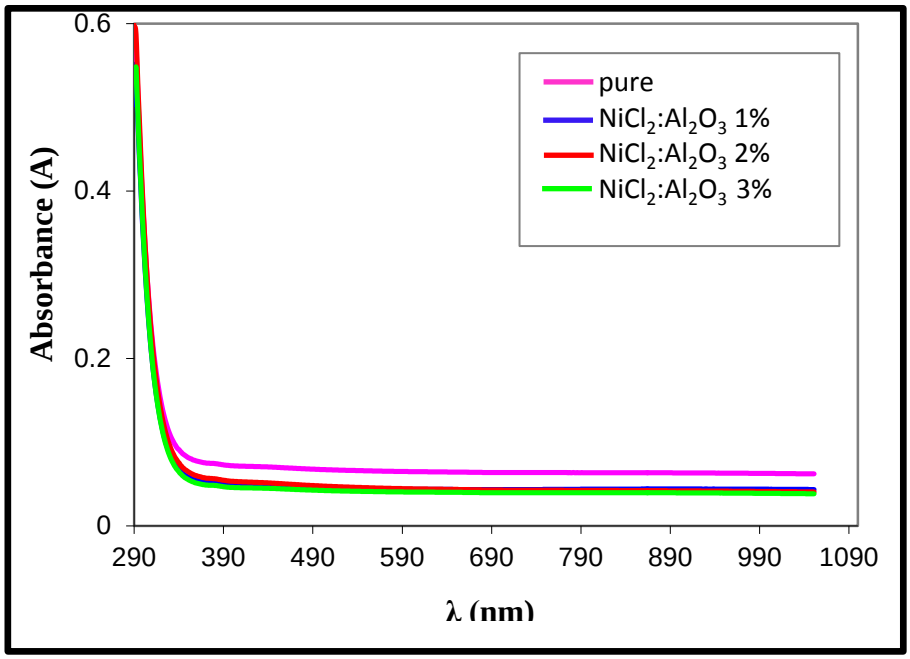

Fig (4.26) : The effect of annealing 350 °C on absorption spectrum .

4.3.2. Transmittance Spectrum

The transmittance spectrum was measured for pure ($NiCl_2$) films doped with (Al_2O_3) and with doping ratios (1,2,3%) under different preparation conditions as a function of the incident photon wavelength within the range (290-1100 nm). We noticed that the permeability decreases by increasing the added inoculation rates, and it has a permeability less than the permeability of pure ($NiCl_2$) films, as shown in figure (4.27), and the reason for this may be attributed to the formation of

levels of (Al_2O_3) impurities within the energy gap that leads to an increase in reflectivity and thus a decrease in permeability .

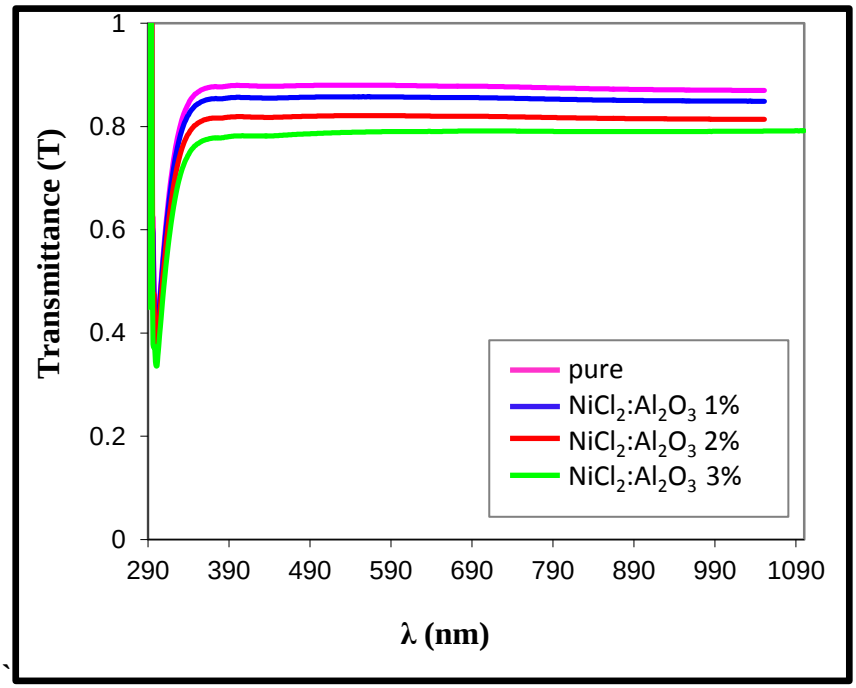

Fig (4.27) : The effect of doping on transmittance spectrum .

Noticed from figure (4.28) that the transmittance of the pure and doped thin films increases with the increase in temperature (annealing), because the porosity of the membrane increases with this increase.

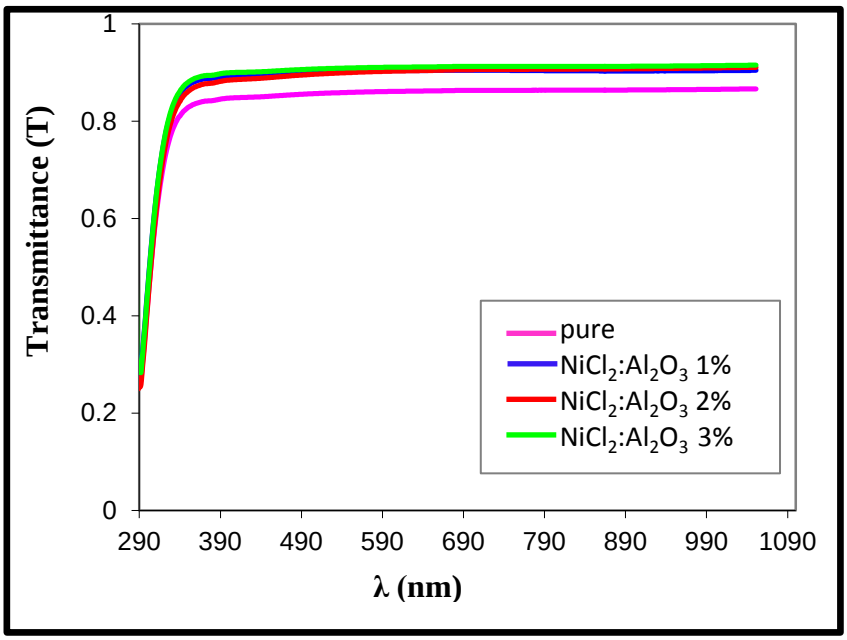

Fig (4.28) : The effect of annealing 350°C on transmittance spectrum .

4.3.3. Absorption Coefficient (α)

The absorption coefficient (α) is defined as the ratio of the decrease in the radiation energy flux relative to the unit distance in the direction of wave propagation inside the medium, and depends on the energy of the incident photons, the wavelength, the nature of the thin film surface, the energy gap of the semiconductor, and the type of electronic transitions that occur between the energy bundles [103]. The absorption coefficient was calculated from equation (2-11) as a function of the photon energy change , and it was found that the absorption coefficient (cm^{-1}) ($\alpha > 10^4$), and this indicates a high probability of direct electronic transitions, and that the high energies at which these values were calculated are the energies of a direct energy gap. The absorption coefficient is low at low photon energies, in which the probability of electronic transitions is few and the values of the absorption coefficient increase at the edge of absorption towards higher energies. The following figures show the effect of temperature and vaccination on the values of the absorption coefficient.

When inoculating the thin film with aluminum oxide (Al_2O_3), the absorption coefficient behaves like absorbance, as it increases with increasing inoculation rates to be levels of impurities added within the energy gap, as shown in figure (4.29), this result is consistent with the research [104].

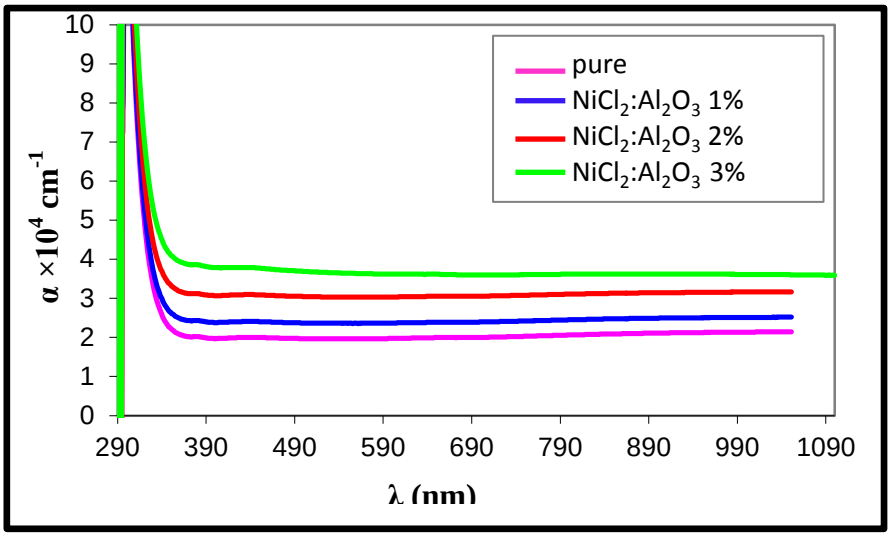

Fig (4.29) : The effect of doping on absorption coefficient .

Noticed from the figure (4.30) below that an increase in temperature (annealing 350 °C) leads to a clear decrease in the absorption coefficient of the pure ($NiCl_2$) and doped films , and this is due to the increase in crystallization of the material, which in turn reduces crystalline defects. This result is consistent with the refer[98] .

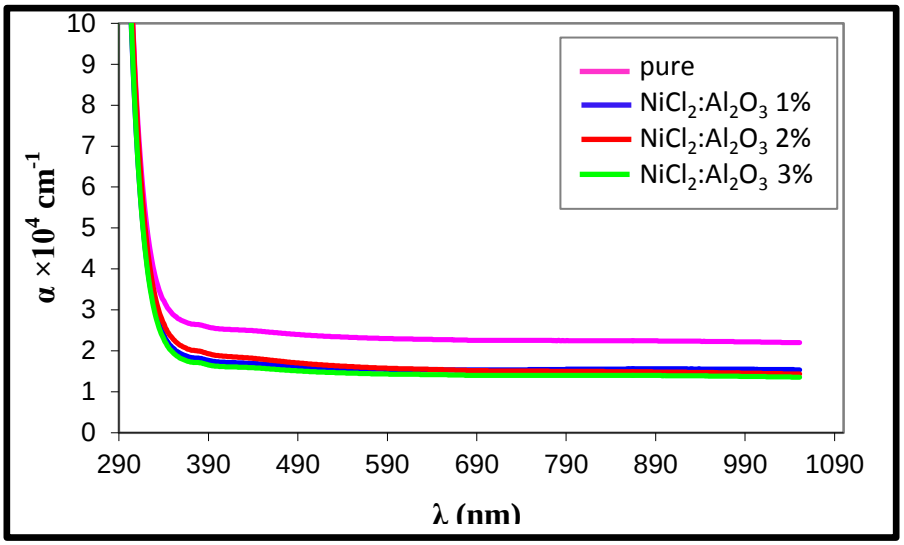

Fig (4.30) : The effect of annealing 350 °C on absorption coefficient .

4.3.4. Energy Gap

($NiCl_2$) semiconductor films with a wide direct energy gap of about (3.8 eV), the value of the optical energy gap for the direct

transitions allowed is calculated through equation (2-14) and the absorption coefficient (α) is associated with the energy of the incident photon through the relation the same, therefore, the relation is drawn between $(\alpha\upsilon h)^2$ and photon energy (υh), then we extend part of the straight line from the curve to cut the photon energy axis at $(0 = (\upsilon h\alpha)^2$ so we get the value of the energy gap for the allowed direct transitions.

Figure (4.31) shows the energy gap value of the pure ($NiCl_2$) thin film doped with different degrees (1,2 , 3)% of aluminum oxide (Al_2O_3) before the annealing process. The decrease in the values of the energy gap leads to the formation of levels of aluminum oxide impurities (Al_2O_3) within the energy gap, and the width of these levels increases with the increase in the inoculation ratios, this result is consistent with the refer [100].

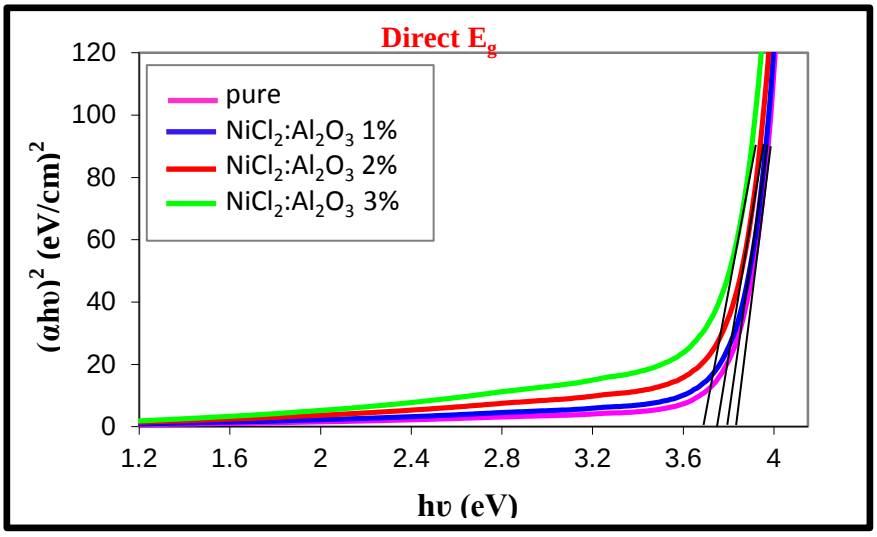

Fig (4.31) : The effect of doping on energy gap .

Noticed from figures (4.32), that the increase in the degree of annealing increases the values of the direct energy gap, and that the reason for this increase in the energy gap is attributed to the improvement of the structural properties of the films , this was confirmed by X-ray examinations and SEM and AFM examinations, this result is consistent with the refer [106].

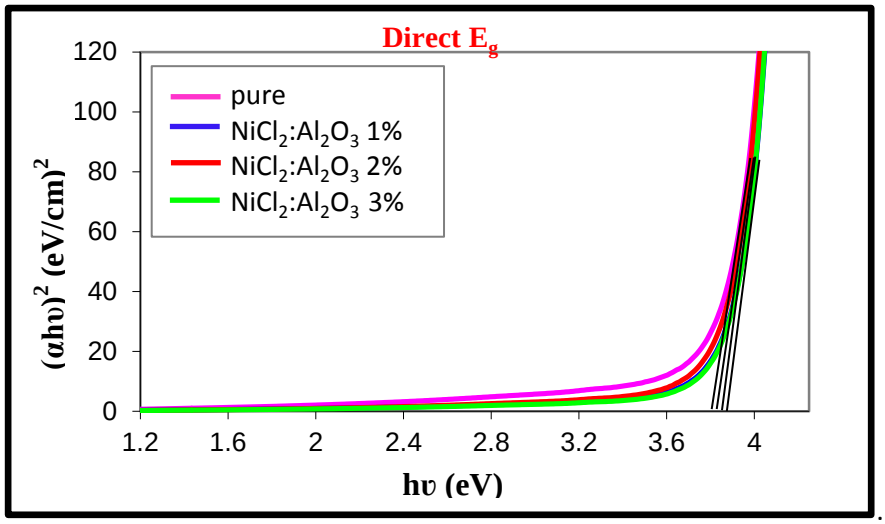

Fig (4.32) : The effect of annealing 350 °C on energy gap .

Table (4.11): Effect of doping on energy gap .

Thin Film	Energy Gap (eV)
$NiCl_2$ pure	3.8
$NiCl_2$:Al_2O_3 (1%)	3.7
$NiCl_2$:Al_2O_3 (2%)	3.65
$NiCl_2$:Al_2O_3 (3%)	3.6

Table (4.12): Effect of annealing 350 °C on energy gap .

Annealing 350 °C	Energy Gap (eV)
Pure	3.81
1%	3.75
2%	3.7
3%	3.69

4.3.5. Extinction Coefficient (k)

The extinction coefficient represents the amount of energy absorbed in the thin film represents the imaginary part of the complex refractive index. The passivity coefficient was calculated from the relation (2-16) and the passivity coefficient is associated with the absorption coefficient as shown in the previous relation. The figure (4.33) it shows the change

of the extinction coefficient of ($NiCl_2$) pure film and doped with (Al_2O_3), where when the inoculation percentage is increased, the extinction coefficient increases, this result is consistent with the refer [100].

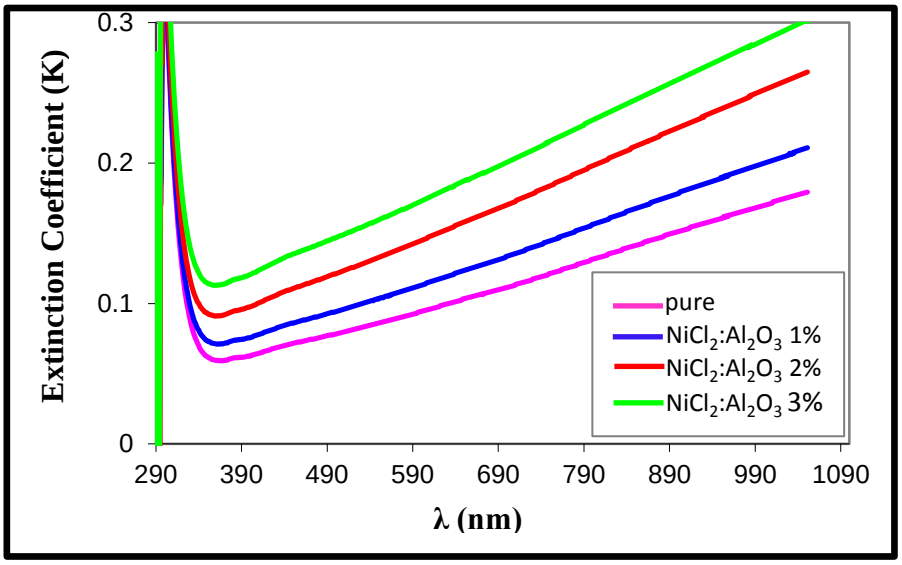

Fig (4.33) : The effect of doping on extinction coefficient .

As for the annealing 350 °C process, it leads to a decrease in the extinction coefficient, which decreases with the increase in temperature, this result is consistent with the refer [105], as shown in the figures .

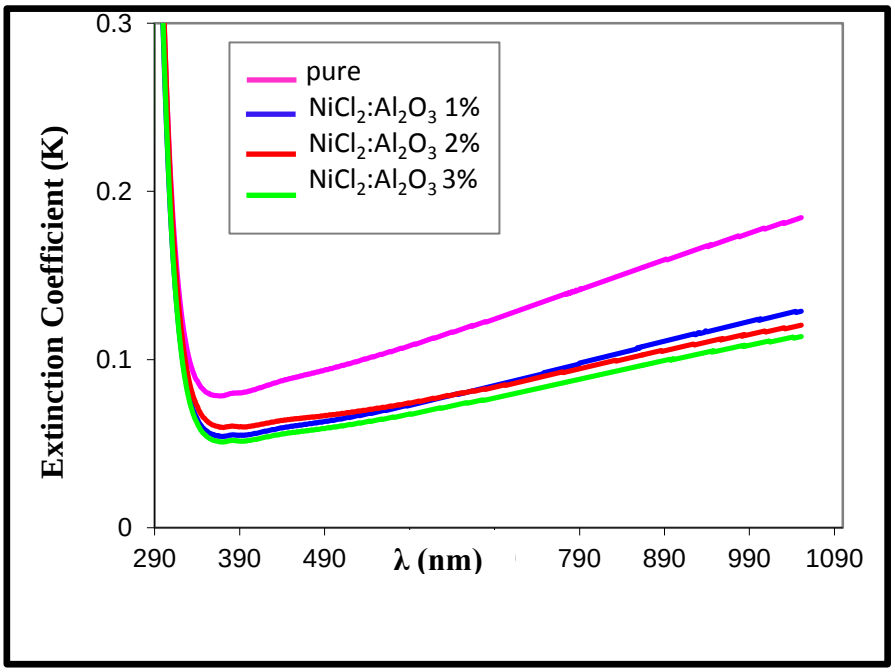

Fig (4.34) : The effect of annealing 350 °C on extinction coefficient .

4.3.6. Refractive Index (n)

We not the values of the refractive index (n) increase with the increase in the doping ratio, the reason bhand is due to the fact that the doping process led to the addition of impurity atoms within the crystalline structure of ($NiCl_2$) films .This leads to the addition of new levels based on reflecting the X- rays in more quantity, which increases the intensity the reflected rays. Thus, increasing the refractive index. The increase in the refractive index is attributed to the increase in the compaction density as a result of the improvement of the crystal structure of the films prepared after doping with aluminum oxide [107].

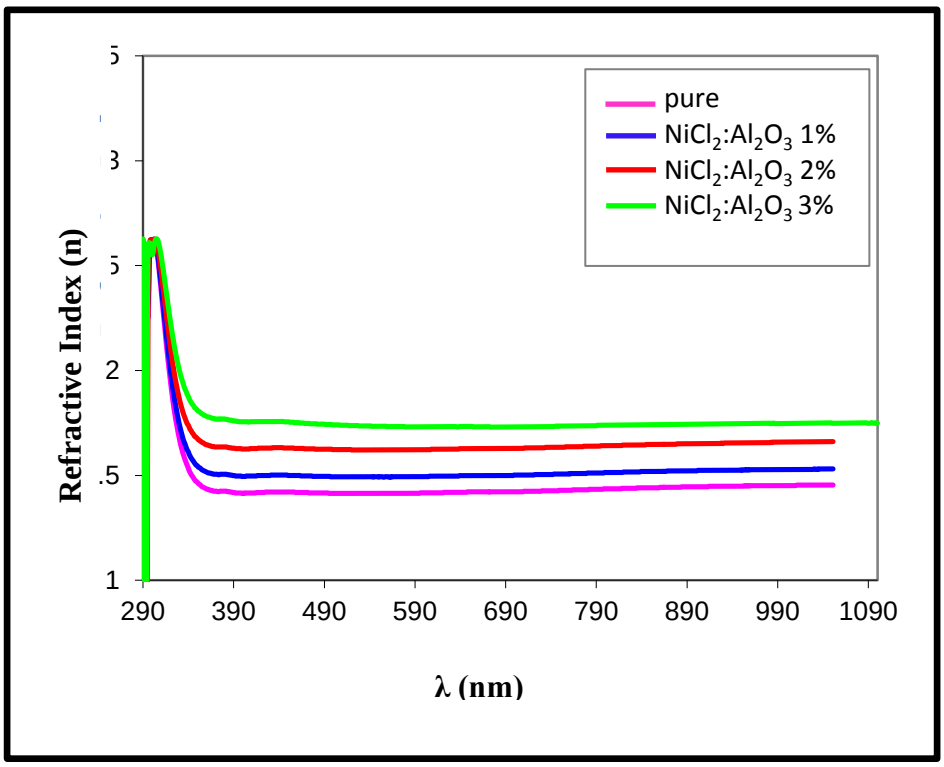

Fig (4.35) : The effect of doping on refractive index .

Noticed that an increase in the annealing 350 °C leads to a decrease in the refractive index, and this is due to a decrease in the reflectivity values, as shown in the following figure (4.36)

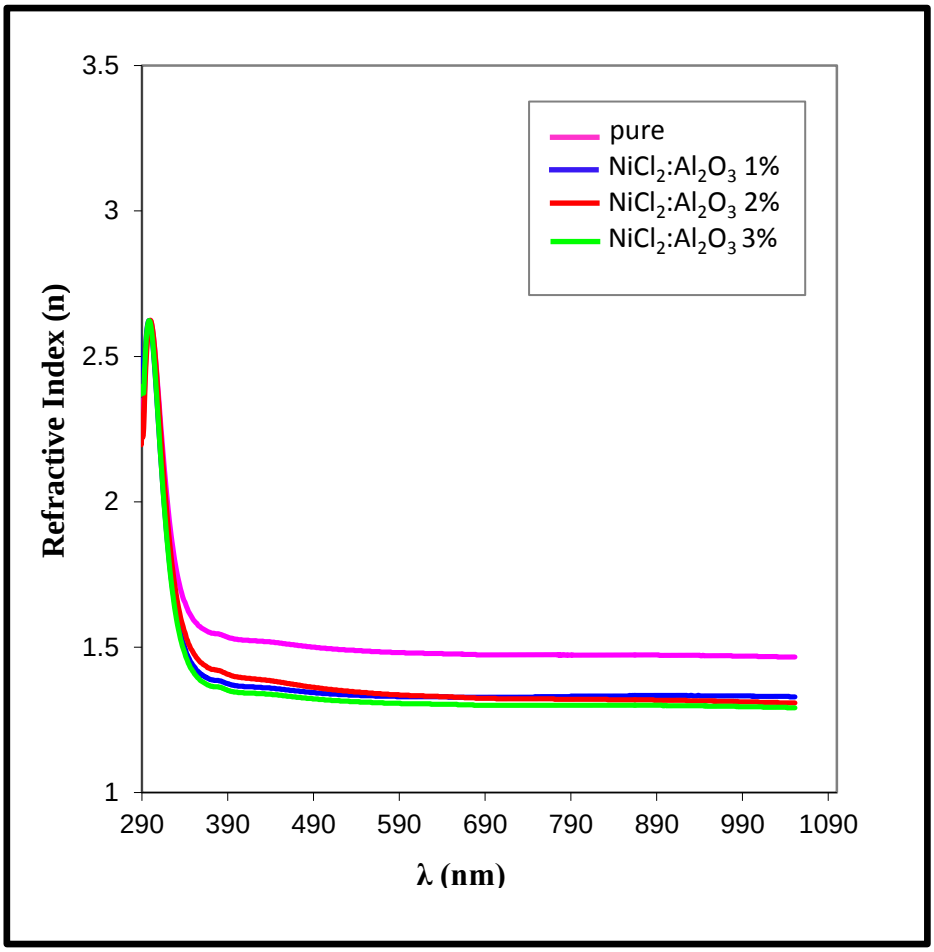

Fig (4.36) :The effect of annealing 350 °C on refractive index .

4.3.7. Dielectric Constant

The interaction between light and the charges of the medium is due to the process of energy absorption in the material and then the polarization of the charges of that medium. This polarization is usually described by the complex dielectric constant of that medium.

Figure (4-37) shows the values of the real part of the dielectric constant increase with the increase in doping percentages with (Al_2O_3) (1,2,3)% similar to the behavior of the refractive index.The reason for this is the high density generated by the dipoles resulting from the increase in the doping ratio, which increases the values of the dipoles optical polarization and refractive index, this result is consistent with the refer [108].

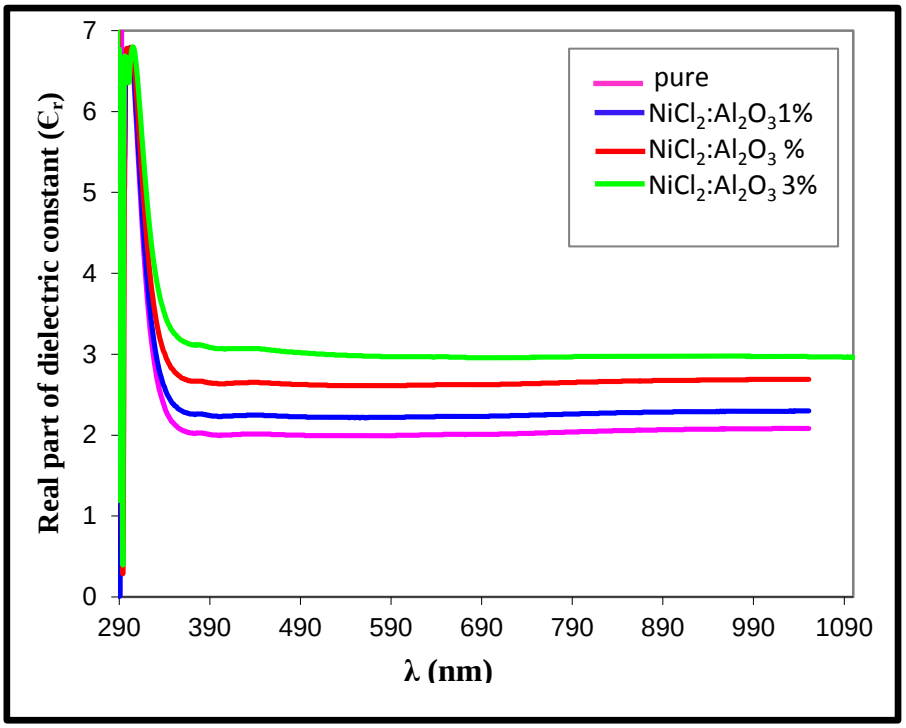

Fig (4.37): The effect of doping on the real part of the dielectric constant .

Also, when the temperature increases, we noticed that the value of the real dielectric constant decreases, as it is similar to the values of the refractive index, as shown in the following figure (4.38).

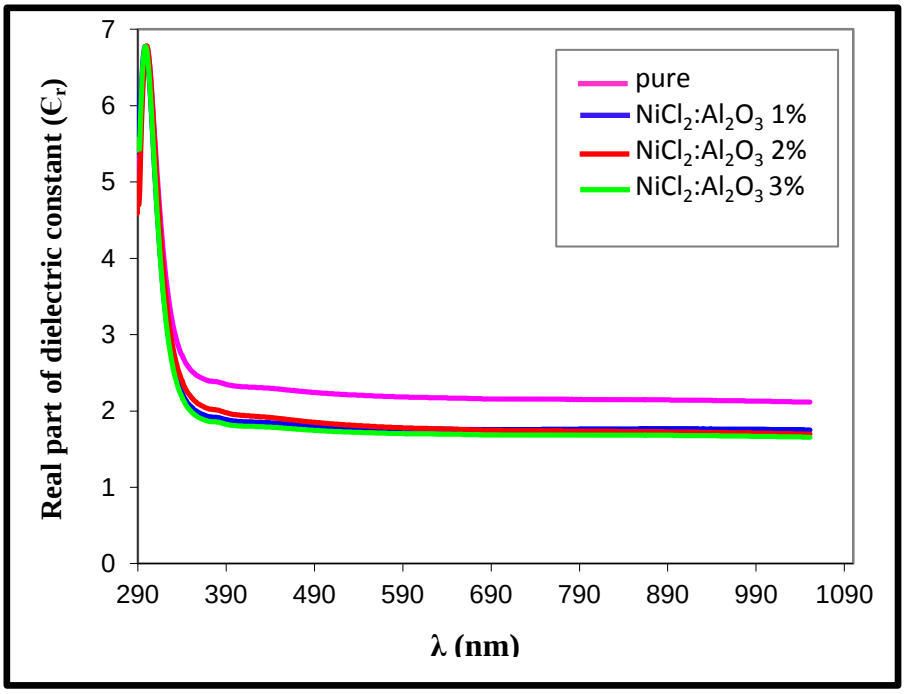

Fig (4.38) : The effect of annealing 350 ^{0}C on the real part of the dielectric constant.

Also, the imaginary part of the dielectric constant increases with increasing doping rates - and it is noticed from figure (4.39) .The reason for that is back to the entry of atoms (Al_2O_3) in the crystalline structure of the pure film material, which has created new levels within the vacuole banned energy, which led to an increase in the polarization ratio of the diodes and an increase in the energy absorbed from the radiation falling, thus increasing the imaginary part of the dielectric constant.As it is evident from the clear similarity of the figure(4.39) and the shape of the extinction coefficient curves, the relation between the damping coefficient, and this is consistent with the research [109].

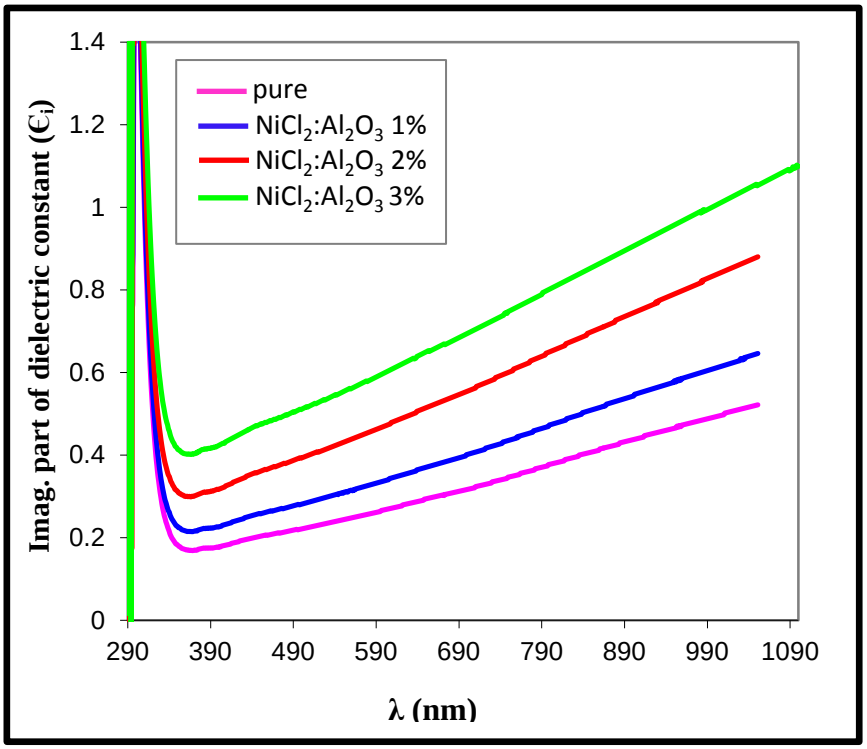

Fig (4.39): The effect of doping on the imaginary dielectric constant .

Also, when the temperature increases, we notice that the value of the imaginary dielectric constant decreases, as it is similar to the values of the extinction coefficient, as shown in the following figure (4.40).

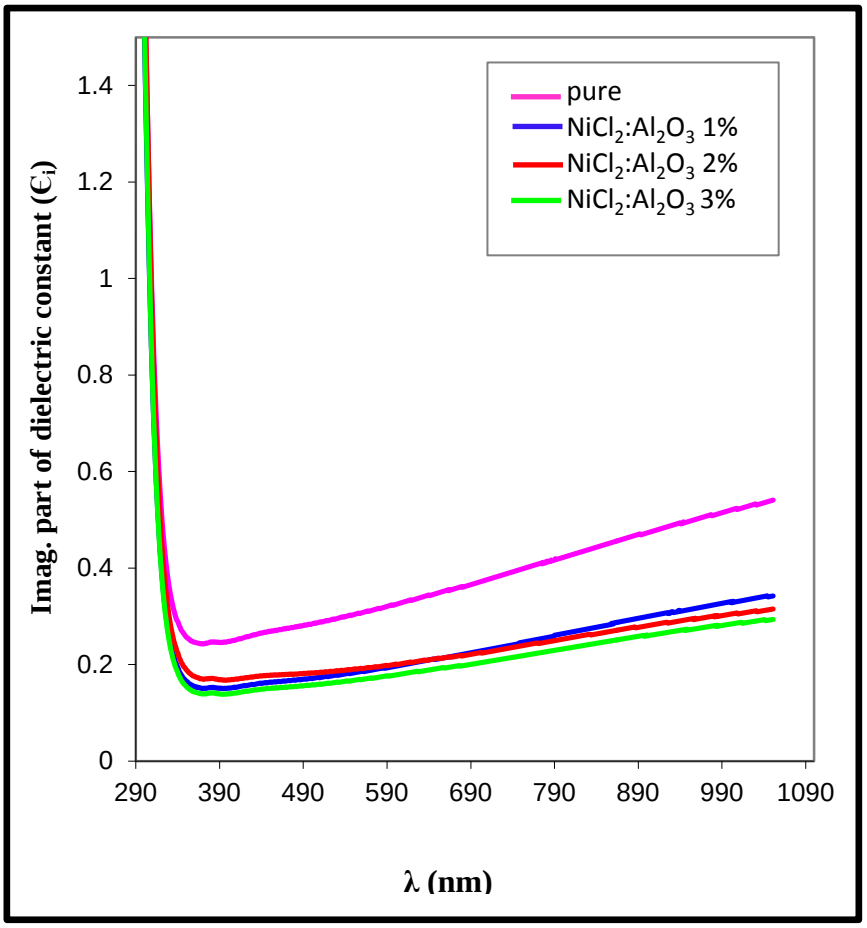

Fig (4.40): the effect of annealing 350 °C on the imaginary dielectric constant .

4.3.8. Reflectance

The reflectance is calculated by using equation (2-7), figure (4.41) show the increase in the amount of reflectivity in general, by increasing the doping ratios, the reason for this is that the optical absorption at energies less than the energy gap is little, so the amount of reflectivity increases, and when the energy of the photons reaches the value of the energy gap, the amount of absorption optical will increase as a result of the occurrence of direct electronic transitions, and thus the amount of reflection decreases and then begins to increase .The rapid increase in the amount of incident energy and the decrease in the amount of absorption when exceeding the energy of the incident photons for the amount of energy gap.

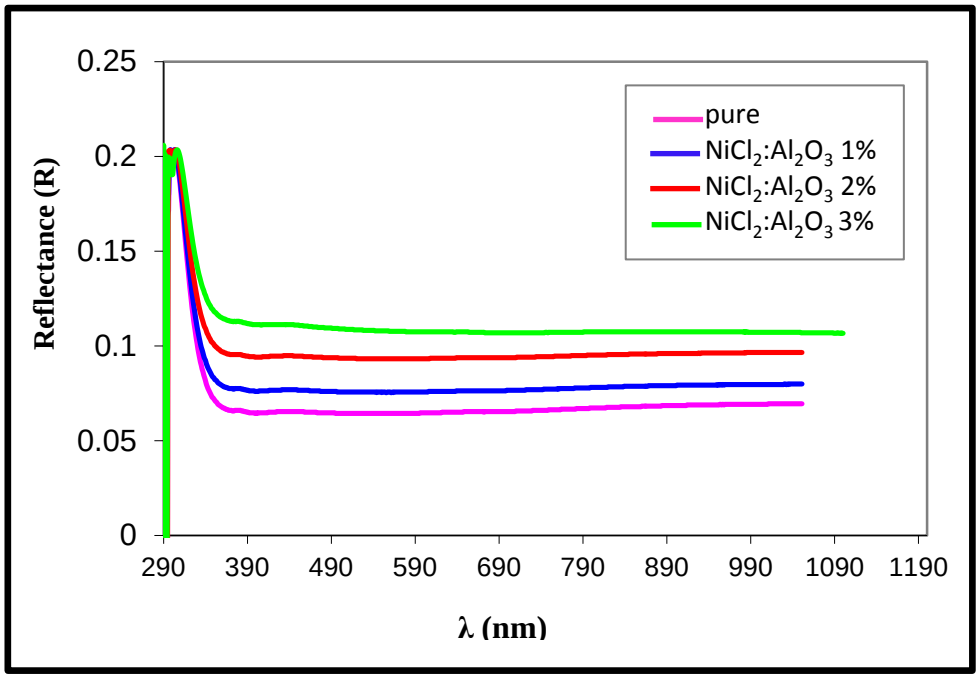

Fig (4.41):The effect of doping on reflectance .

When the temperature is increased (annealing 350 °C), we notice a decrease in the reflectivity curve with the increase in temperature, as shown in the following figure (4.42).

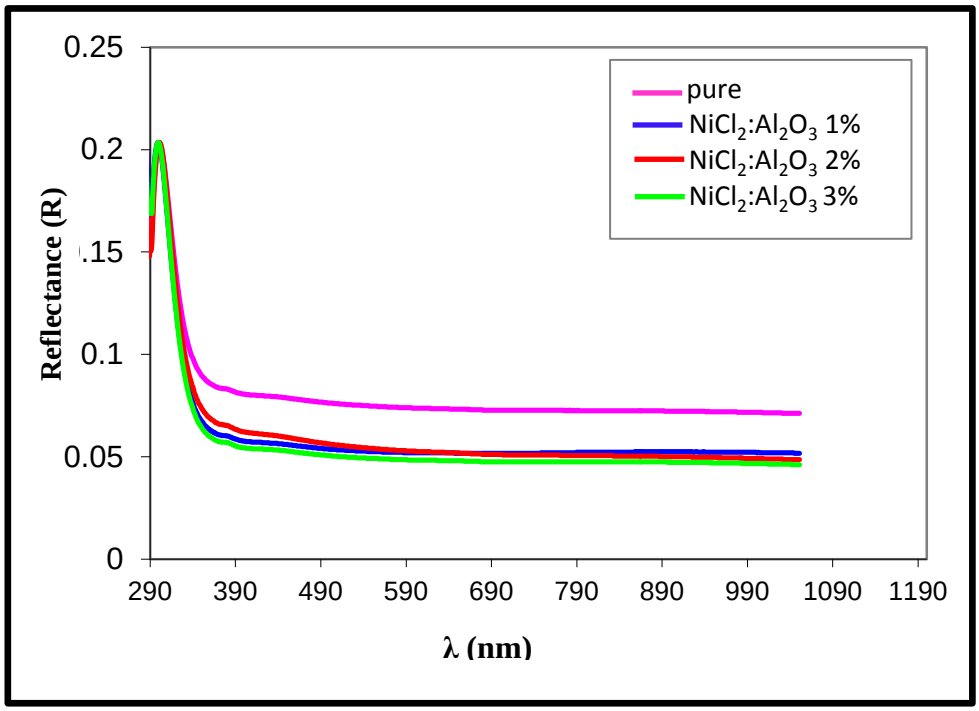

Fig (4.42) : The effect of annealing 350 °C on reflectance .

4.4. The Electrical Properties of ($NiCl_2$:Al_2O_3)Thin Films

The electrical properties of pure $NiCl_2$ thin films and doped with Al_2O_3 deposited on a glass substrate were studied .

4.4.1. I-V Characteristics

It is important to study current-voltage properties $NiCl_2$ thin films deposited on glass substrate, which involve I-V Characteristics , were investigated with increasing doping Al_2O_3 . All the figures show that the current values increase with the increase in the doping ratios , the electrical conductivity increases with the increase in the doping ratios (1,2,3)%, and this is consistent with the optical results, because in the case of doping, the energy gap decreases, This is consistent with the previous study in refer [45].

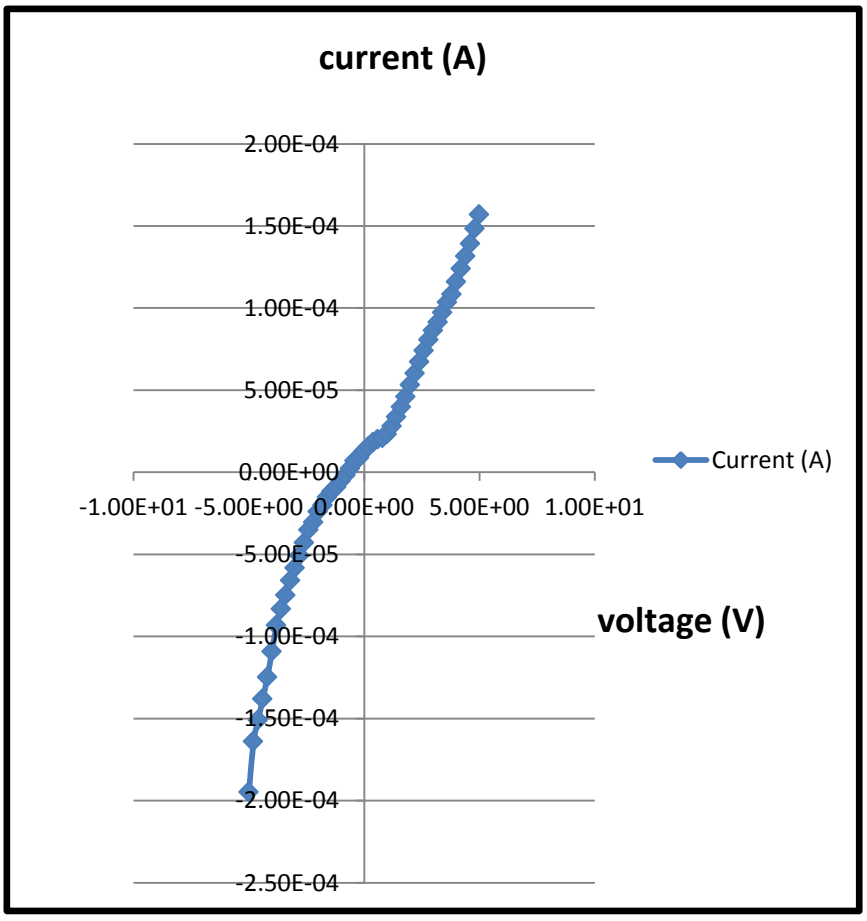

Fig (4.43): I-V Characteristics of $NiCl_2$ thin film (pure) current .

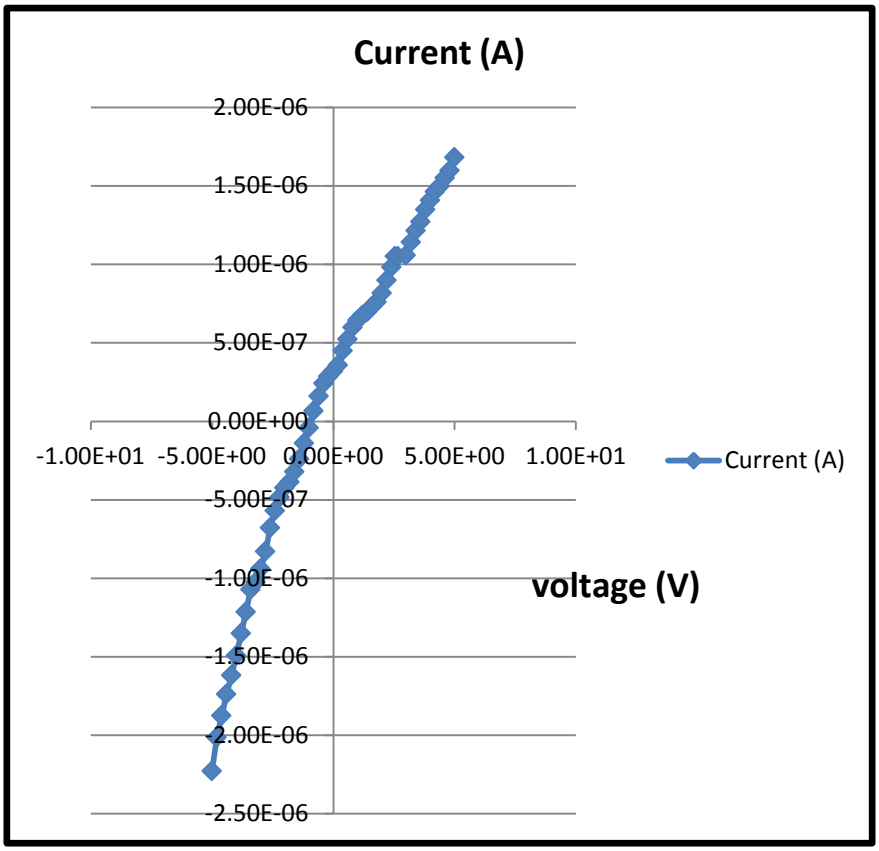

Fig(4.44) : I-V Characteristics of $NiCl_2$:Al_2O_3 thin film at 1% .

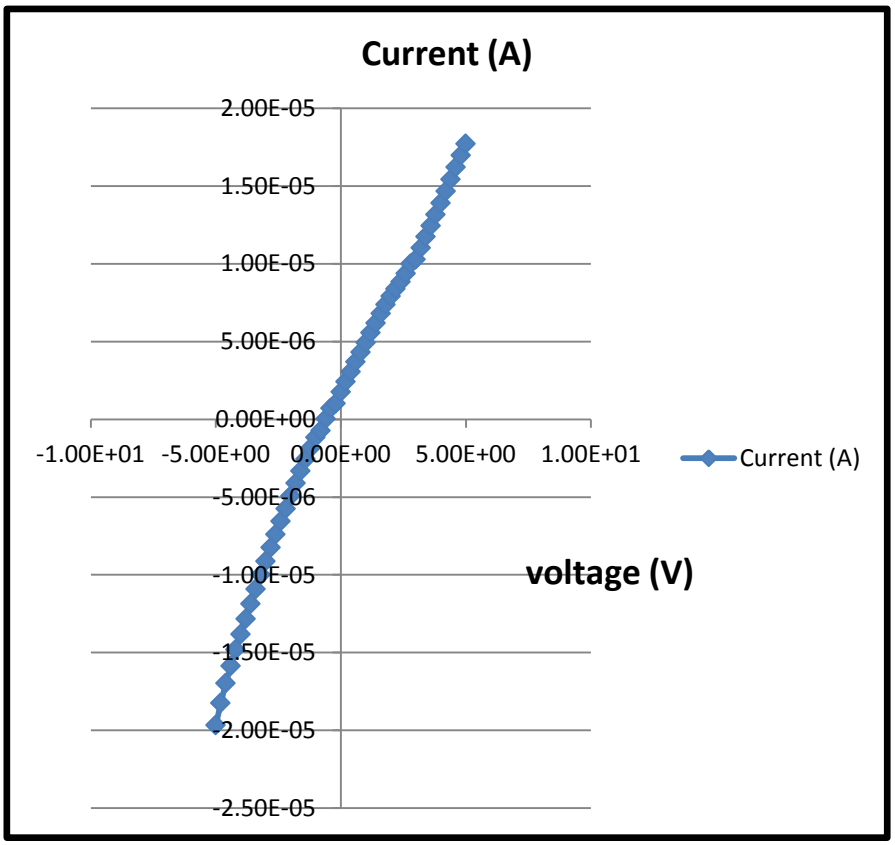

Fig(4.45) : I-V Characteristics of $NiCl_2$:Al_2O_3 thin film at 2% .

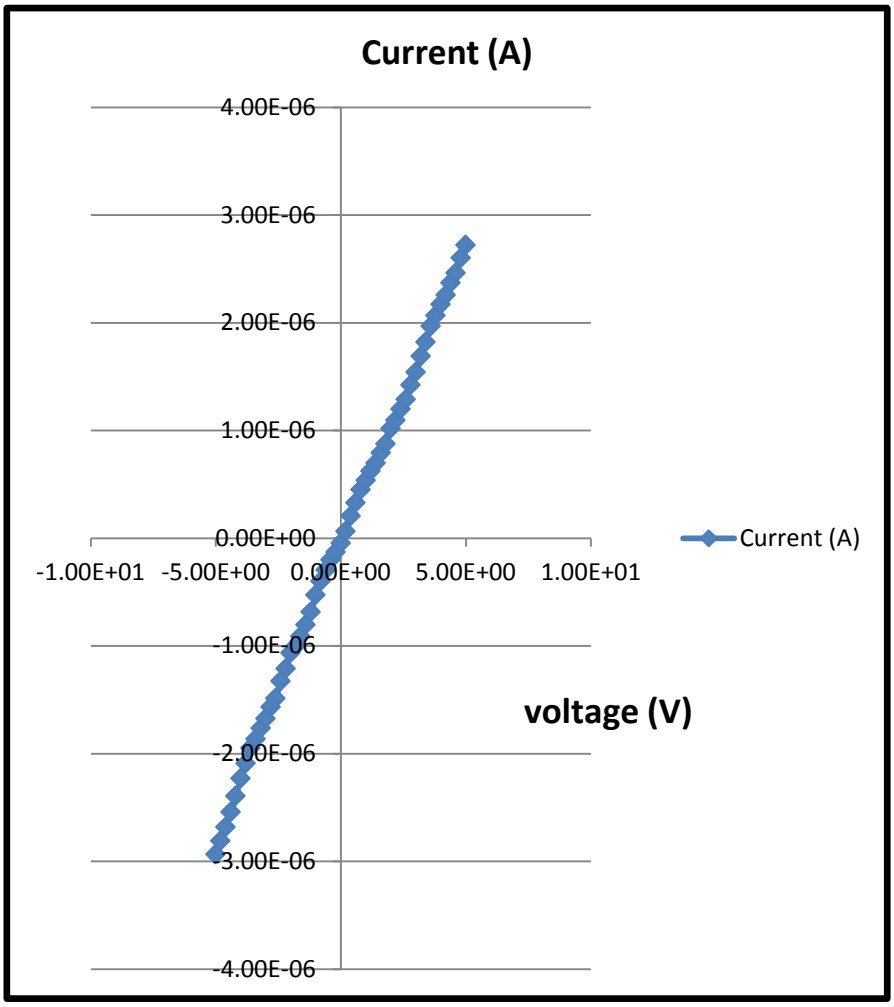

Fig (4.46) : I-V Characteristics of $NiCl_2$:Al_2O_3 thin film at 3% .

Table(4.13): show the effect of doping on conductivity values .

Sample	Conductivity $\sigma(\Omega.cm)^{-1}$
$NiCl_2$ (pure)	0.0102
$NiCl_2$:Al_2O_3 (1%)	0.0447
$NiCl_2$:Al_2O_3 (2%)	0.0988
$NiCl_2$:Al_2O_3 (3%)	0.7980

In the case of annealing 350 ˚C , noticed the opposite as the electrical conductivity decreases due to the increase in the energy gap, as shown in the figures from (4.47) to (4.50) .

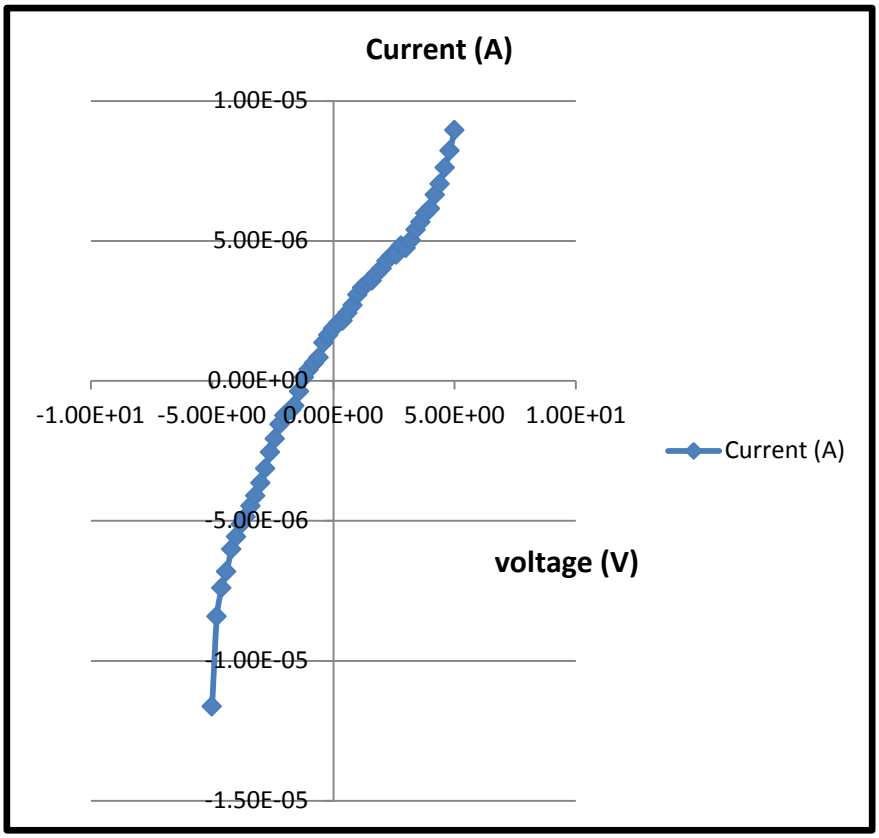

Fig(4.47) : I-V Characteristics of the pure thin film $NiCl_2$ at 350 ˚C .

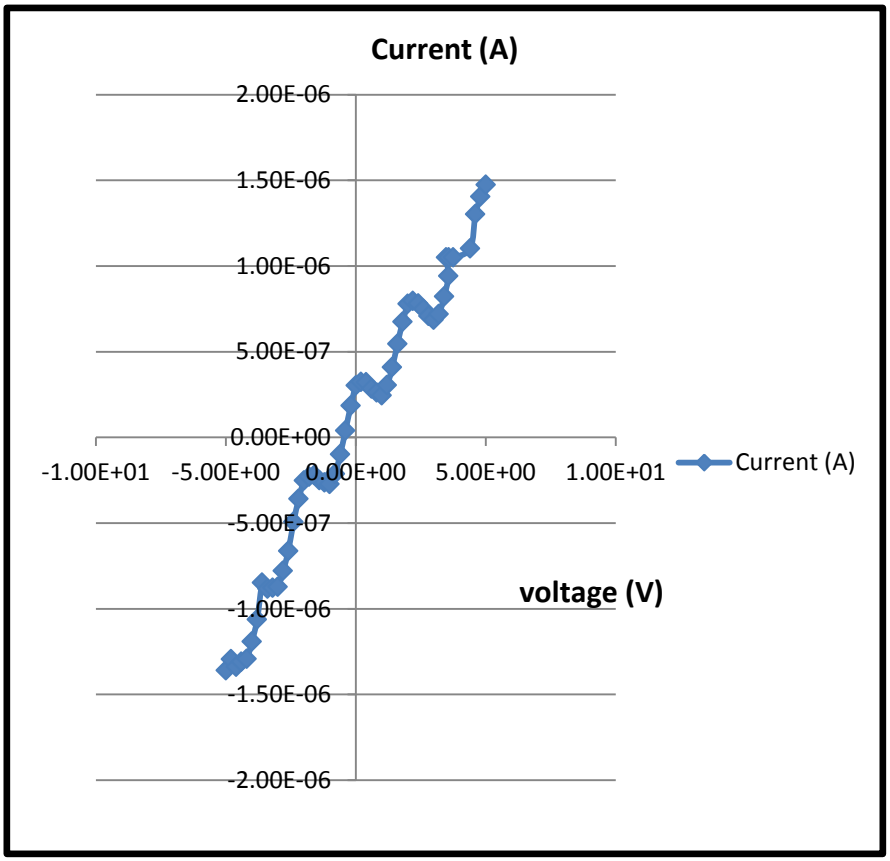

Fig(4.48) : I-V Characteristics of thin film $NiCl_2$:Al_2O_3 (1%) at 350 ˚C .

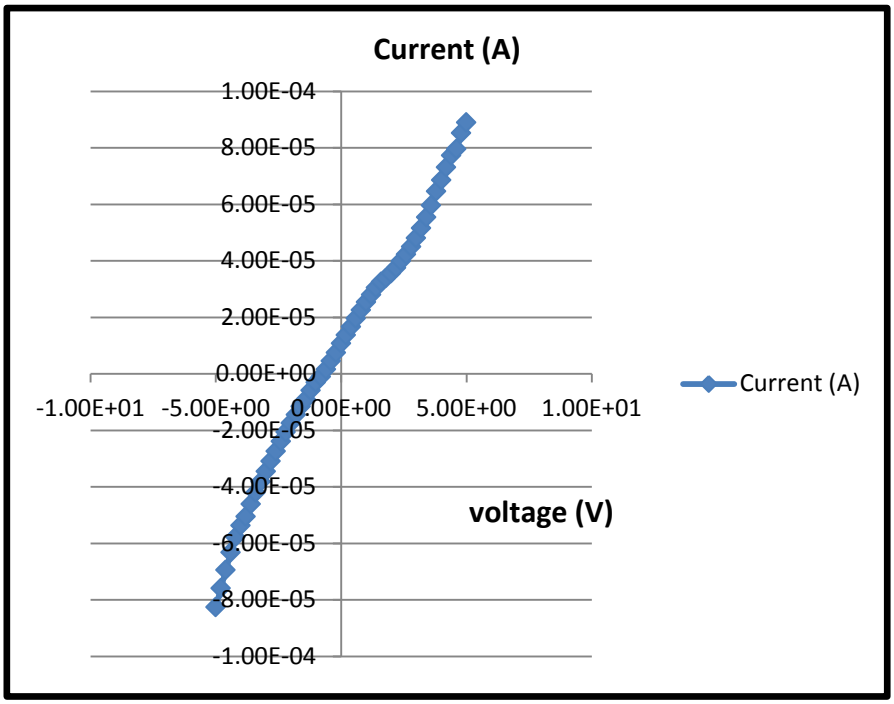

Fig(4.49) : I-V Characteristics of thin film $NiCl_2$:Al_2O_3 (2%) at 350 ˚C .

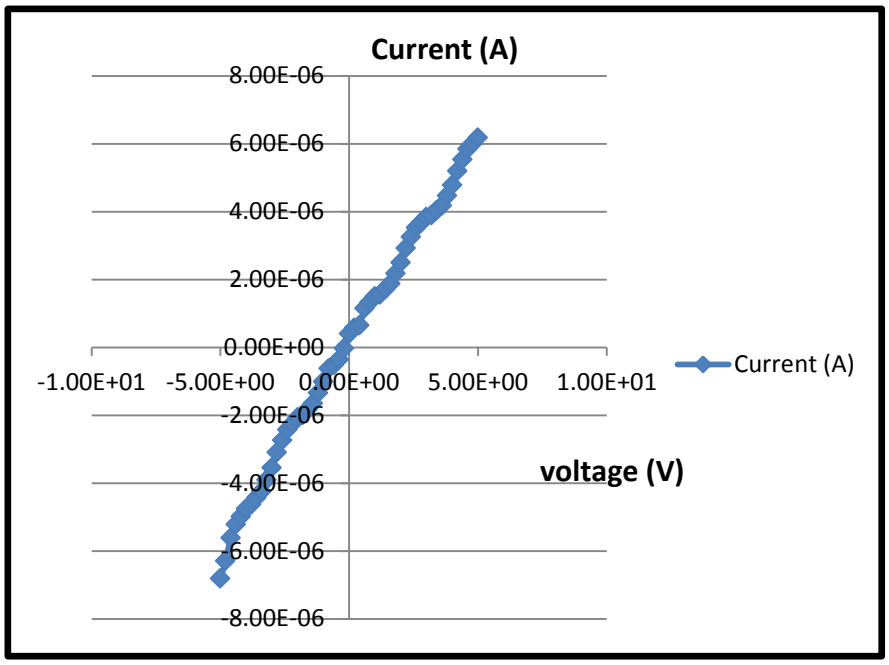

Fig(4.50): I-V Characteristics of thin film $NiCl_2$:Al_2O_3 (3%) at 350 ˚C .

Table(4.14): show the effect of annealing on conductivity values .

Sample	Conductivity $\sigma(\Omega.cm)^{-1}$
$NiCl_2$ (pure)	0.0078
$NiCl_2$:Al_2O_3 (1%)	0.0156
$NiCl_2$:Al_2O_3 (2%)	0.0350
$NiCl_2$:Al_2O_3 (3%)	0.4368

4.5. Conclusions

This section shows the main conclusions that we have obtained in our research. From overall measurements and observations, one can conclude the following:

1. It was concluded that the possibility of doping nickel chloride ($NiCl_2$) with aluminum oxide (Al_2O_3) using the thermal chemical spraying technique .
2. XRD measurements of the $NiCl_2$ thin films show that the structures were of the polycrystalline rhombic type. It can be concluded that all films exhibit a high intensity (111) diffraction peak for the thin films. Also, the average crystal size increases with the increase in the doping ratio and the opposite occurs when the temperature is increased.
3. The SEM and AFM images show that the RMS size, roughness and grain increase with increasing doping ratios and decrease with increasing substrate temperature.
4. It was noticed the absorbance of the films increased with increasing the doping rates and decreased with annealing, and the best absorption was at the doping percentage (3%) , and the best transmittance at the doping ratio (3%) at 350 ^{0}C , as the temperature increases the absorption coefficient decreases and increases with the increase in doping, and the highest value of the absorption coefficient was at the ratio (3%) .
5. It was noticed from the voltage-current characteristics curves that the conductivity increases with increasing doping rates and decreases with annealing . The best conductivity was at the doping ratio 3%, where the energy gap was lowest at this ratio.

4.6. Suggestions for Future Work

For future work it can be suggested the following:

1- Fabrication and characterization of a solar cell from multijunction of $NiCl_2$:Al_2O_3 as an upper layer .
2- Preparation of $NiCl_2$:Al_2O_3 heterojunction on different substrate such as Ge and study the optoelectronic properties for heterojunction .
3- Effect of radiation by neutrons on the optical and structural of un doped Al_2O_3 thin films of different thickness and comparing the result with result of the recent study .

References

[1] K. L. Chopra, “Thin films phenomena”, McGraw-Hill, New York, (1969).

[2] R. A. Smith, “Semiconductors”, 2nd.ed, Cambridge University Press, London, (1987).

[3] K. D. Lever, “Thin Films”, London, (1972)

[4] L. Eckcrtova, “Physics of Thin Films”, Plenum Press, (1977).

[5] K. L. Chopra, “Thin Film Devices Application”, Plenum Press, (1983).

[6] S. M. SZe, “Semiconductor Devices Physics and Technology”, Translated by F. G. Hayaty and H. A. Ahmed, University of Mosul, (1990) .

[٧] على أحمد يوسف"دراسة الخواص البصرية والكهربائية لاغشية كبريتيد الكادميوم المشوب بالفضة" ، رسالة ماجستير، الجامعة المستنصرية ، (٢٠٠١) .

[8] AshishGarg, "Growth and characterization of Epitaxial oxide thin films", Degree of doctor of philosophy at university of Cambridge, December (2001).

[9] Peter B. Barna,"history of thin films gowth techniques ,characterization" , Autumn School 2005 on Advanced Materials Science and Electron Microscopy Humbold University of Berlin , Oct. 4th - Oct.7th, (2005).

[10] Jiho Kang, M.S., "electrochemical studies of coatings and thin films" , Degree Doctor of Philosophy, in the Graduate School of The Ohio State University, (2006).

[11] K. E. Gonsalves, S. P. Rangarajan, and J. Wang, "chemical synthesis of nanostructured metals ,metal alloys , and semiconductors" , Handbook of Nanostructured Materials and Nanotechnology, Volume 1: Synthesis and Processing (2000).

[12] Bhachu, D., "the synthesis and characterization of metal oxide thin films", thesis (Ph.D) university college London, (2013).

[13] Feng, Qi, "Magnetic and magneto- optical properties of magnetic oxide thin films", thesis (Ph.D.), University of Sheffield, EthOS ID: uk.bl.ethos.570169, (2013).

[14] Saba Abdulzahra ALShiaa," Investigation of structural, electrical and optical properties of nickel oxide thin films doped by Ge, Zn and Sn by PVD methods" Ph.D. ,Thesis, College of Science , Iran, Razi University , (2016).

[15] Tribble, "Electrical Engineering Materials and Devices", University of Lowa, (2002).

[16] F. Bueche-D. Jerde, "Principles of Physics", Arabic Edition, International House for Cultural Investments and Publishing, (2001).

[17] Philip Moriarty1, "Nanostructured materials", Rep. Prog. Phys. 64 297–381, (2001).

[18] J. Zhou, R. Skomski, A. Kashyap, K. D. Sorge, Y. Sui, M. Daniil, L. Gao, M. L. Yan, S.-H. Liou, R. D. Kirby and D. J. Sellmyer, "Highly coercive thin-film nanostructures, Magnetism and Magnetic Materials" , pp. 227–230-290-291 (2005).

[19] Pablo Jensen, Albert-l , L6 Barbaki , Hernan larraled , Shlomo Havlin and H.E. stanlley, "Growth and Percolation of Thin Films": A

Model Incorporating Deposition, Diffusion and Aggregation, Volume. 6, pp. 221-236, Elsevier Science Ltd (1995).

[20] Hui Gong, Shi-Gang Sun ,1, Jun-Tao Li, You-Jiang Chen and Sheng-Pei Chen, "Surface combinatorial studies of IR properties of nanostructured Ru film electrodes using CO as probe molecule", Electrochimica Acta 2933_/2942, 48 (2003).

[٢١] N. Hutchinson, T. Coquil, A. Navid and L. Pilon," Effective optical properties of highly ordered mesoporous thin films". Thin Solid Films 518(8), 2141–2146 (2010).

[٢2] قحطان الخزرجي " المعاملات الحرارية للمعادن الحديدية واللاحديدية " دار دجلة ناشرون وموزعون (٢٠٠٩) .

[٢٣] C.A.Keyser,"Materials Science in engineering " 2nd ed.,Chareles E.Merrill pub.co.,(1974).

[24] فراس هاشم احمدو" دراسة تاثير الحراري على بعض الخواص البصرية والكهربائية لاغشية تيتانيت الباريوم الرقيقة"رسالة ماجستير ،الجامعة المستنصرية ،(٢٠٠٣).

[٢٥] S.K.Hsiuang and R.wang,"Chinese Journal of physics, volume.15،No.3(1977).

[٢٦] د.مهدي ناجي الزكوم "كيمياء العناصر الانتقالية"، كلية العلوم ، جامعة البصرة،(١٩٨١) .

[27] Grimsrud, T. K. Andersen, "Evidence of carcinogenicity in humans of water-soluble nickel salts". Journal of Occupational Medicine and Toxicology Aage (2010).

[28] Wells, A. F. "Structural Inorganic Chemistry", Oxford Press, Oxford, United Kingdom, (1984).

[29] C. Barry Carter and M. Grant Norton, " Ceramic Materials " Science and Engineering, Springer, (2007).

[30] Karen Davis, "Material Review: Alumina (Al_2O_3)", School of Doctoral Studies European Union Journal, 2, 109–114,(2010).

[31] Mohsin Abbas Aswad, "Residual Stress and Fracture in High Temperature Ceramics", The University of Manchester, PhD Thesis, (2012).

[32] Mohsin Abbas Aswad, Residual Stress and Fracture in High Temperature Ceramics, The University of Manchester, PhD Thesis, (2012).

[33] Takashi Shirai, Hideo Watanabe, Masayoshi Fuji and Minoru Takahashi, "Structural Properties and Surface Characteristics on Aluminum Oxide Powders", Ceramics Research Lab.,(2009) .

[34] Rahul Anand, "Preparation of Denes Alumina Ceramic By Slip Casting Method", National Institute of Technology, Rourkela: Bachelor of Technology Thesis, (2014).

[35] David W. Richerson, "Modern Ceramic Engineering: Properties, Processing, and Use in Design Second Edition", Revised and Expanded, USA, Marcel Dekker, Inc. (1992).

[36] S. Ilican , M. Caglar , F. Yakuphanoglu , " A study of Structural and Optical Properties of CdO ： Al Films Deposited by Sol-gel Process ″ , Journal of Optoelectronics and Advanced Materials , Volume. 3 , No. 2 , P.135- 140 , (2009) .

[37] Khudheir Abass Mishjil, "study the optical properties and continuous conductivity for Al2O3 films prepared by chemical

spray pyrolysis method", journal, no.2, Al-Mustansiriya University, (2003).

[38] Abeer K. J. Al-Azawee " The effect of annealing on the optical properties of (Al_2O_3) thin films prepared by chemical spray pyrolysis" M.Sc. Thesis , University of Al- Nahrain , (2006).

[39] S. C. Chen, T. Y. Kuo, Y. C. Lin and H. C. Lin, "Preparation and properties of p-type transparent conductive Cu-doped NiO films," Thin Solid Films, volume. 519, no. 15, pp. 4944–4947, (2011).

[40] Y. Zhao, H. Wang, C. Wu, Z.F. Shi, F.B Gao, W.C. Li, B.I. Zhang and G.T. Du, "Structural, electrical and optical properties of nickel oxide films by radio frequency magnetron sputtering " , Vacuum, 103, pp. 14-16, (2014).

[41] M. Jlassi, I. Sta, M. Hajji, and H Ezzaouia, "Optical and electrical properties of nickel oxide thin films synthesized by sol-gel spin coating ", Mater. Sci. Semicond. Processing, 21, pp. 7-13, (2014).

[42] M. Vigneshkumar, S. Muthulakshmi Suganya, J. Pandiarajan, A. Saranya and N. Prithivikumaran , " Structural and optical properties of nanocrystalline nickel oxide thin film by spray pyrolysis technique ", Int J Tech Res Appl 52–6 , (2016).

[43] A.A. Yadav, U. Chavan , "Influence of substrate temperature on electrochemical supercapacitive performance of spray deposited nickel oxide thin films" , J Electroanal Chem, 36–42, (2016).

[44] R. O. Ijeh., "Magnetic and optical properties of electrodeposited nanospherical copper doped nickel oxide thin films ", Phys. E Low-Dimensional Syst. Nanostructures, volume. 113, no. December 2018, pp. 233–239, (2019).

[45] Zaid Mohammed J. Zwaid " Preparation and Characterization of (NiO:Cu/Si) Solar Cell by Aerosol Assisted Chemical Vapor Deposition" M.Sc. Thesis , University of Babylon, (2021).

[46] N. Ramanathan, and H. T. Alan, "Nanoparticles: Synthesis, Stabilization, Passivation, and Functionalization", American Chemical Society, pp.6-329, (2008).

[47] H. Masuo, N. Kiyoshi, N. Makio, and Y. Toyokazu, "Nanoparticle Technology Handbook", Elsevier, pp. 5-11. (2007).

[48] X. Wang, J. Zhuang, Q. Peng, and Y. Li, "Biomimetic Nanoceramic in Clinical Use: From Materials to Applications", Advanced Materials, volume 18, pp. 2031-2034, (2006).

[49] J. Liu, W. Huang, Y. Xing, R. Li, and J. Dai, "Preparation of durable superhydrophobic surface by sol–gel method with water glass and citric acid", Journal of Sol-gel Science and Technology, Volume 58, Issue 1, (2011).

[50] J. Dutta and H. Hofmann, "Nanomaterials", India: Elsevier, pp. 34-35, (2007).

[51] Castro-Hurtado I, Malagu C, Morandi S, Perez N, Mandayo GG and Castano E. "Properties of NiO sputtered thin films and modeling of their sensing mechanism under formaldehyde atmosphere", Acta Mater;61:1146-53(2013).

[52] Mai Mostafa Khalaf 1, 2, Hikmet Gamal Ibrahimov1 and Etibar Hummat Ismailov1 , " Nanostructured Materials : Importance , Synthesis and Characterization - A " , Review , Chemistry Journal, Volume. 02 , Issue 03, pp. 118-125, (2012).

[53] Umair Yaqub Qazi and Rahat Javaid, " A Review on Metal Nanostructures: Preparation Methods and Their Potential Applications " , Advances in Nanoparticles, 5, 27-43, (2016) .

[54] JungdaeKima, ShengyongQina, Wang Yaob, QianNiua, M. Y. Chouc, and Chih-Kang Shiha,1, Quantum size effects on the work function of metallic thin film nanostructures, PNAS |July 20, |volume . 107 |no. 29 |12761–12765,(2010).

[55] Ying, J. Y. " Nanostructured Materials ", Academic, San Diego previously published as : Advances in chemical engineering, volume. 27, (2001).

[56] Chow, G. M., Ovid'ko, I., and Tsakalakos, T. " Nanostructured Filmsand Coatings, NATO Science Series, 3. " High Technology, Volume. 78, KluwerAcademic Publishers, Dordrecht (2000).

[٥٧] ح. بن سالم، " دارسة الخصائص الفيزيائية والكهربائية والضوئية لشرائح أكسيد القصدير مطعم بالأنتموان Sb موضع بطريقة الأمواج فوق الصوتية " ، رسالة ماجستير، جامعة الوادي، (2014) .

[58] N. A. H. Al-Isawi, "Preparation and Characteristic Study of TiO_2/Ag Nanocomposite for Gas Sensing and Optoelectronic Applications," Ph.D ,Al-Mustansiriyah,(2017).

[59] J. M. Hincapié-Zapata, E. Y. Castrillón-González, B. Cruz-Muñoz, M. H. Medina-Barreto, and R. J. Dorantes-Rodríguez, "Instrumentation and control of an aerosol-assisted chemical vapor deposition system (AACVD) " , DYNA, volume. 86, no. 210, pp. 52–57, (2019).

[60] P. Pizá-Ruiz, A. Sáenz-Trevizo, Y. Verde-Gómez, P. Amézaga-Madrid, and M. Miki-Yoshida, "Delafossite CuFeO2 thin films via

aerosol assisted CVD: synthesis and characterization" , Ceramics International, 45(1), pp. 1156-1162, (2019).

[61] E. Chen, " Thin Film Deposition, Applied Physics " , Harvard University, (2004).

[62] N. B. Hasan and M. A. Mohammed, "XRD Investigation of (PbO) 1-x (CdO) x Thin Films Deposited By Spray Pyrolysis Technique," pp. 1–10.,(2014).

[6٣] G. Blandenet, M. Court, and Y. Lagarde, "Thin layers deposited by the pyrosol process," Thin Solid Films , volume. 77, no. 1–3, pp. 81–90, (1981).

[64] W. D. Callister " Materials Science and Engineering" 4th ed., (1997).

[65] C. Kittel "Introduction to solid state physics" John Wiley and sons ,5th edition, (1986).

[66] A. Beiser " Concepts of Modern Physics " Mc Graw – Hill Kogakusha , Ltd , 2nd Edition , (1980) .

[67] L. Pawlowski "The Science and Engineering of Thermal Spray Coatings", John Wiley and sons , 2nd. ed., France , book, (2007).

[68] Y.N.AL-Jammal " Soild state physics" AL- Mousul University ,Arabic version , (1990).

[69] M. G. Yousif " Solid State Physics "Volume.1 ,Baghdad University Arabic Version , (1989).

[70] P.A. Chate, D.J. Sathe and P.P. Hankare, "Electrical and crystallographic properties of nanocrystalline CdSe0.5S0.5 composite thin films deposited by dip method" , Journal of Materials

Science: Materials in Electronics, Volume. 22, No. 2, pp. 111–115, (2011).

[71] J. Pattar , S. N. Sawant , M. Nagaraja , N. Shashank , K. M. Balakrishna , G. Sanjeev and H. M. Mahesh ” Structural Optical and Electrical Properties of Vacuum Evaporated Indium Doped Zinc Telluride Thin Films” Int. J. Electrochem. Sci., Volume. 4,pp 369-376 , (2009).

[72] S. P. Ghiosh, “Synthesis and Characterization of Zinc Oxide Nanoparticles by Sol-Gel Process”, M.Sc. Thesis, Department of Physics, National Institute of Technology, Rourkela-769008, Orissa, India, (2012).

[73] H. A. Banimuslem, “Organic/Carbon Nanotubes Hybrid Thin Films for Chemical Detection”, PhD Dissertation, Sheffield Hallam University, (2015).

[74] E. Meyer, "Atomic force microscopy", Progress in Surface Science, Volume. 41, pp. 3-49, (1992).

[75] A. Said, L. Sajti, S. Giorgio, and W. Marine, " Synthesis of nanohybrid materials by femtosecond laser ablation in liquid medium", IOP Publishing J. of Physics: Conference Series, no.59, pp. 259–265, (2007).

[76] M. Dhanam, R.R. prabhu & P.K. Manoj "Investigations on chemical bath deposited Cadmium Selenide thin films" Materials Ch & Phy,Volume.107, pp289-296, (2008).

[77] M.A. Abdul Majeed,"Optoelectronics Properties of(CdO)1-x(SnO2)x/Si Detector Prepared by Pulsed Laser Deposition", M.Sc.Thesis, Babylon University, College of Science,(2015) .

[78] K.L.Chopra " Thin Film Phenomena " Mc Graw – Hill , New York (1969).

[79] T. Allen, S. Rutherford, S. Murray, S. Reipert, and M.Goldberg, "Field emission scanning electron microscopy and visualization of the cell interior", Cell Biology, Academic Press, Volume 115, pp. 325-333, (2006).

[80] A. H. Clark "Optical properties of polycrystalline and amorphous thin films and devices " edited by Laurece. L. Kazemerki, Academic press, (1960).

[81] S. Ben "Solid State Electronic Devices" Hall International , Inc ,U. S. A. ,(1990).

[82] J. I. Pankove "Optical Processes in Semiconductors" Prentice-Hall, New Jersey, (1971) .

[83] Y. Sirotin ,Y. M. Shaskolskaya "Fundamentals of crystal physics ", Mir Publishers , Moscow, (1982).

[84] S. Elliott, "Physics of Amorphous Materials" , New York: Longman Inc, Volume. 155, p. 98, (1984).

[85] S. Saxena, "Polyvinyl Alcohol (PVA)", Chemical and Technical Assessment, 1st. Ed., JECFA, (2004).

[86] N. Hasan and M . Mohammed, "Electrical Properties of (PbO) 1 - x(CdO)xThin Films Fabricated by Spray Pyrolysis Technique", Advances in Applied Science Research ,Volume. 6,No. 7, (2015).

[87] T. Allen, S. Rutherford, S. Murray, S. Reipert, and M.Goldberg, "Field emission scanning electron microscopy and visualization of

the cell interior", Cell Biology, Academic Press, Volume 115, pp. 325-333, (2006).

[88] D. Newman, "Semiconductor physics and devices", Basis Principles, Richard, University of New Mexico, Volume 435, p.211, (1992).

[89] G. Busch and H. Schade, "Lectures on Solid State Physics" International Series in Natural Philosophy, pergamon press, Elsevier, Volume 79, (2013).

[90] B. Sharma and R. Purohit, "Semiconductor heterojunctions", Pregamon Press, Oxford, New York, (1974).

[91] Amada Loren, "Texturization Processes of Mono Crystalline Silicon with $Na_2Co_3/NaHCo_3$ Solution for Solar Cells", Cienclas Y Tecnologlas I.S.B.N, (2012).

[92] Sami S. Jiyad , " Optical and structural properties of SnO_2 films Fluorized and irradiated with gamma rays " ,M.SC. Thesis , University of Baghdad , College of Science for Girls, (2005).

[93] R. Guinebretière, "X-ray diffraction by polycrystalline materials, Wiley , " (2013).

[94] A. Tonomura and T. Komoda, "Field emission electron microscope" Microscopy, Volume. 22, no. 2, pp. 141–147, (1973).

[95] A. M. • Y. P. • T. Rades and Editors, "analytical techniques in the pharmaceutical sciences" Department of Pharmacy University of Copenhagen Copenhagen Ø, Denmark, (2016).

[96] Subhajit Biswas, Soumitra Kar, and Subhadra Chaudhuri," Journal of Phys. Chem", Volume. 109, pp.17526-17530 , (2005) .

[٩7] V. Gayou , B. Salazar-Hernandez , M. Constantino, E. Rosendo Andre, T. Diaz ,R. Delgado Macuil , M. Rojas Lopez," Journal of Vacuum ", Volume. 84 , pp.1191–1194, (2010) .

[98] Rusul Kadhim M.Jasim " Substrate Temperature Effect on Some Physical Properties of SnS Thin Films Prepared by Chemical Spray Pyrolysis" M.Sc. Thesis , University of Babylon, (2022).

[99] Salam H. Fayyad " Preparation and study of the structural and optical properties of film CdTe:Cu" M.Sc. Thesis, University of Baghdad, (2015).

[100] A. Goudarzi, G. Motedayen Aval, S. Soo Park, M. Choi, R. Sahraei, M. Ullah, A.Avane, and H. ChangSik," Journal of Chem. Mater" , Volume. 21, No. 12, pp.2375–2385 , (2009) .

[١01] M. Y. Nadeem and A. Waqas, " Journal of Turk. J. Phy" Volume. 24 , pp . 651- 659 , (2000) .

[102] G. Rodica, J.P. Elisabeth, L. Maria, S.D. Laura & E. Indrea, " Studia Universitatis Babes-Bolyal, Physica, Special Issue" , Romania, (2003) .

[103] S. O. Kasap, "Principles of Electronic Materials and Devices", 2nd Edition, McGraw-Hill, New York, (2002) .

[104] B. Bhattacharjee , D. Ganguli , K. Iakoubovskii , A. Stesmans and S. Chaudhuri ," Journal of Bull. Mater. Sci, ", Volume. 25, No. 3 ، pp.175–180 , (2002) .

[105] D. Nithyaprakasha, M. Ramamurthya, P.Thirunavukarasub, T. Balasubramaniamc. J. Chandrasekarana , and P. Maadeswarana,

" Journal of Optoelectronic and Biomedical Materials", Volume. 1, Issue 1, pp. 42-51 , (2009) .

[1،6] R. Poulomi , R. Jyoti & S.Srivastava," Journal of Thin Solid Films،" Volume. 515, Issue 4, pp.1912–1917 , (2006) .

[107]F.Y. Mohammed " Characterization Of CdTe/GaAs Heterojunction" Ph.D. ,Thesis, College of Science , University of Baghdad , (2009).

[١08] M. Funaki, Y. Ando, R . Jinnai, A. Tachibana and R. Ohno, "Development of CdTe detectors in Acrorad",Acrorad Co. Ltd ,(2006).

[١09] S.M.Ali "Studies Structure and optical properties of CdTe thin films dopant of Zn " University of Baghdad ,(2011).